



KHCO₃/CO₂ ELECTROREDUCTION FOR FUEL CELL APPLICATIONS: REACTION AND REACTOR OPTIMIZATION, PROTOTYPING WITH 3D PRINTING AND AUTOMATIC TESTING.

Andreu Bonet Navarro

ADVERTIMENT. L'accés als continguts d'aquesta tesi doctoral i la seva utilització ha de respectar els drets de la persona autora. Pot ser utilitzada per a consulta o estudi personal, així com en activitats o materials d'investigació i docència en els termes establerts a l'art. 32 del Text Refós de la Llei de Propietat Intel·lectual (RDL 1/1996). Per altres utilitzacions es requereix l'autorització prèvia i expressa de la persona autora. En qualsevol cas, en la utilització dels seus continguts caldrà indicar de forma clara el nom i cognoms de la persona autora i el títol de la tesi doctoral. No s'autoritza la seva reproducció o altres formes d'explotació efectuades amb finalitats de lucre ni la seva comunicació pública des d'un lloc aliè al servei TDX. Tampoc s'autoritza la presentació del seu contingut en una finestra o marc aliè a TDX (framing). Aquesta reserva de drets afecta tant als continguts de la tesi com als seus resums i índexs.

ADVERTENCIA. El acceso a los contenidos de esta tesis doctoral y su utilización debe respetar los derechos de la persona autora. Puede ser utilizada para consulta o estudio personal, así como en actividades o materiales de investigación y docencia en los términos establecidos en el art. 32 del Texto Refundido de la Ley de Propiedad Intelectual (RDL 1/1996). Para otros usos se requiere la autorización previa y expresa de la persona autora. En cualquier caso, en la utilización de sus contenidos se deberá indicar de forma clara el nombre y apellidos de la persona autora y el título de la tesis doctoral. No se autoriza su reproducción u otras formas de explotación efectuadas con fines lucrativos ni su comunicación pública desde un sitio ajeno al servicio TDR. Tampoco se autoriza la presentación de su contenido en una ventana o marco ajeno a TDR (framing). Esta reserva de derechos afecta tanto al contenido de la tesis como a sus resúmenes e índices.

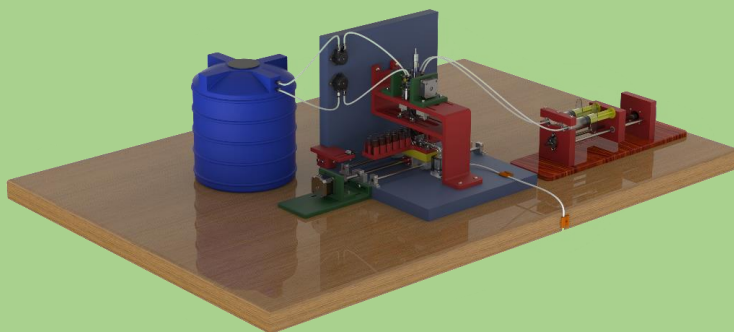
WARNING. Access to the contents of this doctoral thesis and its use must respect the rights of the author. It can be used for reference or private study, as well as research and learning activities or materials in the terms established by the 32nd article of the Spanish Consolidated Copyright Act (RDL 1/1996). Express and previous authorization of the author is required for any other uses. In any case, when using its content, full name of the author and title of the thesis must be clearly indicated. Reproduction or other forms of for profit use or public communication from outside TDX service is not allowed. Presentation of its content in a window or frame external to TDX (framing) is not authorized either. These rights affect both the content of the thesis and its abstracts and indexes.



KHCO₃/CO₂ ELECTROREDUCTION FOR FUEL CELL APPLICATIONS

**Reaction and reactor optimization, prototyping with 3D
printing and automatic testing.**

Andreu Bonet Navarro



DOCTORAL THESIS 2021

UNIVERSITAT ROVIRA I VIRGILI

KHCO₃/CO₂ ELECTROREDUCTION FOR FUEL CELL APPLICATIONS: REACTION AND REACTOR OPTIMIZATION,
PROTOTYPING WITH 3D PRINTING AND AUTOMATIC TESTING.

Andreu Bonet Navarro

Andreu Bonet Navarro

KHCO₃/CO₂ ELECTROREDUCTION FOR FUEL CELL APPLICATIONS

**Reaction and reactor optimization, prototyping with 3D
printing and automatic testing.**

Doctoral Thesis

Supervised by Dr. Ricard Garcia Valls and

Dr. Adrianna Nogalska

Chemical Engineering Department



UNIVERSITAT ROVIRA i VIRGILI

Tarragona

2021

UNIVERSITAT ROVIRA I VIRGILI
KHCO₃/CO₂ ELECTROREDUCTION FOR FUEL CELL APPLICATIONS: REACTION AND REACTOR OPTIMIZATION,
PROTOTYPING WITH 3D PRINTING AND AUTOMATIC TESTING.
Andreu Bonet Navarro



UNIVERSITAT ROVIRA I VIRGILI

Departament d'Enginyeria Química
Avinguda dels Països Catalans, 26,
43007 Tarragona
977 55 97 00

I STATE that the present study, entitled KHCO₃/CO₂ ELECTROREDUCTION FOR FUEL CELL APPLICATIONS: Reaction and reactor optimization, prototyping with 3D printing and automatic testing presented by Andreu Bonet Navarro for the award of the degree of doctor, has been carried out under my supervision at the Department of Chemical Engineering of this university.

Tarragona, 01/09/2021

Doctoral Thesis Supervisors

A stylized, handwritten signature in black ink, consisting of several overlapping loops and a long horizontal stroke.

Ricard Garcia-Valls

A handwritten signature in black ink, written in a cursive style. The name 'Nogalska' is clearly legible, followed by a small 'R'.

Adrianna Nogalska

UNIVERSITAT ROVIRA I VIRGILI
KHCO₃/CO₂ ELECTROREDUCTION FOR FUEL CELL APPLICATIONS: REACTION AND REACTOR OPTIMIZATION,
PROTOTYPING WITH 3D PRINTING AND AUTOMATIC TESTING.
Andreu Bonet Navarro

Table of content

AWKNOLEDGEMENTS	11
1. SUMMARY.....	1
List of abbreviations	6
List of figures	7
List of tables	13
2. MOTIVATIONS.....	15
3. GENERAL INTRODUCTION	25
3.1. Zero CO₂ emission energy generation.....	27
3.2. Photocatalytic reduction of CO₂	30
3.3. Electrocatalytic reduction of CO₂	31
3.4. Fuel cell technologies	34
3.5. 3D printing technologies	36
3.6. Automation and 4th industrial revolution.....	39
3.7. Hardware for automatic control.....	42
3.7.1. Electric motors.....	42
3.7.2. Solenoid valves.....	44
3.7.3. Peristaltic pumps	46
3.7.4. Mechanical endstops	47
3.7.5. Microcontroller ESP32.....	47
3.7.6. Stepper motor drivers.....	49
3.8. Electronic circuits and components	50
3.8.1. Protoboard	50
3.8.2. Printed circuit board	52
3.8.3. Transistors	53
3.8.4. Diodes.....	54

3.8.5. DC-DC Controllers	54
3.8.6. Capacitors.....	55
4. OBJECTIVES AND HYPOTHESIS.....	57
5. DIRECT ELECTROCHEMICAL REDUCTION OF BICARBONATE	63
5.1. Introduction.....	65
5.2. Experimental	66
5.2.1. Materials and reagents	66
5.2.2. Linear Sweep Voltammetry.....	67
5.2.3. Electroreduction experiments	71
5.2.4. Product Analysis.....	72
5.3. Results and discussion	73
5.3.1. Linear Sweep Voltammetry.....	73
5.3.2. Chronoamperometry.....	75
5.3.3. Analysis and quantification of products by ¹ H NMR.....	76
5.4. Conclusions	79
6. DESIGN AND FABRICATION OF REACTOR WITH 3D PRINTING	81
6.1. Module design with SolidWorks	83
6.2. Reactor printing with SLA technology and assembly.....	91
6.3. Workshop-made reactor vs 3D printed	94
6.4. Conclusions	97
7. AUTOMATIC AND REMOTE TESTING SYSTEM	99
7.1. Introduction.....	101
7.2. Schematic design of the automated system.....	102
7.3. Design of the system with SolidWorks	105
7.3.1. Support for the reactor.....	105
7.3.2. Solenoid valves.....	105
7.3.3. Stirring Motors.....	105
7.3.4. Autosampler	109

7.3.5. Peristaltic Pump	111
7.3.6. Syringe Pump	112
7.4. Printing of the system.....	115
7.5. Electronic circuit design.....	117
7.6. System assembly	123
7.7. MicroPython programming for control.....	126
7.8. Web for remote control programming with node	132
7.9. Conclusions	138
8. AUTOMATIC SYSTEM TESTING	139
8.1. Introduction.....	141
8.2. Experimental	141
8.2.1. Materials and Methods.....	141
8.3. Results and discussion	143
8.3.1. Electroreduction with Tin catalysts	143
8.3.2. ESEM characterization of ceria-based catalysts.....	147
8.3.3. Electroreduction with Ceria catalysts	148
8.3.4. Characterization of products using NMR.....	150
8.5. Conclusions	153
9. DIRECT FORMATE/FORMIC ACID FUEL CELL	155
9.1. Introduction.....	157
9.2. Experimental	159
9.2.2. Methods and reagents.....	159
9.3. Results and discussion	163
9.4. Conclusions	173
10. GENERAL CONCLUSIONS AND FUTURE WORK.....	175
REFERENCES.....	179
APPENDIX.....	191

List of publications	193
Congresses	194
Code used for calculation of HCOOH production	195
Code used for calculation of CH₃COOH production	200
Code used for solutions preparation	205
Code used for NMR spectra processing and analysis	210

ACKNOWLEDGEMENTS

In this section, I would like to show my appreciation to all the people who supported, me either academically or personally, during this three-year period, of learning extremely useful knowledges that enriched me to confront and solve real world problems.

I would like to show my appreciation to my tutor/mentor Ricard Garcia Valls, that helped me with his “old men” advice and all the freedom and trust he gave to me, which is not very easy to find in a PhD tutor and allowed me to try something very crazy and different.

I would like to show my gratitude to my co-tutor/co-mentor Adriana Nogalska who helped me in with any problem I had during these 3 years and mainly with her strong knowledge in chemistry.

I would like to acknowledge all the members in Eurecat Tarragona team whom I worked with: Victor, Anna, Aitor, Bartek, David Santiago, David Domingo, Emma, Isabel, Iuliana, Monika, Laia, Magda, Miriam and Roger.

I would especially like to thank Dr. Alexey Shavel who advised and helped me with electrochemistry and electronics fields, Montse Carrasco and Dr. Josep Maria Montornes, who managed the buying of lab supplies and helped me with administrative issues. Also, my PhD mate Víctor Llamas Martínez in Eurecat that helped me with engineering problems and shared with me knowledge and difficulties during these three years.

I would like to acknowledge all the members of the URV research group MEMTEC, who I shared knowledge with: Ania, Pepa, Marta, Toni, Yaride and Alberto, with a special mention to Ania and Pepa for all the technical and administration help from the URV side.

Another very important help comes from two people from *Servei de Recursos Científics i Tècnics* of the URV. One of them is Ernest Arce Alcarraz, that manufactured some of the reactors I used during the thesis and helped me with his mechanical issues, and Ramon Guerrero Grueso for NMR analysis help and advice.

First, I would like to acknowledge the extremely competent and beloved friends whose unconditionally gave to me technical support during these three years: Marc Roig Campos for helping and advising me with 3D printing issues, electronics, and data analysis. Christian Callau Romero for the assistance in computer engineering, Carlos Bertomeu Marin for the help in in web design, Marc Navarro Pons for the advice in electronics field and Aïda Ibrahim Camps that helped me in revising the thesis.

Finally, the financial support received by the Regional Agency for Business and Competitiveness of the Generalitat de Catalunya (EURECAT-ACCIÓ). Moreover, the Vincente Lopez scholarship from EURECAT provided for Andreu Bonet Navarro pre-doctoral studies and Ministerio de Economía y Competitividad (ENE2017-86711-C3-3-R).

KHCO₃/CO₂ electroreduction for fuel cell applications

Reaction and reactor optimization, prototyping with 3D printing and automatic testing.

1. SUMMARY

1. Summary

KHCO₃/CO₂ electroreduction for fuel cell applications*Reaction and reactor optimization, prototyping with 3D printing and automatic testing.*

The main effects of climate change, like more frequent and severe climate, dirtier air, higher wildlife extinction rates, more acidic oceans, and higher sea levels, can be devastating for the Earth ecosystem, humans and global economy in the decades ahead. Therefore, it is very important to reduce greenhouse gas emissions. There are multiple approaches to solve this, but we focused on the following **i)** reduce dependency on fossil fuels by increasing the competitiveness of renewable energies, **ii)** CO₂ extraction from the atmosphere to convert it into useful products and **iii)** increase efficiency of industrial processes. During this thesis, I will work on CO₂ electroreduction to convert it into products suitable for fuel cells using an automatic testing system to attack climate change using these three tools at once.

The previous work of Adrianna Nogalska and Ricard Garcia Valls consisted of a leaf-like system that can capture CO₂ by making it pass through membrane pores to the next compartment to be finally converted to potassium bicarbonate, which is a reagent that can be used directly for electroreduction to hydrocarbons. One of the most promising hydrocarbons obtained is formic acid (FA), because it is relatively stable at atmospheric conditions and is also easy to transport and store, together with high energy density, that makes it a very attractive hydrogen carrier. With the previously commented method, CO₂ can be absorbed from the atmosphere by transforming it into formic acid rather than the most conventional methods used nowadays to obtain FA, that rely on fossil fuels emitting large concentrations of CO₂ instead of removing it. The disadvantage of obtaining FA via electroreduction in front the conventional ones is the lower efficiency and scalability of the reaction, that makes it way less competitive in the market yet. The electroreduction of CO₂ is attractive because the electrical energy used to trigger the reaction is stored in form of formic acid which

1. Summary

is a product with way higher energy density than common lithium batteries, therefore a good ally to be able to store large quantities of energy. That is necessary to overcome the main problem of renewable energies, which is its non-continuous generation and the difficulty to store large quantities of energy in conventional lithium batteries.

Hence, during this thesis, the electroreduction of raw potassium bicarbonate acting as a CO₂ source is performed to study its parameters to make the reaction more efficient. Along this research, we focused on bulk Tin (Sn) as electrocatalyst due to its low cost, easiness to use and its selectiveness toward FA among other novel ceria based (CeO₂) GDL catalysts prepared by Eva Chinarro Martín from Instituto de Cerámica y Vidrio, ICV-CSIC. Some reaction parameters are studied to evaluate their effect on the reaction efficiency: KHCO₃ concentration, pure CO₂ gas pre-saturation, applied potential.

Due to the high number of parameters to be studied and therefore, the high number of experiments to be performed, it is necessary to design a reactor as small as possible, easy to assembly-disassembly and manipulate. For this purpose, novel additive manufacturing techniques have been used, such as Fused Deposition Modelling and Stereolithography 3D printing. Those manufacturing techniques present several advantages in front of conventional subtractive ones, like faster prototyping, possibility to print more complex objects therefore reducing the total number of parts, simplifying the assembly, and reducing its size and manufacturing price.

To conclude, we were able to obtain electroreduction efficiencies around 20% when only bicarbonate was using as CO₂ source and efficiencies up to almost 50% when the bicarbonate solution was pre-saturated with pure CO₂. An automatic testing system was also developed to improve

KHCO₃/CO₂ electroreduction for fuel cell applications*Reaction and reactor optimization, prototyping with 3D printing and automatic testing.*

repeatability and reduce human error, while increasing massively the total number of experiments due to the possibility to escalate the system. This system, together with a very small 3D printed reactor are also able to reduce the price of the experiments, therefore, we open the possibility to use machine learning for the optimization of the parameters.

List of abbreviations

Abbreviation	Full name
¹ H NMR	Proton nuclear magnetic resonance
DMSO	Dimethylsulfoxide
D ₂ O	Deuterated water
LSV	Linear Sweep Voltammetry
CV	Cyclic Voltammetry
WE	Working electrode
CE	Counter electrode
RE	Reference electrode
FDM	Fused deposition modelling
FFF	Fused Filament Fabrication
SLA	Stereolithography
AI	Artificial Intelligence
SPI	Serial Peripheral Interface
MEA	Membrane Electrode Assemblies
PdB	Palladium Black
PdC	Palladium activated on Carbon
PCB	Printed Circuit Broad
LED	Light Emitting Diode
PVC	Polyvinyl chloride
MOSFET	Metal-Oxide-Semiconductor Field-Effect Transistor
FA	Formic Acid
CNC	Computer Numerical Control
CO ₂	Carbon Dioxide
GC	Gas Chromatography

KHCO₃/CO₂ electroreduction for fuel cell applications

Reaction and reactor optimization, prototyping with 3D printing and automatic testing.

List of figures

Figure 1: CO ₂ concentration in atmosphere and global temperature since 1850.	18
Figure 2: Global average long-term atmospheric concentration of carbon dioxide (CO ₂), measured in parts per million (ppm).....	19
Figure 3: Environmental degradation Kurnet's curve.	21
Figure 4: China's CO ₂ emissions per capita since 1900 in MT.....	22
Figure 5: Evolution of number of published about CO ₂ capture methods articles each year in Scopus.	28
Figure 6: Net CO ₂ emission cycle.	29
Figure 7: A schematic representation of photocatalytic reduction of CO ₂ to chemical fuels. Photo taken from [21].....	30
Figure 8: Scheme of electroreduction of CO ₂ to formic acid (cross section of a rendered reactor).	33
Figure 9: Scheme of formic a formic acid fuel cell (render of an exploded view).	35
Figure 10: Schematic representation of the FMD 3D printing technology taken from [34].	37
Figure 11: Schematic representation of laser-based SLA 3D printing technology taken from [35].....	37
Figure 12: Types of additive manufacturing processes. Taken from [29].	38
Figure 13: Cross section of a direct acting solenoid valve. Drawing from [45].....	45
Figure 14: Schematic representation of a peristaltic pump seen from the top. Scheme taken from [47].....	46
Figure 15: Schematic representation of a standard mechanical endstop...	47
Figure 16: Photo of a microcontroller ESP32.	48
Figure 17: Interior of a standard protoboard.	51
Figure 18: Standard protoboard.	51

1. Summary

Figure 19: Protoboard used to connect a led with an Arduino microcontroller.	51
Figure 20: Example of common PCBs.....	52
Figure 21: Standard three terminal transistors.....	53
Figure 22: Schematic representation of a diode.....	54
Figure 23: Scheme of a DC-DC controller and photo of a standard one. ..	54
Figure 24: Schematic representation of a capacitor.	55
Figure 25: 3D rendered design of Teflon H-cell used for the experiments.	68
Figure 26: Cross section of Teflon H-cell used for the experiments.....	69
Figure 27: Photo of the module used for the electroreduction experiments.	69
Figure 28: Nafion membrane cleaning procedure.	70
Figure 29: Scheme of sample preparation before for NMR analysis.....	72
Figure 30: LSV of non-CO ₂ saturated solutions compared with pre-saturated ones.....	74
Figure 31: LSV at different potassium bicarbonate solutions (KHCO ₃) concentrations.....	74
Figure 32: Chronoamperogram at -1.6V of bicarbonate solutions.	75
Figure 33: Chronoamperograms at -1.6V KHCO ₃ solution compared non-CO ₂ saturated solutions.....	76
Figure 34: ¹ H NMR spectra of the products in cathodic compartment.....	77
Figure 35: Rendered design of one compartment of the first prototype of reactor.	84
Figure 36: Rendered design of first prototype of reactor.....	85
Figure 37: Rendered design of first prototype of reactor with supporting parts for D.C. stirring motors.	86
Figure 38: Top view of a rendered design of the final prototype of the reactor.	88

KHCO₃/CO₂ electroreduction for fuel cell applications

Reaction and reactor optimization, prototyping with 3D printing and automatic testing.

Figure 39: General view of a rendered design of the final prototype of the reactor.	88
Figure 40: Comparison of a 3D render design of the first module prototype (right) against the final one (left).....	89
Figure 41: 2D sketch of the final reactor prototype with its main measures.	90
Figure 42: 2D drawing of the first reactor prototype with its main measures.....	90
Figure 43: Preview of all the components of the reactor of the slicing program Preform.	91
Figure 44: Photo of one of the final reactor compartments after post-curing.	92
Figure 45: Silicone sheet cut with CO ₂ laser used to seal both reactor compartments.....	93
Figure 46: Photo of the final prototype assembled.	94
Figure 47: Size comparison of the workshop manufactured reactor (on the left) against 3D printed reactor (on the right).	96
Figure 48: Weight in grams of the workshop manufactured reactor (on the left) against 3D printed reactor (on the right).....	96
Figure 49: Flow diagram of the automatic cleaning and reagents injection of the system.....	103
Figure 50: Diagram of the different sensors inside the reactor.	104
Figure 51: 3D render view of the designed support for the electrochemical reactor.	106
Figure 52: 3D render view of the designed reactor on the designed support (without screwed bolts).....	107
Figure 53: 3D render view with the solenoid valves at the bottom of the reactor.	108
Figure 54: 3D render view of the system with the stirring motors for tuneable agitation.....	108

1. Summary

Figure 55: 3D render view of the system with the magnet for stirring on the wall of the reactor.....	109
Figure 56: Photo of the real linear two simple rail system used for the home-made autosampler.	110
Figure 57: 3D render of the system with the autosampler, endstop and evacuation channel.	111
Figure 58: 3D render of the system with the two peristaltic pumps.	112
Figure 59: 3D render of the system with the home-made syringe pump.	113
Figure 60: Rendered design of all the system.	114
Figure 61: Photo of the system with the protoboard.	118
Figure 62: Scheme of electronic circuit used to control all the electronic components for the experiments.	119
Figure 63: Realistic render of the final PCB.	120
Figure 64: Photo of the final PCB with all the components soldered.....	121
Figure 65: Photo of a general view of the system.....	124
Figure 66: Photo of a general view of the system.....	124
Figure 67: Interface for individual control of the experiments.	135
Figure 68: Interface for programming the sequences of the experiments.	136
Figure 69: The 3 different real time views of the system using cameras.	137
Figure 71: Three repetitions of CV's using Tin catalysts and automatic system.	145
Figure 72: Three repetitions of chronoamperometries using non-treated Tin catalysts oxidated in atmosphere and the automated system.....	145
Figure 73: Three repetitions of chronoamperometries using new Tin catalysts non-oxidated in atmosphere and automatic system.	146
Figure 74: Three repetitions of chronoamperometries using pre-treated Tin catalysts and automatic system.....	146

KHCO₃/CO₂ electroreduction for fuel cell applications*Reaction and reactor optimization, prototyping with 3D printing and automatic testing.*

Figure 70: ESEM images of Ceria catalysts dopped with Ni, Cu and blank. The green dots correspond to the CeO ₂ while red dots represent the Ni and Cu atoms respectively.	147
Figure 75: Cyclic voltammetry of using copper dopped Ceria catalysts performed with automatic system.	148
Figure 76: Cyclic voltammetry of using Nickel dopped Ceria catalysts performed with automatic system.	149
Figure 77: Chronoamperometry of all the Ceria-based catalysts performed with automatic system.	150
Figure 78: NMR spectra of the products obtined in the first repetition of electroreduction experiments using tin catalyst in cathodic compartment.	151
Figure 79: NMR spectra of the products obtined in the third repetition of electroreduction experiments using tin catalyst in cathodic compartment.	152
Figure 80: NMR spectra of the products obtined in the first repetition of electroreduction experiments using tin catalyst in anodic compartment.	152
Figure 81: NMR spectra of the products obtined for the electroreduction experiments using Ceria-based catalysts in cathodic compartment.	153
Figure 82: Schematic illustration of membrane electrode assembly (MEA) fabrication.	160
Figure 83: Home-made system for MEA fabrication.	161
Figure 84: 3D render of an exploded view of fuel cell.	162
Figure 85: Diffractograms of catalysts.	164
Figure 86: A general formic acid oxidation mechanism on Pd and Pt anodes of direct formic acid fuel cells (DFAFCs) by Elnabawy et al. Reproduced from [101].	165
Figure 87: Polarization curves of the developed formate/formic acid fuel cells.	166

1. Summary

Figure 88: Comparison of homogeneous dispersion of catalyst in inks. . 166
Figure 89: Formate/Formic acid fuel cells performance..... 168
Figure 90: Constant current discharging efficiency at 20 mA and
maximum power current (MP). 172

KHCO₃/CO₂ electroreduction for fuel cell applications

Reaction and reactor optimization, prototyping with 3D printing and automatic testing.

List of tables

Table 1: Comparison table between additive and subtractive manufacturing	39
Table 2: Differences between machines humans. Taken from: [COTEC]. (2019, April 19). #MiEmpleoMiFuturo: un documental sobre robots, economía, clase media... y el fin del mundo. [Video]. YouTube. https://www.youtube.com/watch?v=htAnVeMtrr8	41
Table 3: Angles and step values for the different microstepping modes for standard stepper motor drivers.	43
Table 4: Candidate stepper motor drivers.	49
Table 5: Summary of the effects of the potassium bicarbonate (KHCO ₃) concentration and the CO ₂ pre-saturation on the faradaic efficiency of the electroreduction to formate.	78
Table 6: Summary of CO ₂ electroreduction efficiencies towards HCOOH/HCOOK of similar bulk catalysts.	78
Table 7: Comparison between first and final prototypes of reactors.	87
Table 8: Comparison of the workshop-made reactor against 3D printed one.	95
Table 9: Summary of all the 3D printed parts with FDM technology used for the automatic system (Table 10 for the 3D printed parts used in the syringe pump)	115
Table 10: Summary of all the 3D printed parts with FDM technology used for the syringe pump.	116
Table 11: Summary of all the 3D printed parts cost in time and price with SLA technology.	116
Table 12: Summary table of all the electronic components soldered on the designed PCB.....	122
Table 13: Summary of the price of components used for the automatic system.	125

1. Summary

Table 14: Summary of the price of components related to electroreduction.....	126
Table 15: List of ceria-based catalyst used.....	142
Table 16: Fuel cell parameters	163
Table 17: Theoretical reaction potential and measured open circuit potentials of the studied cells.	167
Table 18: Formate/formic acid fuel cells' maximum power peak data.	169
Table 19: Comparison of obtained results with literature findings.	170

KHCO₃/CO₂ electroreduction for fuel cell applications

Reaction and reactor optimization, prototyping with 3D printing and automatic testing.

2. MOTIVATIONS

2. Motivations

KHCO₃/CO₂ electroreduction for fuel cell applications*Reaction and reactor optimization, prototyping with 3D printing and automatic testing.***What is causing global warming?**

The Earth's average temperature can be modified by different factors such as a change in the Earth's orbit, solar intensity variations, volcano eruptions, and changes in the atmospheric composition, among others [1]. Any variation on one of these agents can significantly affect the average temperature on Earth. For example, one of the most common phenomena is the greenhouse effect produced mainly due to CO₂, Methane and N₂O. Those gasses have the property to not absorb most of the arriving sunlight but absorbing the reflected sunlight by the earth crust. This phenomenon is the so-called greenhouse effect and it's the main responsible of regulate the average atmospheric temperature on earth. This effect keeps the earth warm around an average temperature of 15°C, that allows to accommodate life on it. Without greenhouse gases this temperature would be around -18°C Celsius degrees [2]. Therefore, greenhouse gasses are in fact necessary for life in earth, but a certain equilibrium over time must be maintained to not overheat or over freeze the earth out of the acceptable limits for life.

Since the start of the first industrial revolution (18th century) and crafting of the steam engine, we started to burn fossil fuels and liberating significant amounts of CO₂, increasing the concentration of it in the atmosphere. As you can see, in **Figure 1**, the CO₂ concentration increased in more than 50% in less than 200 years [3], at the same time the temperature also increased around 1°C [4].

The earth's global temperature and CO₂ concentration have always fluctuated over time (**Figure 2**) and it is due to natural cycles that humans do not have control on, but since the beginning of the industrial revolution in 1760, humans have been liberating significative amounts of greenhouse

2. Motivations

gases to the atmosphere (Mainly CO₂) which can accelerate this natural processes [5].

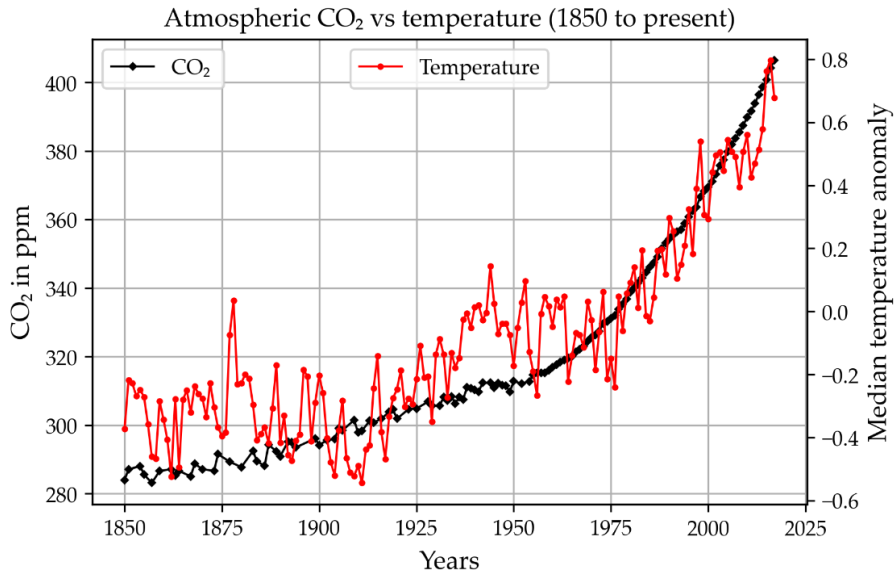


Figure 1: CO₂ concentration in atmosphere and global temperature since 1850.

Despite climate change being a natural process that has been always present, every climate change on earth had consequences in its ecosystem and life, sometimes leading to catastrophic consequences [6]. The most important factor was the speed at which this change was occurring, because living species can't tolerate or evolve fast enough to adapt to the new conditions [7].

The additional anthropogenic CO₂ emissions are threatening its natural readjustment and balance. From the industrial revolution we observed a rapid increase in global temperatures of more than 1 degree in just around one century. 2015 was the first year in which the annual average of CO₂ levels were above 400ppm [8], reaching a never seen level during the last 800.000 years, according to the CO₂ concentration in tapered air bubbles

KHCO₃/CO₂ electroreduction for fuel cell applications

Reaction and reactor optimization, prototyping with 3D printing and automatic testing.

inside Antarctica's ice sheets [9]. Despite CO₂ not being the only responsible of global changes in temperature, it is true that it has a great effect on it as you can see in **Figure 2**.

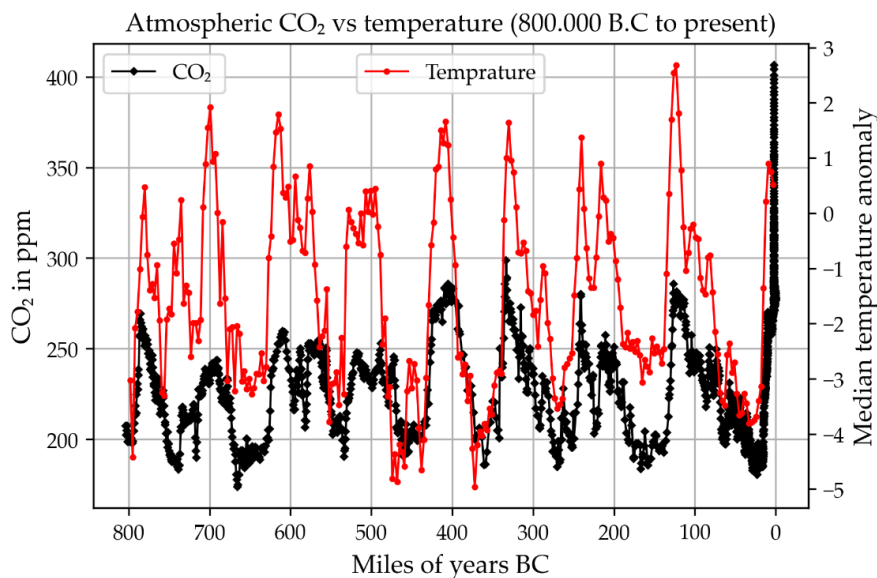


Figure 2: Global average long-term atmospheric concentration of carbon dioxide (CO₂), measured in parts per million (ppm).

What are the consequences of global warming?

Some of the effects of global warming are desertification, more aggressive weather, permafrost melting and increase of the sea level among others. Those effects produce consequences on the ecosystem of the planet with some species starting to go extinct at an alarming rate, with more on the way of being endangered. For humans, the consequences of the climate change will be mainly related with health [10], life quality and economy [11], even though the three of them are quite correlated.

2. Motivations

For humans, the development as a civilization has been always in its nature, leading to incredibly things and increasing life quality and expectancy of life, creating a better world to live in. Nevertheless, the modern human development and industrialization came at a cost of destroying natural ecosystems and changing composition of the atmosphere, and that will decrease the big three (health, life quality and economics), so human development is a double-edged sword that must be managed carefully.

Is it possible to fight against climate change while maintaining the standards in development and industrialization?

Nowadays, climate change is already inevitable, but to mitigate its negative effects while maintaining the level of human development and industrialization is going to be one of the biggest challenges for humanity during the fourth coming years [12].

Since the start of the first industrial revolution, greenhouse emissions and ecosystem invasion has been directly proportional to human development, and most of us were not aware of the consequences. In addition, there was no other possibility to improve our living standards, because non-contaminant technologies are more advanced and required superior technology, that were not accessible few years ago. Therefore, it can be said that first years of the industrial revolution there was no other way to develop our civilization, but now renewable and clean energies are starting to be cost effective, hence, is the time to invest in CO₂ reutilization and renewable energies to minimize CO₂ emissions.

KHCO₃/CO₂ electroreduction for fuel cell applications

Reaction and reactor optimization, prototyping with 3D printing and automatic testing.

To depict what was discussed before we can use the environmental Kurnet's curve (**Figure 3**) [13] that describes the level of environmental degradation in front of GDP per capita. As can be seen, when the wealth of a country increases the level of environmental degradation also increases, but there is a maximum in which the investment on renewable energies becomes viable, and at that point, the level of environmental degradation starts to decrease. A country that is a clear example of that is China (**Figure 4**), being a developing country that has increased drastically its CO₂ emissions since the beginning of the 21st century, and nowadays is already reaching its maximum due to the increase in purchasing power that makes viable the investment in renewable energies and environmental laws application.

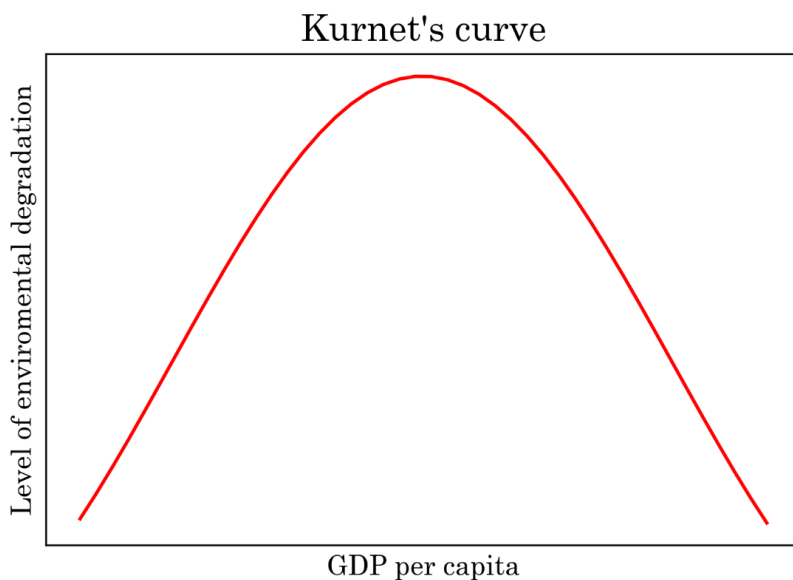


Figure 3: Environmental degradation Kurnet's curve.

Why should we invest in renewable energies?

In most developed countries there are no more excuses today, even for people that is only interested in economics should understand that not trying to mitigate the climate change is going to have catastrophic consequences in long/medium term.

Nowadays we not just reached historic records on CO₂ concentration, but we increased it at a record rate generating an unstoppable inertia, powered by self-accelerating processes like ice melting in poles, in which the great potential of reflecting light that ice has will disappear, and liquid water that absorbs light will take its place.

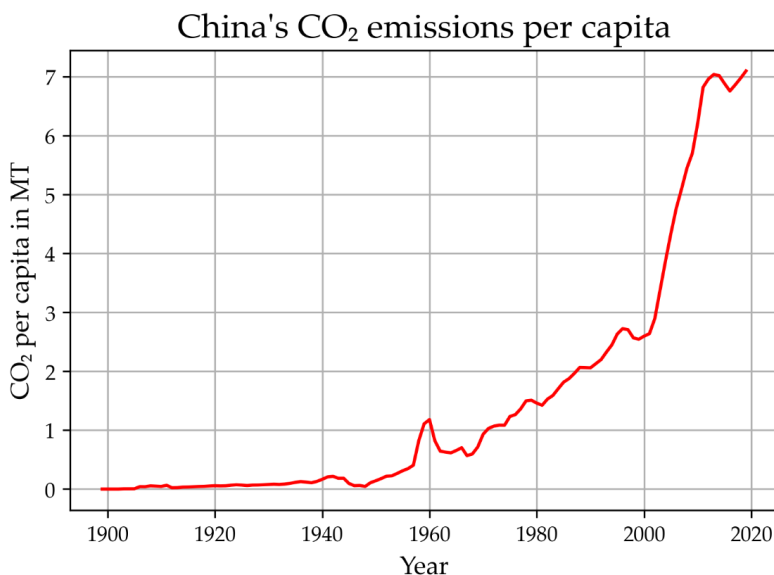


Figure 4: China's CO₂ emissions per capita since 1900 in MT.

Even if there are global initiatives to reduce CO₂ emissions, those are not being compiled to achieve its effective reduction, so complementary techniques should be envisaged. In our research group, we work with CO₂

KHCO₃/CO₂ electroreduction for fuel cell applications*Reaction and reactor optimization, prototyping with 3D printing and automatic testing.*

absorption techniques, that can help mitigate the catastrophic consequences of global warming. Nowadays, CO₂ absorption technologies are an emerging reality, opening the door to reuse the absorbed CO₂ to produce something useful. This is possible, but the challenge is to make this technology efficient enough to be economically viable and competitive.

Our new approach of rechargeable batteries based on absorbing CO₂ technologies [14] and converting it into an energy carrier [15], to be used for fuel cells [16] that could have an energy density around 500 times higher than current lithium batteries, higher lifespan and no rare earth elements politically controlled for manufacturing it [17]. These advantages can help electric cars, autonomous houses and any other devices that depends strongly on battery self-sufficiency to be more competitive and economic in a future when fossil fuels will disappear.

2. Motivations

KHCO₃/CO₂ electroreduction for fuel cell applications

Reaction and reactor optimization, prototyping with 3D printing and automatic testing.

3. GENERAL INTRODUCTION

3. General introduction

In this section a brief introduction of all the topics developed during the thesis will be done to give a better understanding to the reader about the technologies and instrumentation used during this work

KHCO₃/CO₂ electroreduction for fuel cell applications

Reaction and reactor optimization, prototyping with 3D printing and automatic testing.

3.1. Zero CO₂ emission energy generation

As described in the previous section, humanity now should be focused on generate energy without emitting CO₂, following the European Green Deal which is to reach that milestone in 2050 [18]. Nowadays, the two main ways to generate energy without emitting CO₂ is by using renewable energies and nuclear energy, even though, both energies present significant disadvantages.

The challenge with renewable energies, as solar and wind, is that they are very irregular and hard to predict and adapt the peak demands. Therefore, we can't rely solely on them. Nuclear energy has the advantage to have a stable production but cannot be switched off immediately when needed and the nuclear residues generated by nuclear plants have a bad social perception. One of the current approaches is to store the excess of energy generated during production peaks in form of hydrogen, which is a compound with high energy density, but the problem with hydrogen is its low stability that makes it costly and hard to store and transport. To overcome this problem, the coupling of CO₂ absorption technologies and CO₂ reduction technologies appears. Atmospheric CO₂ can be fixated by using different technologies such as absorption, adsorption, membranes, thermodynamics and enzymatic methods [19]. However, the first 3 are the most used and the ones that experienced a drastic increase over the last decades as you can see in **Figure 5**. CO₂ can be reduced to stable hydrogenated products that act as a hydrogen carrier in order to facilitate hydrogen transportability.

One of the most promising CO₂ capture technologies consists on a system that combines absorption with membranes developed by A. Nogalska and R. Valls [14]. This system absorbs the atmospheric CO₂ inside

3. General introduction

an aqueous solution. The captured CO₂ can be electroreduced into an energy/hydrogen carrier [20]. After that, the energy stored in that compound can be released together with CO₂ at the desired moment, using fuel cell technology. Therefore, coupling these systems on the actual energy production network, can solve the extreme irregularity and the impossibility to switch off nuclear power plants, with the possibility to store large quantities of that excess of energy (see **Figure 6**).

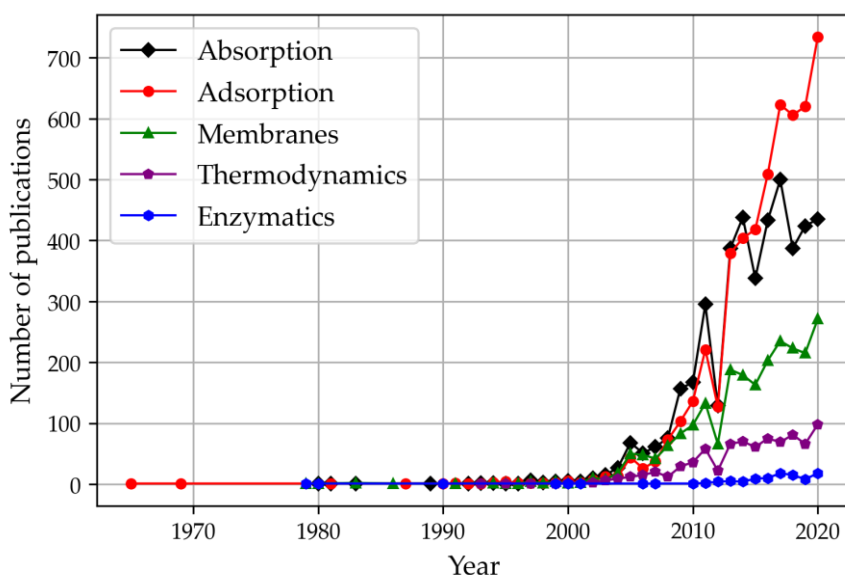


Figure 5: Evolution of number of published about CO₂ capture methods articles each year in Scopus.

KHCO₃/CO₂ electroreduction for fuel cell applications

Reaction and reactor optimization, prototyping with 3D printing and automatic testing.

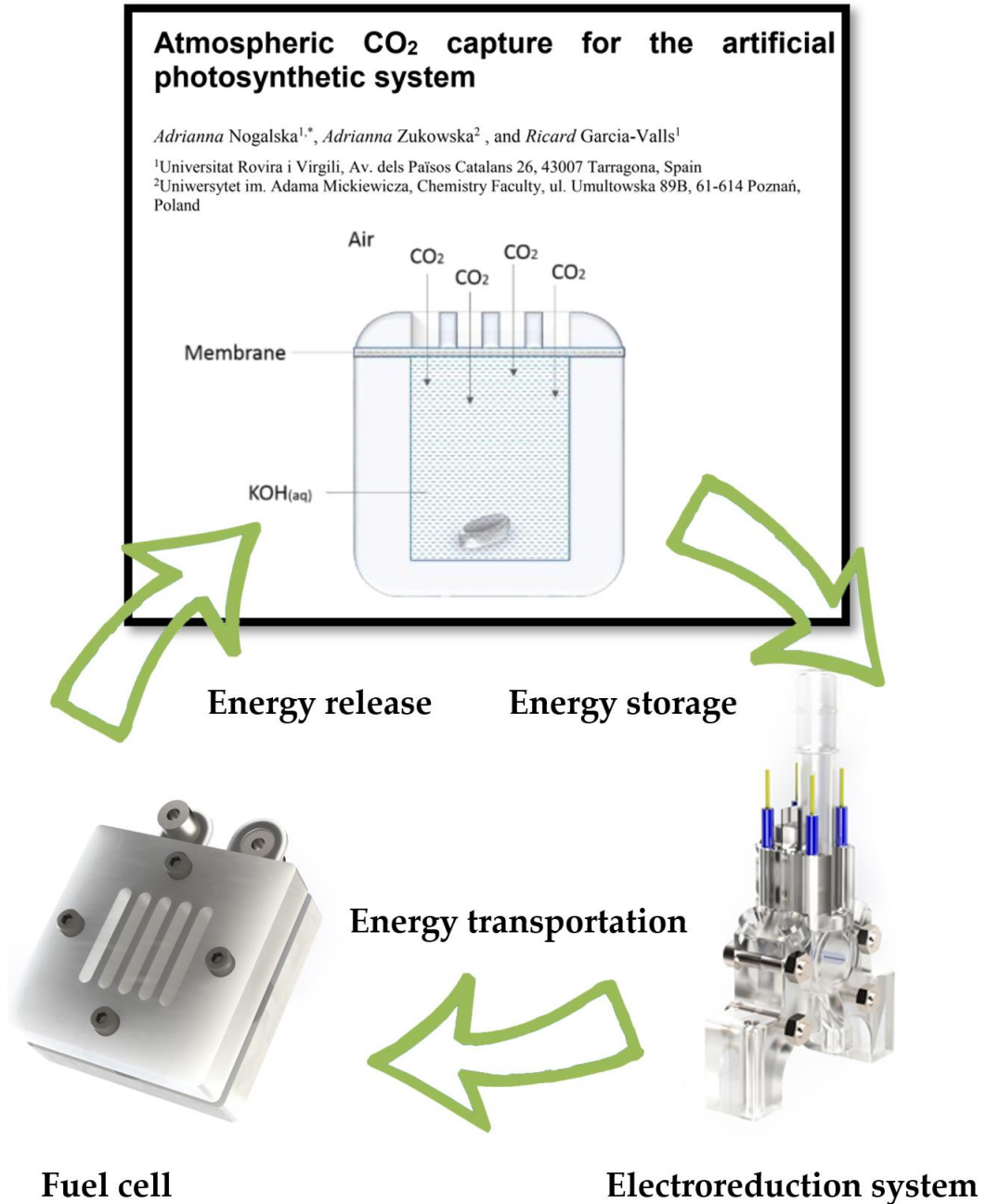


Figure 6: Net CO₂ emission cycle.

3.2. Photocatalytic reduction of CO₂

Photoreduction consists in triggering the reaction using direct sunlight. The energy from the sun energizes the electrons in the last band, liberating them from the nuclei. This is used to form hydrogenated products together with protons, as can be seen in **Figure 7** [21]. Photocatalysis seems to be a very simple and direct method to transform the CO₂ from the atmosphere into higher value chemicals and store the sunlight energy. However most of the photocatalytic processes show reduced efficiencies, which doesn't make it competitive in the market yet [22][23][24].

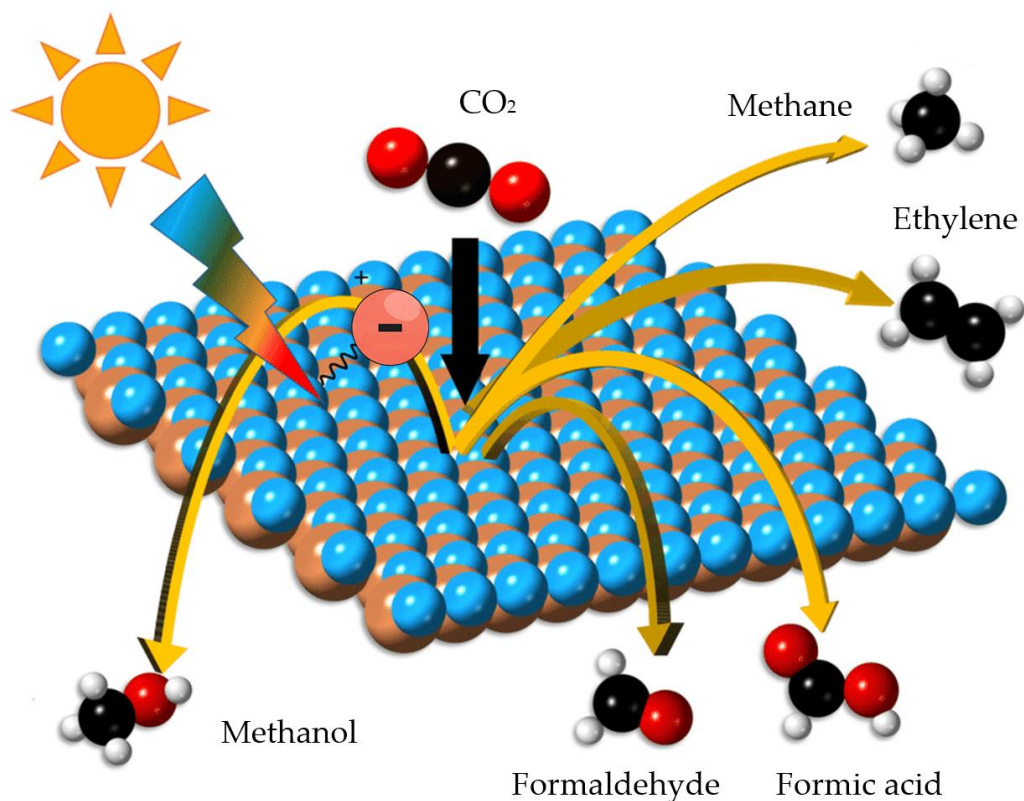


Figure 7: A schematic representation of photocatalytic reduction of CO₂ to chemical fuels. Photo taken from [21]

KHCO₃/CO₂ electroreduction for fuel cell applications

Reaction and reactor optimization, prototyping with 3D printing and automatic testing.

3.3. Electrocatalytic reduction of CO₂

The most common way to reduce CO₂ is by electrocatalysis, due to its greater efficiency compared to photocatalytic reduction. The electrocatalytic reduction of CO₂ can be performed by homogeneous and heterogeneous catalysis. Typically, the reduction with homogeneous catalysts tends to be faster and more efficient, even though the catalysts are usually not reusable and need to be separated from the products [25]. This step increases the price of the reaction all together with the usually expensive catalysts [26].

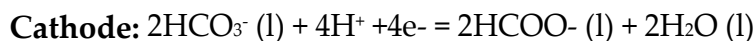
On the other side, electroreduction with heterogeneous catalysis shows great efficiencies compared with photocatalysis, and the reusable catalyst doesn't need to be separated from the products, therefore this is one of the most attractive ways to electro-reduce CO₂ at low price in industry. In the present thesis, we will describe the investigations performed to reduce CO₂ by electroreduction using heterogeneous catalysts because seems to be the most interesting for industrial production in the future [27].

The electroreduction using bulk metal catalysts is performed as shown in **Figure 8** (The scheme is considering that the CO₂ is reduced only to formic acid for simplification but other products can be obtained during this process), where a potential applied between two electrodes, the working electrode (also called catalyst) in the cathodic compartment and the counter electrode in the anodic compartment, makes water molecules split in the anode, producing protons (H⁺) and electrons. Then, the protons are electrically attracted by the negatively charged working electrode, and tend to move to the cathodic compartment, but before that, they must cross a proton exchange membrane (Nafion membrane). That membrane is designed to let those protons cross freely and avoid as much as possible the

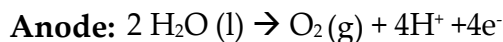
3. General introduction

pass of other species. Once those protons are in the cathodic compartment, they interact with the excess of electrons and the CO₂ molecules to form the formic acid and O₂ (following the (Eq. 1), (Eq. 2) and (Eq. 3)) or other hydrogenated products. Thanks to the previously mentioned proton exchange membrane, the products cannot go to the anodic compartment and therefore cannot be re-oxidized.

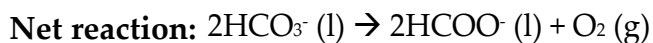
(Eq. 1)



(Eq. 2)



(Eq. 3)



KHCO₃/CO₂ electroreduction for fuel cell applications

Reaction and reactor optimization, prototyping with 3D printing and automatic testing.

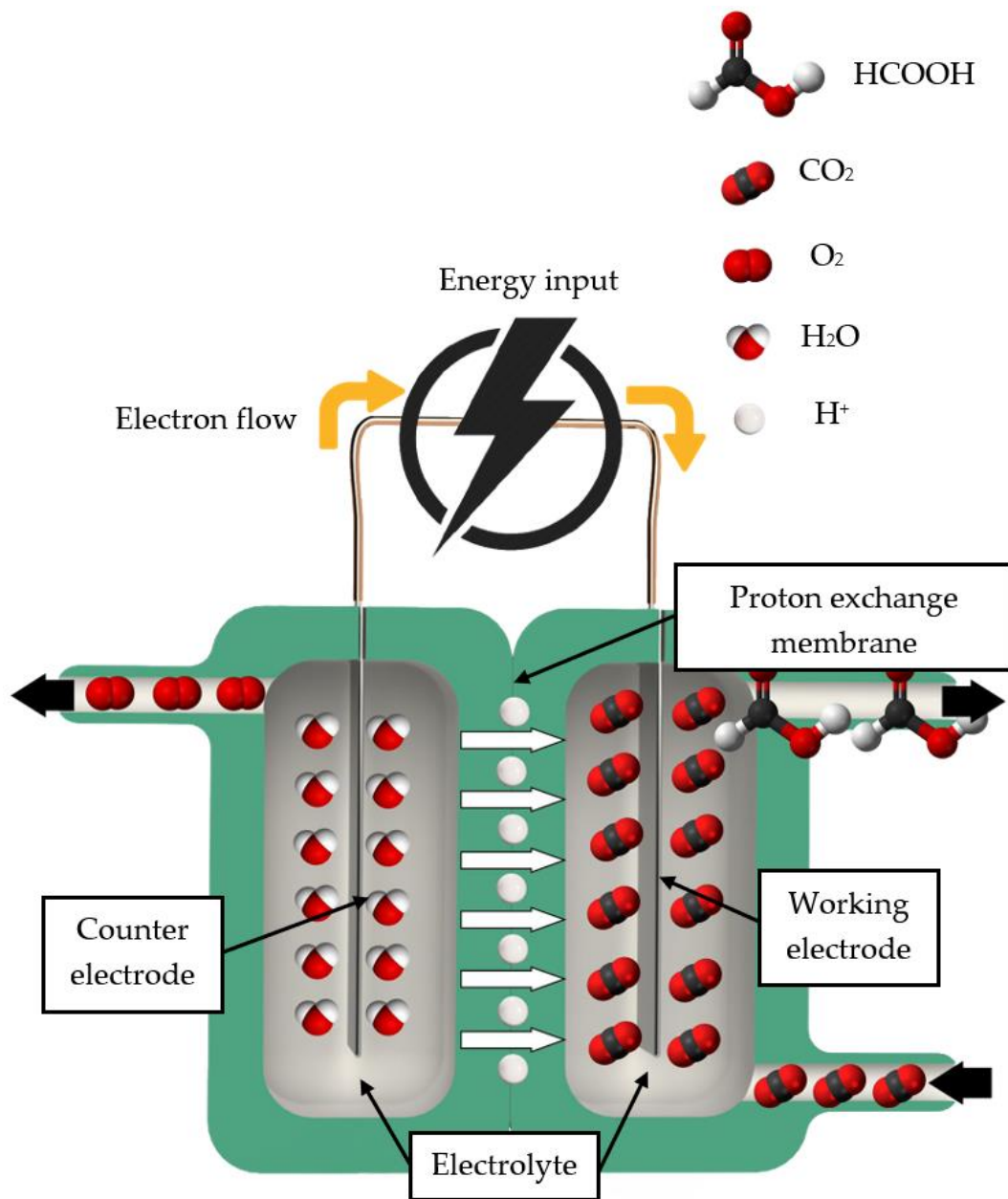
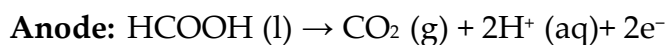


Figure 8: Scheme of electroreduction of CO₂ to formic acid (cross section of a rendered reactor).

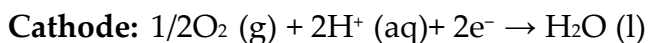
3.4. Fuel cell technologies

A fuel cell consists of a device that transforms chemical energy from a fuel directly into electrical energy. The most common ones are hydrogen fuel cells, but as we will work with formic/formate fuel cells during this thesis, a description of them will be done. A formic/formate fuel cell converts this reagent to water and CO₂, liberating electrical energy (**Figure 9**). The chemical reaction is performed as follows: the formic acid is oxidized to CO₂ (**Eq. 4**), liberating protons (H⁺) and electrons in the anode. The protons cross through a proton exchange membrane (normally Nafion) to meet the cathode. Those protons and electrons, together with oxygen molecules form water (**Eq. 5**). Finally, the global balance is formic acid plus oxygen being converted into CO₂ and water (**Eq. 6**) liberating electrons that can be used to power any electric device.

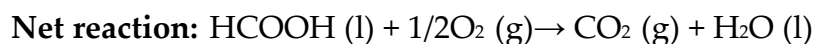
(Eq. 4)



(Eq. 5)



(Eq. 6)



KHCO₃/CO₂ electroreduction for fuel cell applications

Reaction and reactor optimization, prototyping with 3D printing and automatic testing.

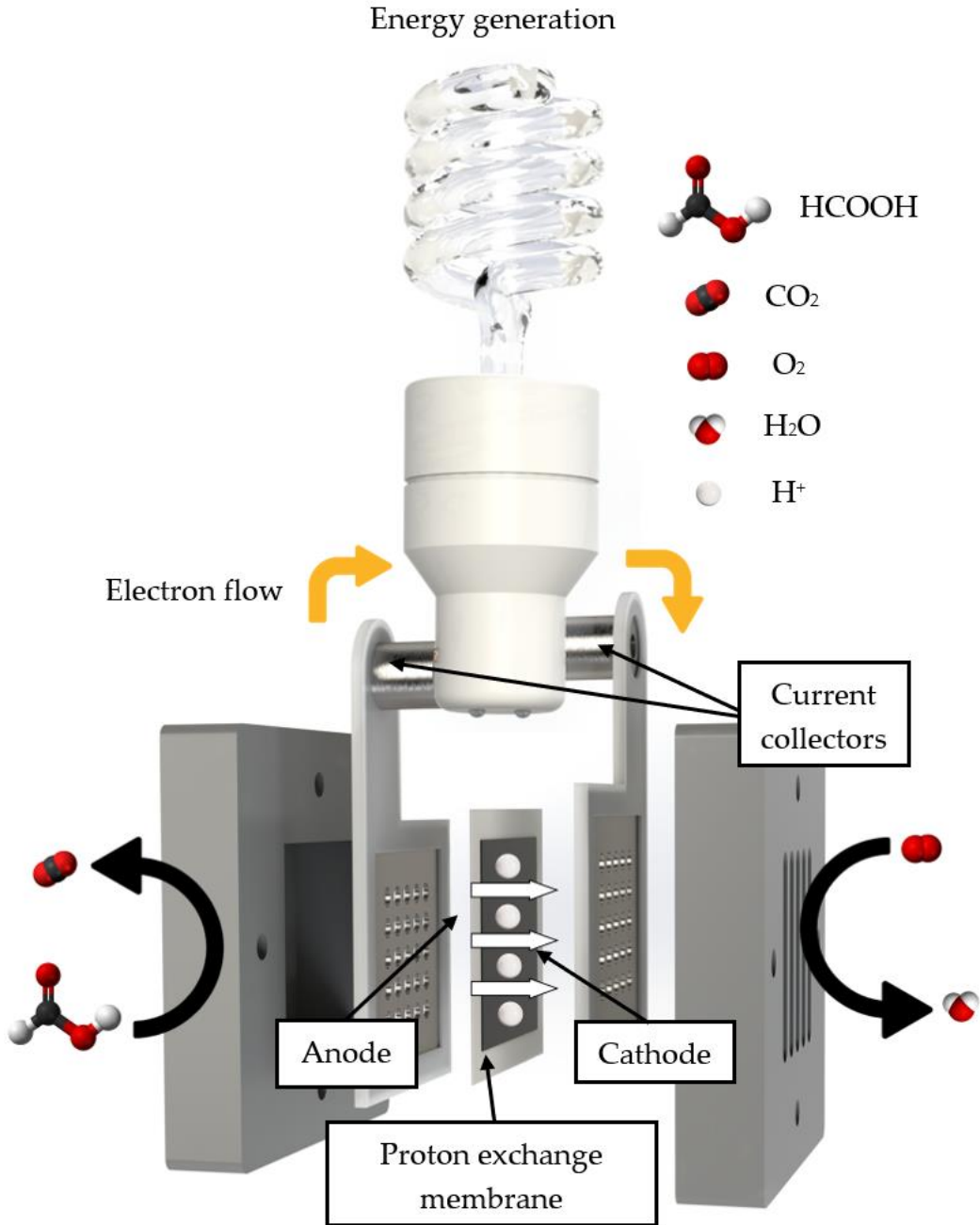


Figure 9: Scheme of formic a formic acid fuel cell (render of an exploded view).

3.5. 3D printing technologies

For several decades, rapid prototyping techniques have been present [28], but required a very expensive equipment and demanded long times. Those techniques were also called laser-induced techniques, consisting of a laser, solidifying a polymer layer by layer to obtain the final product as shown in **Figure 11**. Nowadays, those techniques form part of a big group of techniques called additive manufacturing [29] (**Figure 12**), as its name says the final product is obtained by addition of material, contrary to traditional subtractive techniques which consists on material removal [30]. Those techniques have evolved drastically during the last decade [31], decreasing the price of the instrumentation and also decreasing the time of prototype production.

Nowadays two of these new emerging additive manufacturing techniques called Fused Deposition modelling (FDM) [32] and Stereolithography (SLA) [33], are gaining importance in a lot of fields due to its very interesting advantages. The FDM technique consists of melting a thermoplastic polymer and extruding it through a nozzle, layer by layer to form the final piece, as you can see in **Figure 10**. On the other side, SLA that is a laser-based technique technology, consists of a solidifying a photopolymer tank using a laser, as described before.

Another important factor that allowed 3D printing techniques to emerge in the industry and even for personal uses is the increase of the quality and user-friendliness of the slicing software used to process the 3D models. The slicing software is used to break down the 3D model in layers to make the model printable.

KHCO₃/CO₂ electroreduction for fuel cell applications

Reaction and reactor optimization, prototyping with 3D printing and automatic testing.

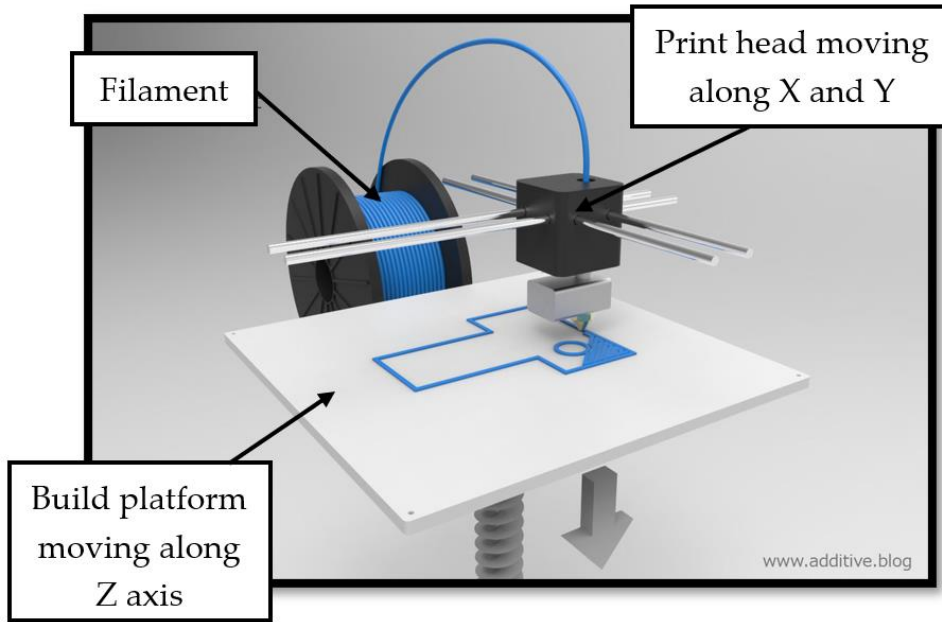


Figure 10: Schematic representation of the FMD 3D printing technology taken from [34].

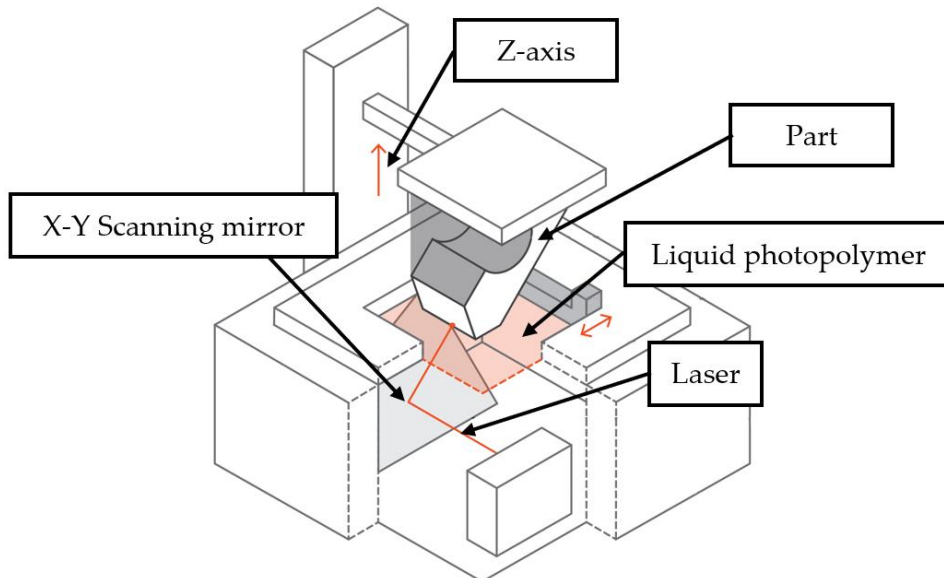


Figure 11: Schematic representation of laser-based SLA 3D printing technology taken from [35].

3. General introduction

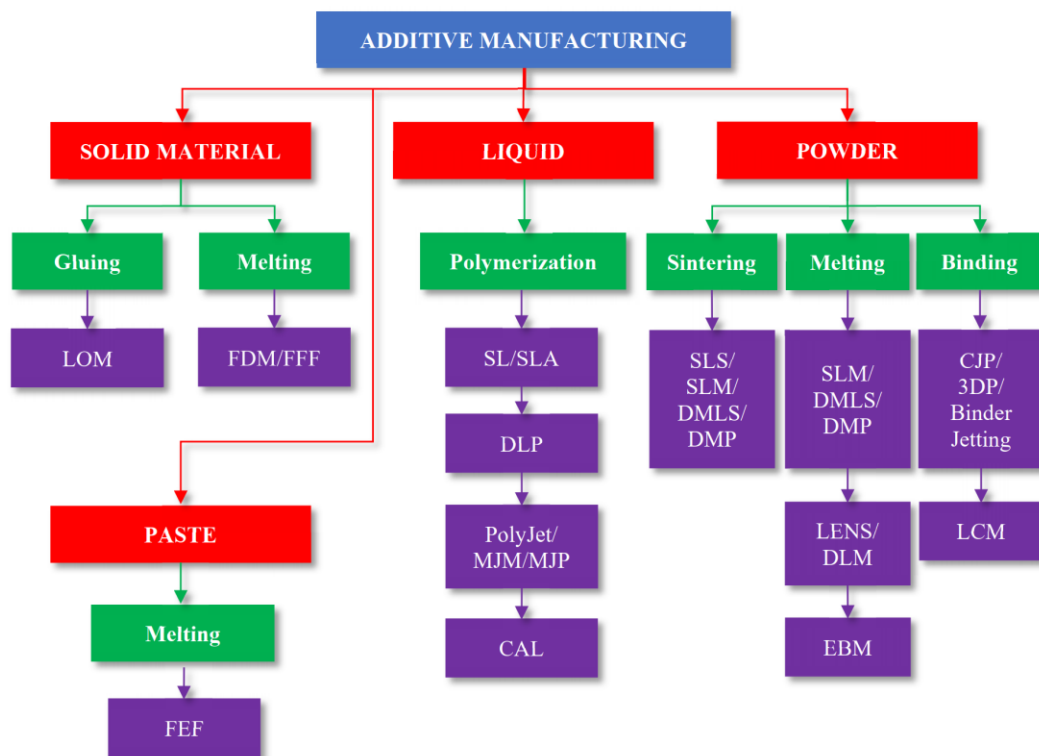


Figure 12: Types of additive manufacturing processes. Taken from [29].

We started to work with SLA printing because these technologies present some advantages in front of conventional subtractive techniques, listed in **Table 1**. That allows us to decrease the size of modules, increasing sensitivity and reducing reactants usage for the experiments due to reduced volumes of the reactors (as you will see in **section 6**), producing more complex modules for better sensors fitting and reducing production and time costs. That allows us to design a lot of different prototypes and chose the most suitable depending on the electrodes and sensing gear that we want to use with them. The only drawback is that in aggressive reaction conditions, the module might decompose. In our case, the reaction

KHCO₃/CO₂ electroreduction for fuel cell applications*Reaction and reactor optimization, prototyping with 3D printing and automatic testing.*

conditions are mild, so that would not affect the experiment. Furthermore, compatibility tests are being run, and more and more resin types are available.

Table 1: Comparison table between additive and subtractive manufacturing

	Additive manufacturing (SLA, FDM)	Subtractive manufacturing (CNC)
Price	Low	High
Manufacturing time	Fast	Slow
Personnel	Low qualified	High qualified
Tolerance	High	Very high
Waste	Low	High
Geometric complexity	High	Low

3.6. Automation and 4th industrial revolution

In 1786, when the steam machine was invented, the first industrial revolution started. From that time a lot of technological advances have appeared in the world, increasing our quality of life, and making ourselves more productive. For example, the steam machine busted the productivity of the textile, agriculture, iron, and mining industry [36]. The second industrial revolution resulted in an extensive installation of railroads and telegraphs as well as electricity, which permitted the faster transportation of ideas and people [37]. The third industrial revolution consisted on the digitalization and the whispered use of computers [38]. Finally, nowadays the fourth industrial revolution or also called the automation revolution is

3. General introduction

starting. This revolution consists of the automatization of simple and repetitive processes thanks to the great advances of robotics and AI. It is true that automation can destroy some of the occupations related to the medium class workers, but it's expected to create even more work positions related of new emerging works that don't even exist now [39]. Machines and computers are expected to substitute us humans in most of the very specific, repetitive and data analysis works, because they are already performing better than us in those fields. In addition, can work non-stop [40]. Until very recently, most of the education systems have trained us to be like machines because they focused us to get specialized, to do repetitive work, memorize data and follow the rules, therefore the old education system has trained us to compete against someone we cannot win, but forgot to train us in the things we are far away better than machines [41]. For example, we are good crossing different subjects, mixing ideas and working interdisciplinary, contrary to machines, which are extremely bad on that. In addition, we are better managing the unpredictable and understanding people emotions. And finally, the golden characteristic of humans which is the critical thinking, that led us to evolve technologically and as a society by generating new ideas and creating new things [42]. Those mentioned characteristics are not very well trained nowadays, because labour world needed people to work like machines, but now instead to see machines stealing our jobs, we should see them as liberators from the repetitive works to let us work on more human skills, or in other words to let us be more human. In **Table 2** there is a summary of all the things mentioned before.

KHCO₃/CO₂ electroreduction for fuel cell applications*Reaction and reactor optimization, prototyping with 3D printing and automatic testing.***Table 2:** Differences between machines humans. Taken from: [COTEC]. (2019, April 19). #MiEmpleoMiFuturo: un documental sobre robots, economía, clase media... y el fin del mundo. [Video]. YouTube. <https://www.youtube.com/watch?v=htAnVeMtrr8>

Work in danger	Computers	Education system	Human brain	Most wanted skills in the future world
Specialized	Specialized	Specialized in one thing	Good cross-ing disciplines	Create new ideas
Repetitive	Repetitive	Repetitive exercises	We are good with the unpredictable	Solve unpredictable problems
Data management	Data related	Learn to memorize	We need emotions	Understand emotions
-	Obey blindly	Obey	Critical thinking	Critical thinking
-	No salary	Compete	We are complementary	Complement each other

3.7. Hardware for automatic control

In the following section the components used for automatizing some of the testing procedures will be described.

3.7.1. Electric motors

One of the most used precision electric motors in industry are the brushless DC motors, due to its high speed and high-power density. However, they require expensive drivers, and they are difficult to control.

The other option was the stepper motors [43]. Those motors are way easier to control, and they are even more precise, together with a more interesting market price. The position of these motors can be controlled in open loop without any kind of feedback while is maintained below the maximum speed and torque.

To control the position of the motors a pulse is send to the motor driver, where each pulse corresponds to one step of the motor. Normally, a stepper motor contains 200 steps per revolution, where each step its around 1.8 degrees.

To increase the resolution of the stepper motors, most of the drivers offer different types of step modes: Fullstep, Halfstep and Microstep.

With the fullstep mode, the motor needs 200 steps to complete a full revolution and the halfstep needs 400 steps. The driver can regulate the current of the coils to divide even more the number of steps. In **Table 3** there is an example of most of the used microstepping modes.

KHCO₃/CO₂ electroreduction for fuel cell applications

Reaction and reactor optimization, prototyping with 3D printing and automatic testing.

Table 3: Angles and step values for the different microstepping modes for standard step-per motor drivers.

Step properties	Full Step	Half Step	Micro-steps			
Divisor	1	1/2	1/4	1/8	1/16	1/32
Step per revolution	200	400	800	1600	3200	6400
Angle per step (°)	1.8	0.9	0.45	0.225	0.112	0.056

The advantages of the stepper motors can be summarized as:

- Easy to control its position
- High retention torque
- High repeatability and precision
- Open loop control
- Good response in start, stop and reversal rotation
- Good behaviour at low speeds

3.7.2. Solenoid valves

Solenoid valves [44] are used to automatically and remotely control the flow of any fluid (gas or liquid), this allow the system to be run more efficiently and safely. Those valves can be found in a lot of applications, from washing machines to space rockets, and work by converting electrical energy to mechanical energy.

The valves can be divided in two parts, the body valve, which is at the bottom, where all the mechanical components are found. That part is constructed with different sizes and different materials depending on the application, flow and working pressure. The other one is the top part, where there is a block with all the electric components (**Figure 13**).

There are two main types of solenoid valves, the Normally Closed (N.C) and the Normally Open (N.O). For the N.C valves, the valve remains closed when no electrical current is applied on the solenoid coil, but when current is applied, the magnetic field generated pushes the core of the valve up, opening the valve. When, the current is shut off, the spring returns the core of the valve to the bottom, closing the valve. The N.O valves function in the opposite way, when no current is applied to the valve the valve remains open.

KHCO₃/CO₂ electroreduction for fuel cell applications
Reaction and reactor optimization, prototyping with 3D printing and automatic testing.

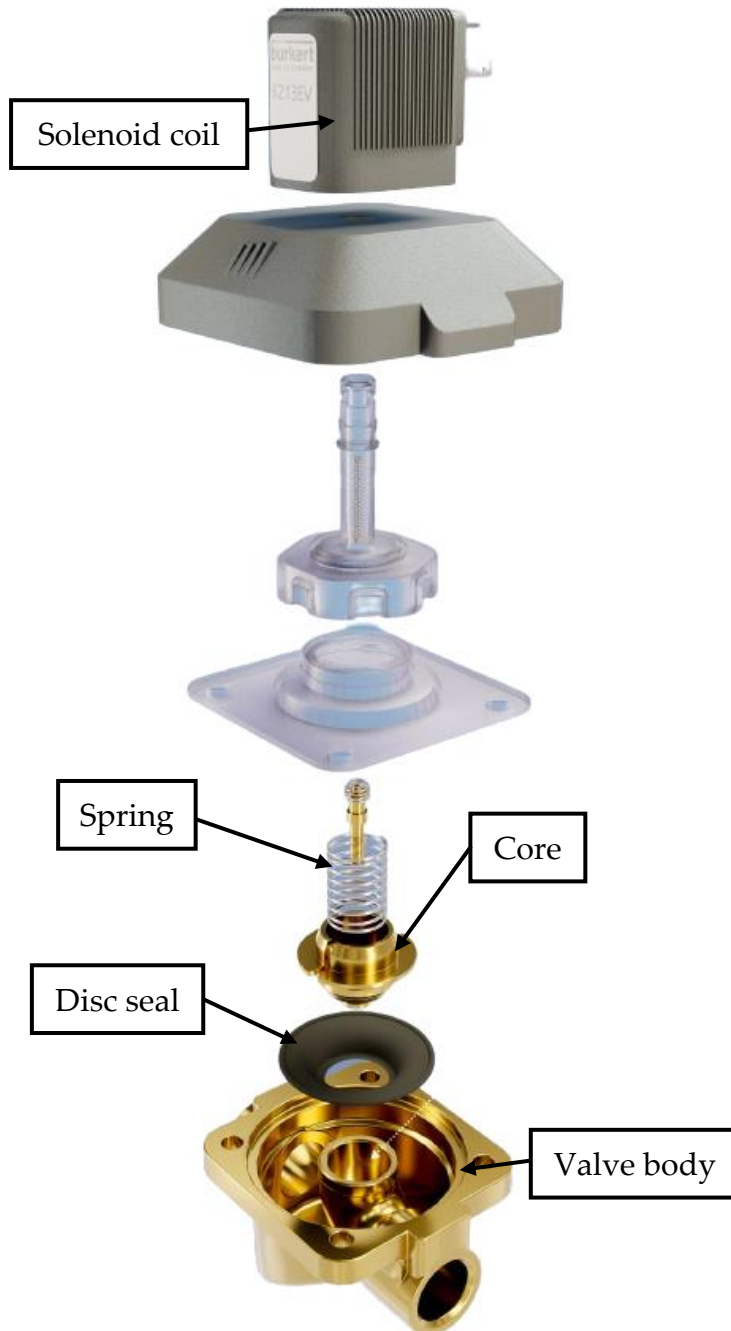


Figure 13: Cross section of a direct acting solenoid valve. Drawing from [45].

3.7.3. Peristaltic pumps

Peristaltic pumps [46] are commonly used for pumping or recirculate liquid. A common peristaltic pump consists of (Figure 14) a spinning rotor driven by an electric motor (usually, either a stepper motor or standard D.C. motors are used, depending on the precision needed). On the rotor multiple rollers (from 2 up to more than 10, depending on the regularity of the flow needed) are attached. That compress a flexible tube while rotating, thereby moving pockets of liquid from intake to outlet.

The advantage of peristaltic pumps is that large amounts of water can be moved, and the main disadvantage is that discrete pockets create an unsteady flow rate, resulting in difficulty to deliver small volumes of liquid, and therefore are not indicated as injection pumps or to deal with pressure.

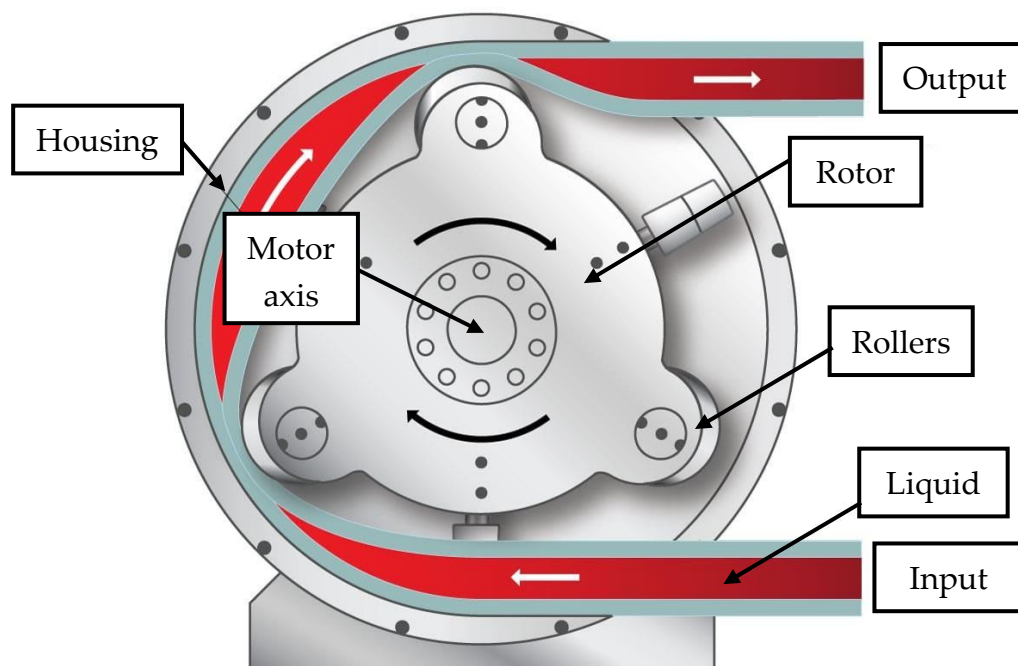


Figure 14: Schematic representation of a peristaltic pump seen from the top. Scheme taken from [47].

KHCO₃/CO₂ electroreduction for fuel cell applications

Reaction and reactor optimization, prototyping with 3D printing and automatic testing.

3.7.4. Mechanical endstops

A mechanical endstop [48] is normally used to detect when the axis of an automatic machine has reached the minimum or maximum bound. They function using a mechanical switch (**Figure 15**) positioned to trigger when a RepRap's axis reaches the limits of motion. Most of these endstops are normally used for 3D printers. The main advantages of these in front of optical endstops is that they are cheaper and easier to use and program.

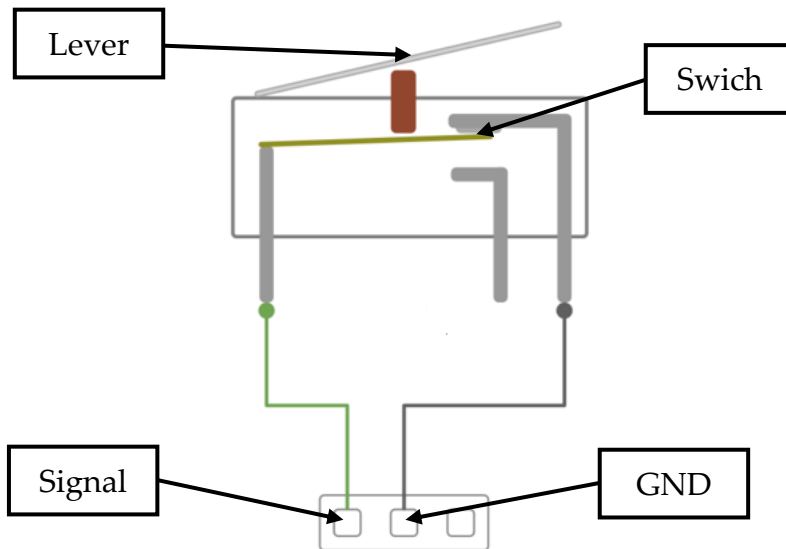


Figure 15: Schematic representation of a standard mechanical endstop.

3.7.5. Microcontroller ESP32

For the automatic control and programming of the components such as stepper motor, solenoid valves and peristaltic pumps, a microcontroller with Wi-Fi and SPI is required. The most used microcontrollers such as Arduino Uno and Arduino Mega offer shields with Wi-Fi and support

3. General introduction

communication with SPI and can be used to control stepper motors. However, the processing speed of all Arduino boards is slow (16 MHz) and can limit motors at very high speeds, therefore the alternative is to use an ESP32 (**Figure 16**), with 10 times higher processing speed (160 MHz), together with the following characteristics:

- Wi-Fi
- Bluetooth
- Higher processing speed (10x higher than Arduino boards)
- Ability to encrypt flash data
- Hardware module to generate hashes with SHA-256
- Hardware module for floating point calculations among several other functionalities



Figure 16: Photo of a microcontroller ESP32.

KHCO₃/CO₂ electroreduction for fuel cell applications



Reaction and reactor optimization, prototyping with 3D printing and automatic testing.

3.7.6. Stepper motor drivers


The stepper motors are controlled by a driver. To do that control we had to choose between 3 three candidates shown on

Table 4. The driver TB6600 is normally used for more powerful motors than the 17HS4401 motors used during this thesis, where they only reach a maximum of 1.5A at maximum acceleration, and this is far away from the maximum 4.5A acceptable for the driver. Therefore, that driver is discarded because of the over dimensioning but also due to its higher price. Between the TMC2130 and the DRV8825, the choice is harder. The TMC2130 is six times more expensive but also gives eight times more step resolution and has more functioning modes. However, the DRV8825 was chosen because extreme resolution is not required for the purposes of this thesis and its price is lower.

Table 4: Candidate stepper motor drivers.

Driver name	Driver photo	Price (€)	Maximum microstepping	Maximum current (A)
DRV8825		1	1/32	2.5
TMC2130		6	1/256	2 (2.5 pic)

3. General introduction

<p>TB6600</p>		<p>10</p>	<p>1/16</p>	<p>4 (4.5 pic)</p>
----------------------	---	-----------	-------------	--------------------

3.8. Electronic circuits and components

This section explains the main electronic components and circuits used in the experimental research.

3.8.1. Protoboard

To create the electrical connections between the microcontrollers, stepper motor drivers, and other electrical components it is necessary to design an electronic circuit.

The first step is to use a protoboard [49] to make the raw connections and the first prototype of the electronic design. A protoboard, or also called “solderless board”, consists of layers of metallic conductive material pads at the inside (**Figure 17**), covered in plastic with holes, as you can see on **Figure 18**. The holes are designed to fit the breadboard cables **Figure 19**.

This configuration allows to make fast modifications of the electronic circuit and tests different electronic designs. Nevertheless, for the final application it is necessary to design a PCB or integrated circuit to reduce size and solder everything with tin to ensure good contact and durability, as will be described in the following section.

KHCO₃/CO₂ electroreduction for fuel cell applications

Reaction and reactor optimization, prototyping with 3D printing and automatic testing.

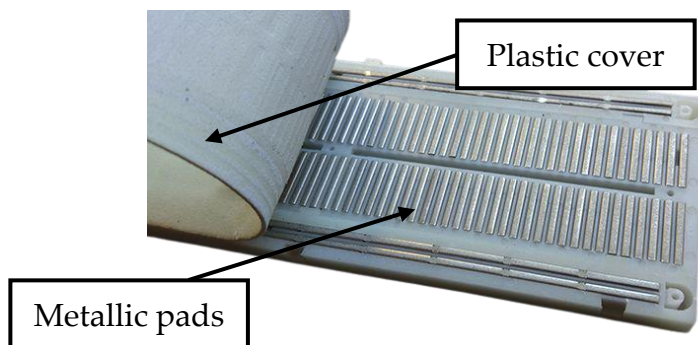


Figure 17: Interior of a standard protoboard.

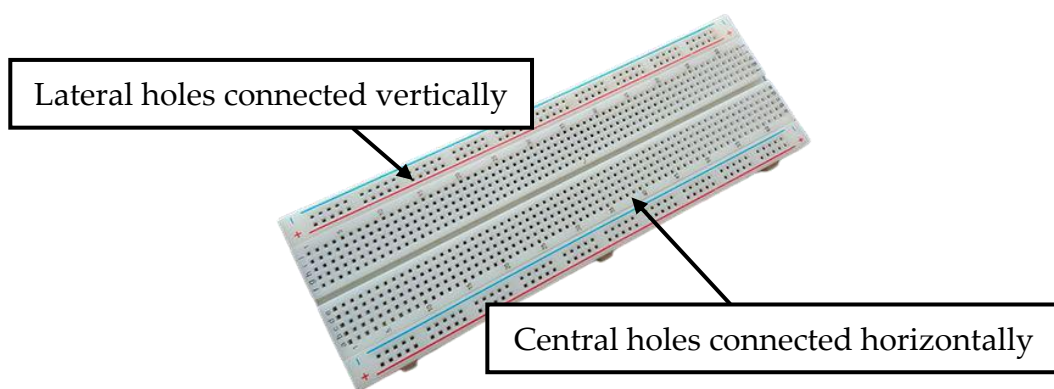


Figure 18: Standard protoboard.

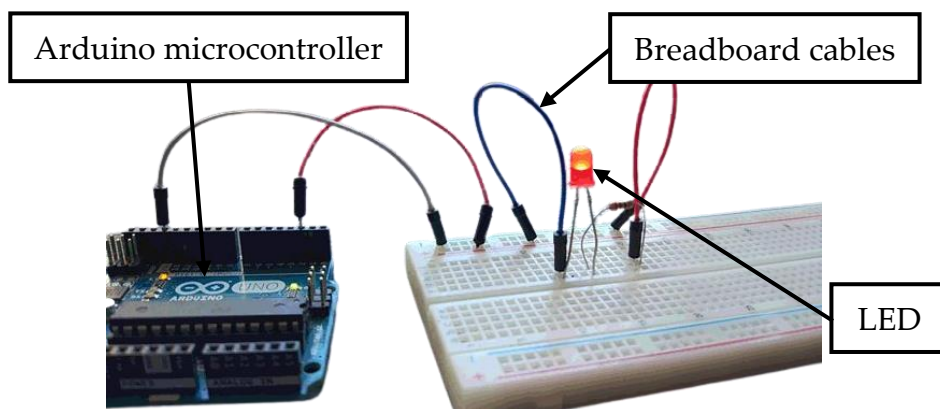


Figure 19: Protoboard used to connect a led with an Arduino microcontroller.

3.8.2. Printed circuit board

A Printed Circuit Board or PCB [50] is used to mechanically and electrically support the connection between electronic components, by using conductive tracks, pads or any other features etched from one or more sheets layers of copper between non-conductive sheets (Figure 20). The electronic components are normally soldered on the copper pads of the PCB. Contrary to the protoboards, the electrical connections here are permanent, therefore more stable, and robust but once made they cannot be modified unless new PCB is manufactured.

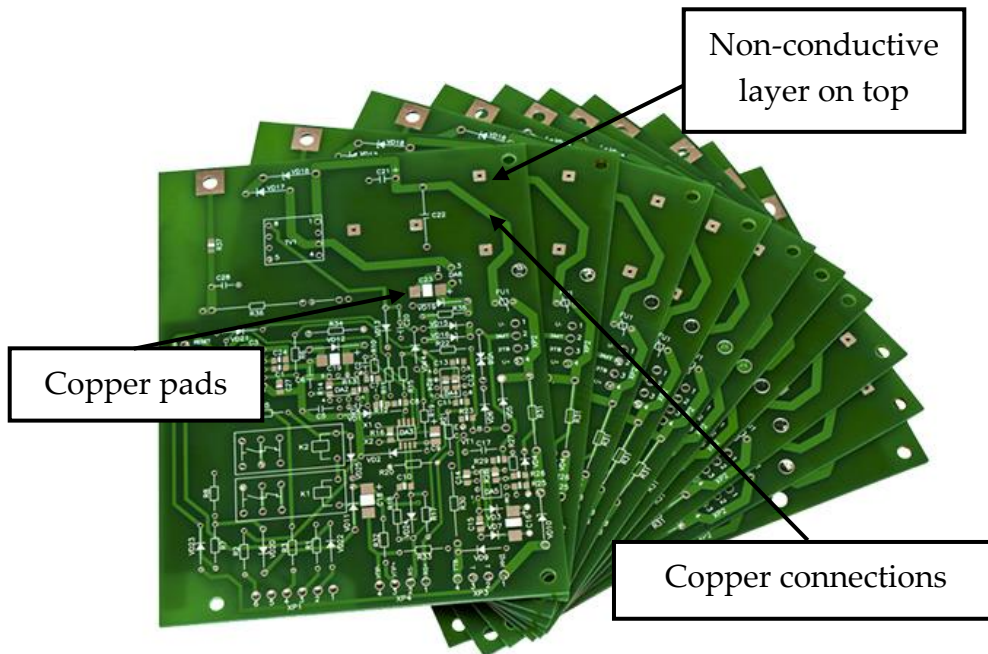


Figure 20: Example of common PCBs.

3. General introduction

3.8.4. Diodes

The diodes [52] are designed to let the electrical current flow in one direction (**Figure 22**), just as non-return valves do with liquids, to avoid rebounds of the current and to protect electrical components.

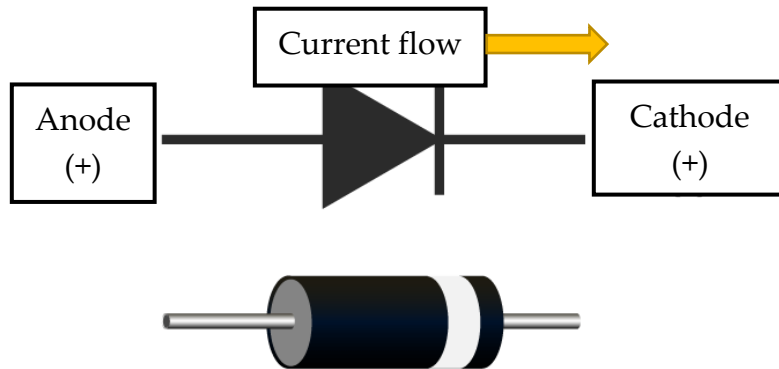


Figure 22: Schematic representation of a diode

3.8.5. DC-DC Controllers

DC-DC converters [53] are widely used to efficiently produce a regulated voltage from a source that may or may not be well controlled to a load that may or may not be constant (**Figure 23**), to protect some devices for to high voltage peaks.

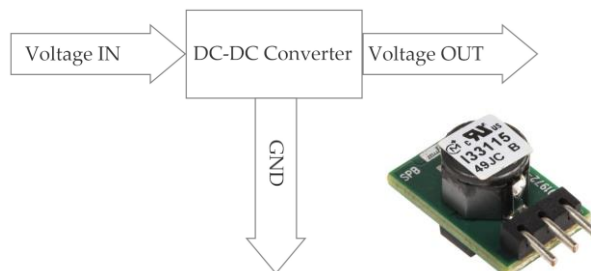


Figure 23: Scheme of a DC-DC controller and photo of a standard one.

KHCO₃/CO₂ electroreduction for fuel cell applications

Reaction and reactor optimization, prototyping with 3D printing and automatic testing.

3.8.6. Capacitors

A Capacitor [54] is an electronic component made of 2 close conductors (usually plates) that are separated by a dielectric material that stores electric charge. The plates accumulate electric charge when connected to a power source. One plate accumulates positive charge while the other accumulates negative charge (**Figure 24**). They can be used to store energy like batteries, but on electronic circuits they are used to make the currents more homogenous and prevent fluctuations. For example, when the electrical current is shoot down for a moment, the capacitors release the stored electric energy to maintain the circuit on.

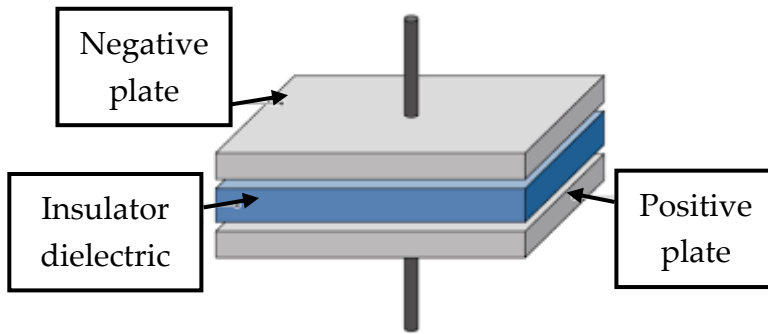


Figure 24: Schematic representation of a capacitor.

3. General introduction

KHCO₃/CO₂ electroreduction for fuel cell applications

Reaction and reactor optimization, prototyping with 3D printing and automatic testing.

4. OBJECTIVES AND HYPOTHESIS

4. Objectives and hypothesis

KHCO₃/CO₂ electroreduction for fuel cell applications

Reaction and reactor optimization, prototyping with 3D printing and automatic testing.

The main hypothesis are:

- Bulk Tin (Sn) acts as a very selective electroreduction catalyst towards formic acid in raw bicarbonate solutions (No CO₂ pre-saturation)
- 3D printing it's an outstanding technique to reduce the price and time of chemical reactors prototyping.
- 3. Most of the repetitive work can be automatized and controlled remotely to increase repeatability, avoid human error, and increase the efficiency of researchers.
- 4. With automation, the testing capacity can be escalated, thus increasing the size of data.
- 5. The produced formic acid quantity and purity is enough to feed Direct formic Acid fuel cells.

The main objectives of the doctoral dissertation are:

➤ **Perform the electroreduction of a bicarbonate solution:**

We will perform electroreduction experiments using a raw bicarbonate solution to convert it using bulk Tin (Sn) as working electrode and Platinum wire as counter electrode to obtain the desired products.

➤ **Determine the efficiency of the reaction:**

The effect of the following parameters on the reaction efficiency will be determined: electroreduction potential, bicarbonate concentration, stirring speed, catalyst used and CO₂ pre-saturation.

➤ **Optimize and manufacture the reactor for the electroreduction experiments using 3D printing techniques:**

To overcome some of the limitations of conventional CNC manufacturing techniques, we will fabricate a reactor with 3D printing to reduce its size, manufacturing time and costs.

➤ **Design an assembly automatic testing system:**

Increase the repeatability and diminish the human error in the experiment, while augmenting testing capacity.

KHCO₃/CO₂ electroreduction for fuel cell applications

Reaction and reactor optimization, prototyping with 3D printing and automatic testing.

➤ **Design a remote control of the experiments:**

We will implement remote control to initiate, monitor, and control the experiment Remotely. With that we increase the time in which we can perform and the experiment while reducing the dangerousness of being in a chemical lab.

➤ **Use the formic acid/formate to power a fuel cell**

We will use the formic acid/formate obtained by CO₂ electroreduction for powering a fuel cell.

4. Objectives and hypothesis

KHCO₃/CO₂ electroreduction for fuel cell applications

Reaction and reactor optimization, prototyping with 3D printing and automatic testing.

5. DIRECT ELECTROCHEMICAL REDUCTION OF BICARBONATE

***Based on:** Andreu Bonet Navarro, Adrianna Nogalska, Ricard Garcia-Valls, *Direct Electrochemical Reduction of Bicarbonate to Formate Using Tin Catalyst*, *Electrochem 2* (2020) 64-70.

5. Direct electrochemical reduction of bicarbonate

In this section, a method for bicarbonate/CO₂ electroreduction using bulk tin (Sn) as catalysts will be described, where Tin shows great selectivity towards formic acid formation and the efficiency of the reaction increases with the pre-saturation of the solution with pure CO₂ gas.

KHCO₃/CO₂ electroreduction for fuel cell applications*Reaction and reactor optimization, prototyping with 3D printing and automatic testing.***5.1. Introduction**

Since the start of the industrial revolution, the atmospheric CO₂ levels increased drastically and exceeded the 400 ppm in 2016 [55]. -For this reason, some studies indicate that just cutting off or reducing the CO₂ emissions will not be enough to avoid or mitigate the effects of climate change, and CO₂ removal from the atmosphere is going to be necessary [56]. One way to absorb atmospheric CO₂ is by transforming it into bicarbonate using hydroxide solutions, like the system developed by A. Nogalska and R. Garcia [57]. Bicarbonate is a product with low value and not many applications, but its conversion to more useful and valuable hydrocarbons is becoming an economically viable way to reuse it [58].

Many different direct CO₂ electroreduction techniques use bicarbonate solutions previously saturated with pure CO₂ gas to obtain hydrocarbons or alcohols showing significant selectivity. The main inconvenient of these techniques are its practical applications because it's almost impossible to saturate a bicarbonate solution with atmospheric air, due its low content in CO₂. There are just a few studies performing it on non-CO₂ saturated bicarbonate solutions [59]–[65]. Theoretically, direct CO₂ electroreduction is performed by CO₂ activation on a catalyst surface and its following reaction with two protons (2H⁺). Generally, the bicarbonate acts as an electrolyte, favouring the CO₂ dissolution and increasing the conductivity of the aqueous solution, but, since dissolved bicarbonate is always in equilibrium with dissolved CO₂, it is still not clear if the carbon source is bicarbonate or CO₂ [66]–[70].

The electrochemical reduction of CO₂ into formate performed with water as a proton source is a very attractive technology, due to the great energy density of formate that can be used to power formate fuel cells [16],

5. Direct electrochemical reduction of bicarbonate

[71], [72], as a future alternative to lithium batteries [73], [74]. In addition, this liquid fuel may be easily stored and transported using existing infrastructures. This way, renewable energy, which is intermittent, unpredictable, and with irregular production peaks, could be stored as formate and released during low production periods without any additional emissions of CO₂ into the atmosphere. Our goal is to study the viability of reducing a non-CO₂ saturated bicarbonate solution into formate using a bulk tin catalyst, which is a relatively cheap material, simple to use and with great selectivity towards formate in mild conditions [75]–[79]. For this purpose, electrochemical studies were performed with the use of potassium bicarbonate. Moreover, the influence of CO₂ saturation on faradic efficiency of conversion was evaluated.

5.2. Experimental

5.2.1. Materials and reagents

Tin foil (99.8% trace metals basis), 0.25 mm thick, provided by Alfa Aesar (Haverhill, MA, USA), was used as a working electrode and highly pure KHCO₃ (Bio Ultra 99.5%), supplied by Sigma-Aldrich (St. Louis, MO, USA), with a content of iron lower than 5 mg/Kg was used for preparation of the electrolyte. Milli-Q water was used to prepare solutions. Proton exchange membrane was Nafion 117 membrane (Sigma-Aldrich). Hydrogen peroxide 30% (v/v) (Sigma-Aldrich) and 95–97% H₂SO₄ (Serviquimia) were used to prepare cleaning solutions for Nafion membrane. To prepare a standard for ¹H NMR analysis, 99.8% D₂O from Panreac and 99.7% DMSO (Chromasolv Plus) from Sigma Aldrich were used. CO₂ gas used for the electrolyte saturation was pure liquid carbon dioxide (CO₂ Premier X10) purchased from Carbueros Metálicos.

KHCO₃/CO₂ electroreduction for fuel cell applications

Reaction and reactor optimization, prototyping with 3D printing and automatic testing.

5.2.2. Linear Sweep Voltammetry

Linear sweep voltammetry (LSV) was performed prior to electroreduction experiments to evaluate which is the lowest potential that is high enough to allow significant product formation, without experimenting excessive H₂ gas formation. To study the effects of KHCO₃ concentration, three solutions with different concentrations (0.1, 0.5, and 1.5 M) were prepared. Finally, the 1.5 M KHCO₃ solution was submitted to saturation with CO₂ gas during 30 min at a flow rate of 14.47 sccm to test its effects. Constant stirring was applied to ensure homogeneous solution, improve bicarbonate migration to the electrode, and facilitate the release of residual gas bubbles formed during reaction.

All experiments were carried out in a gas-tight Teflon H-cell (**Figure 25, Figure 26 and Figure 27**) equipped with the standard three-electrode system. The cell consists of two compartments (Anodic and Cathodic of 25 mL each) filled with bicarbonate solution and separated by a proton exchange membrane (Nafion membrane) to prevent reoxidation of reduced products on the cathode. The anodic compartment contains the counter electrode (platinum foil (Pt) foil of 1 cm²), where water splitting takes place. In the cathodic compartment there is the working electrode (Tin (Sn) foil of 5 cm²) where the CO₂ is reduced and the reference electrode (Ag/AgCl/3M KCl (0.21 V)), is used to maintain a stable potential reading. For the saturation of solution with CO₂ outlets and inlet for gas were used.

The membrane was washed by immersion in an 80°C aqueous solution, for 1 h each, in the following order: 0.5M H₂SO₄, H₂O₂ 3% and distilled water to eliminate possible contamination (**Figure 28**). The working electrode was not pre-treated before experiments, as the native SnO₂ layer is reported to increase the catalytic activity [80]. The whole system

5. Direct electrochemical reduction of bicarbonate

was leaned with distilled water between each experiment. An AutoLab PGSTAT 302N potentiostat (Metrohm, Autolab B.V.) was used in all the electrochemical experiments. All the LSV were conducted at a scan rate of 100 mV/s in a range of potentials between 0 and -2.0 V in the presence of the reference electrode.

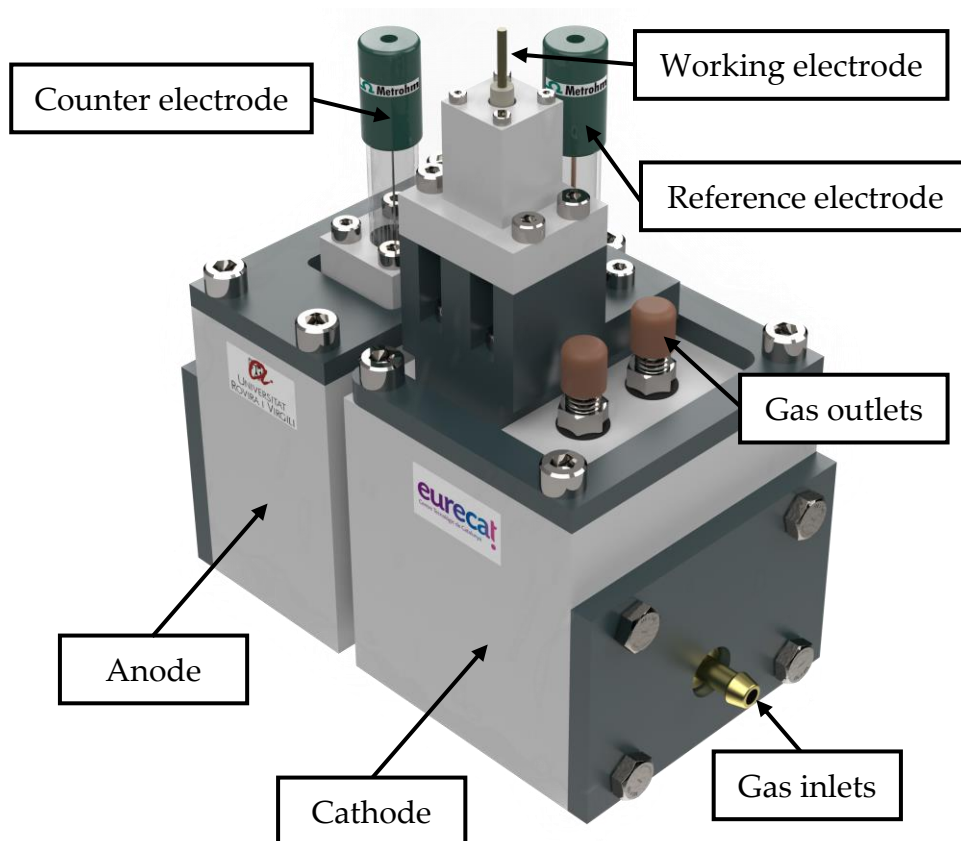


Figure 25: 3D rendered design of Teflon H-cell used for the experiments.

KHCO₃/CO₂ electroreduction for fuel cell applications

Reaction and reactor optimization, prototyping with 3D printing and automatic testing.

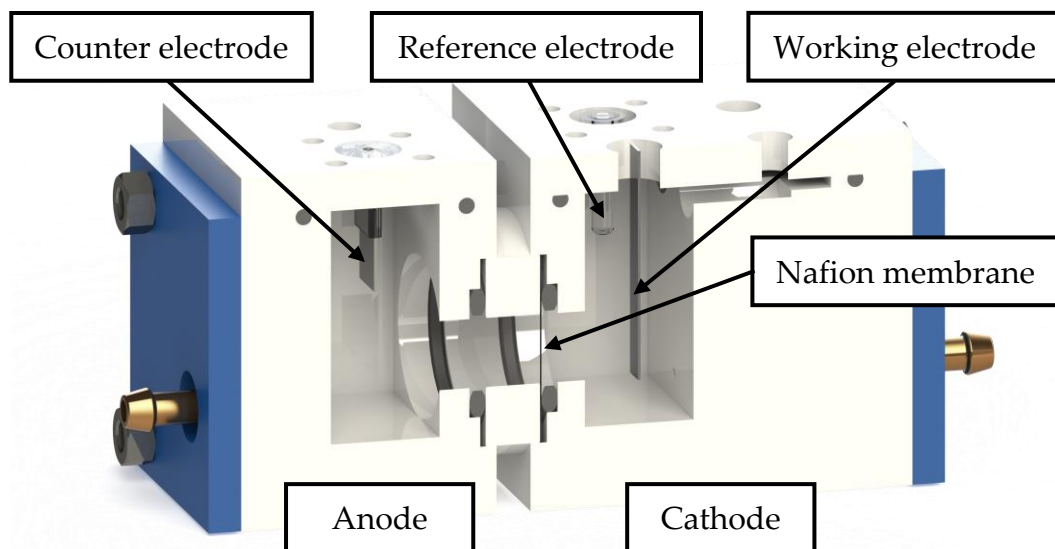


Figure 26: Cross section of Teflon H-cell used for the experiments.

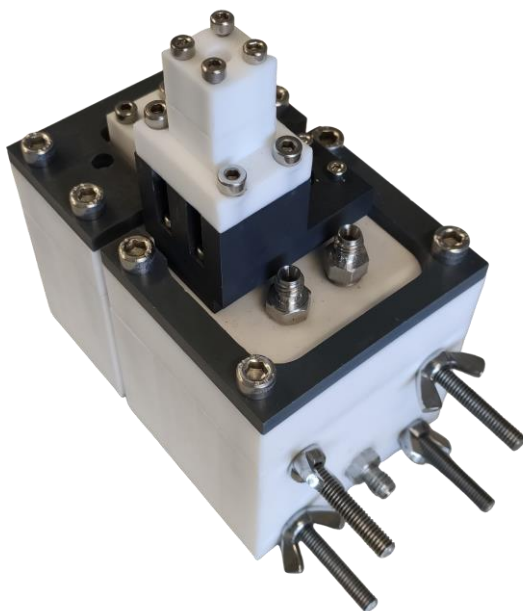


Figure 27: Photo of the module used for the electroreduction experiments.

5. Direct electrochemical reduction of bicarbonate

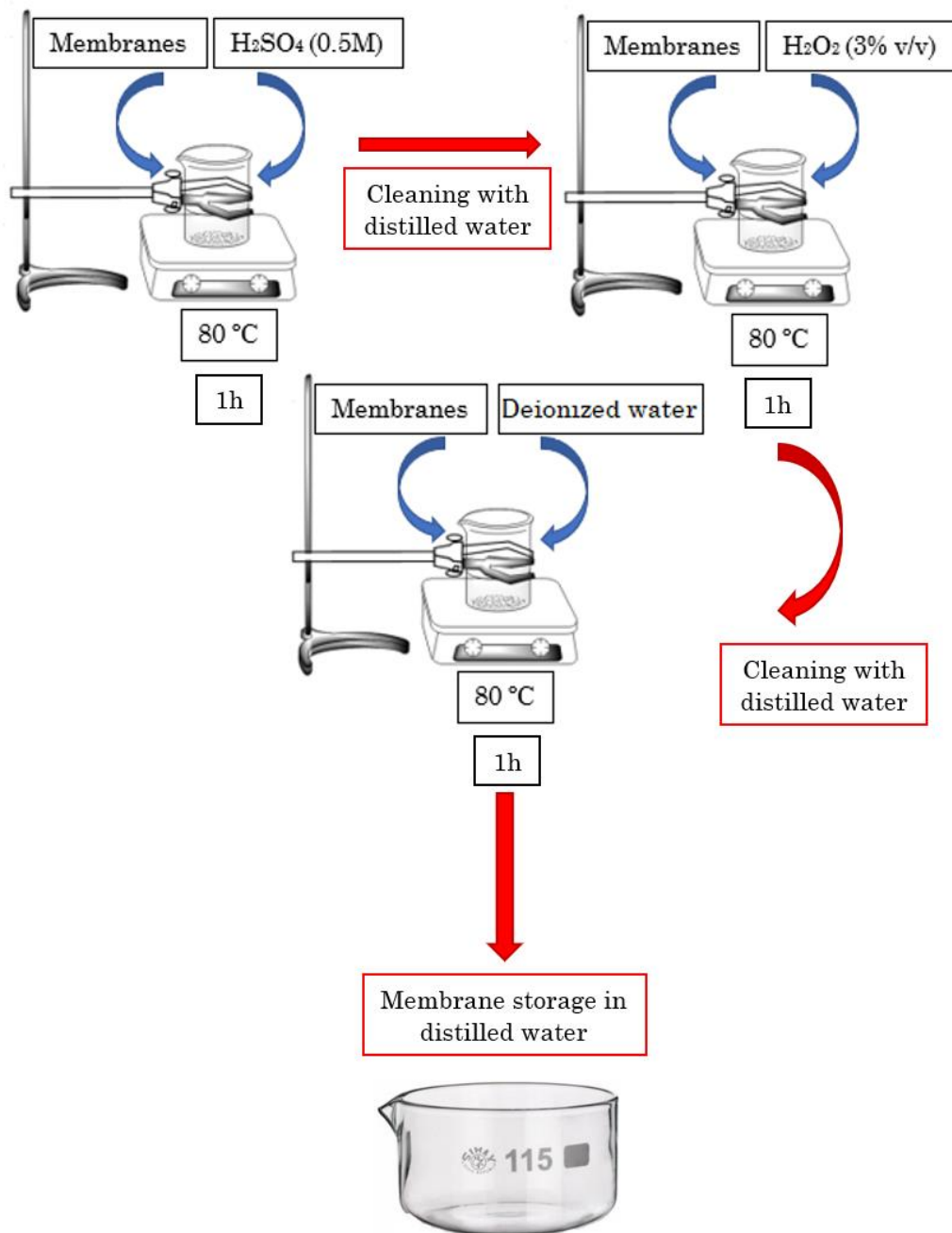
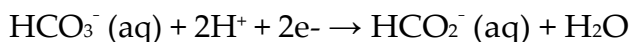


Figure 28: Nafion membrane cleaning procedure.

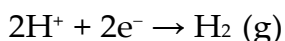
KHCO₃/CO₂ electroreduction for fuel cell applications*Reaction and reactor optimization, prototyping with 3D printing and automatic testing.***5.2.3. Electroreduction experiments**

The electroreduction experiments were carried out in potentiostatic conditions for 1.5h in the same Teflon H-cell used for LSV analysis. In addition, constant stirring, CO₂ pre-saturation, and membrane-system cleaning were performed as described in the previous section and for the same purposes.

The electroreduction potential was chosen based on the LSV analysis and set to -1.6 V. Beyond that, a significant increase of reduction current and gas bubble formation associated with CO (**Eq. 8**) and H₂ (**Eq. 9**) formation can be observed [81]. Some of those bubbles stayed in the working electrode surface, diminishing its active area, and reducing the efficiency of the reaction. The materials and the samples used are the same described in the voltammetry section. The most probable electroreduction reaction is from bicarbonate to formate (**Eq. 7**), but some studies suggest that bicarbonate acts just as a CO₂ source [70]:

(Eq. 7)

The most likely side reactions of CO and H₂ formation are:

(Eq. 8)*(Eq. 9)*

5.2.4. Product Analysis

The analysis of the reaction's products was performed by ¹H NMR (VARIAN Mercury VX400). As reference, an internal standard consisting of 1 droplet of DMSO (weight with analytical balance) mixed with 1ml of D₂O was used. Catholyte samples of 600 μL were mixed with 100 μL of standard (**Figure 29**). To obtain the peaks coming from products, we suppressed the water peak by irradiation.

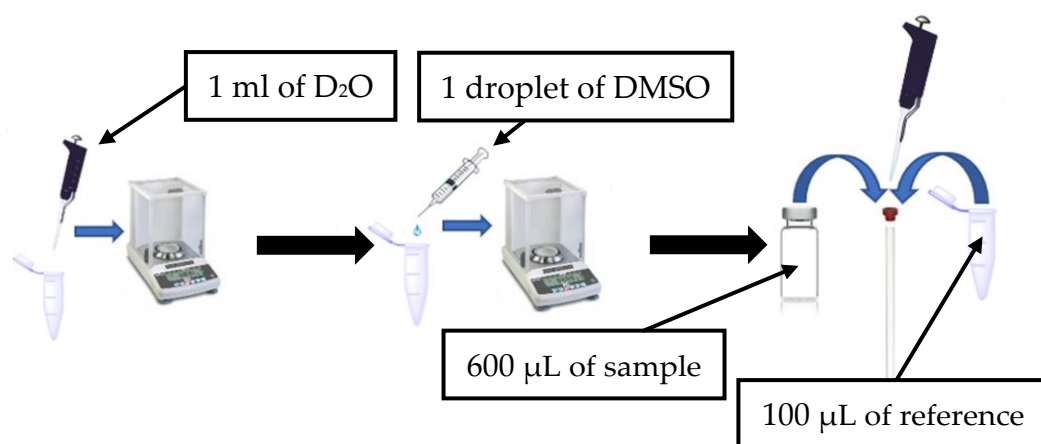


Figure 29: Scheme of sample preparation before for NMR analysis.

Based on the determination of formate concentration through the NMR analysis using the nmrglue ("<https://www.nmrglue.com/>") Python library, Faradic efficiency FE (%) was calculated considering passed charge and electrons transferred with the following

(Eq. 10)

$$\text{FE (\%)} = q_{\text{exp}}/q_{\text{theo}} \times 100$$

Experimentally used charge [C] q_{exp} (Eq. 11) is calculated by:

KHCO₃/CO₂ electroreduction for fuel cell applications*Reaction and reactor optimization, prototyping with 3D printing and automatic testing.***(Eq. 11)**

$$q_{\text{exp}} = Fnz$$

F stays for Faraday constant $9.6485 \cdot 10^4$ [C/mol], n is the amount of formate moles obtained by proton NMR, and z are electrons needed for bicarbonate conversion to formate based on chemical reaction ($2e^-$). In addition, theoretical charge q_{theo} (**Eq. 12**) [C] passed charge is obtained chronocamperograms by:

(Eq. 12)

$$Q_{\text{exp}} = -It$$

where I is the total current [A] and t is the reaction time [s]

5.3. Results and discussion**5.3.1. Linear Sweep Voltammetry**

The LSV measurements show a small peak between -0.9 V to -1.0 V corresponding to reduction of the small SnO₂ layer usually present on bulk Sn [74] (**Figure 30**).

At potentials below -1.2 V, current density increases exponentially in all cases, probably associated with bicarbonate and hydrogen electroreduction. In addition, as current density increases, CO₂ bubbling on the working electrode (Sn foil) is observed, probably associated with H₂ or CO and other residual gasses [82]. Furthermore, oxygen bubbles are observed on the platinum counter electrode. Current density is higher when CO₂ pre-saturation is used (**Figure 30**), and similar tendency is observed when bicarbonate concentration increases (**Figure 31**).

5. Direct electrochemical reduction of bicarbonate

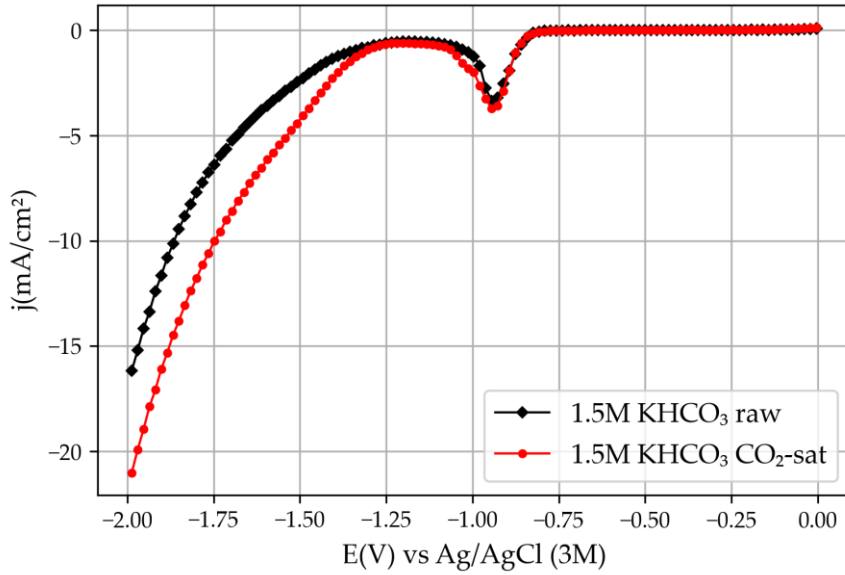


Figure 30: LSV of non-CO₂ saturated solutions compared with pre-saturated ones.

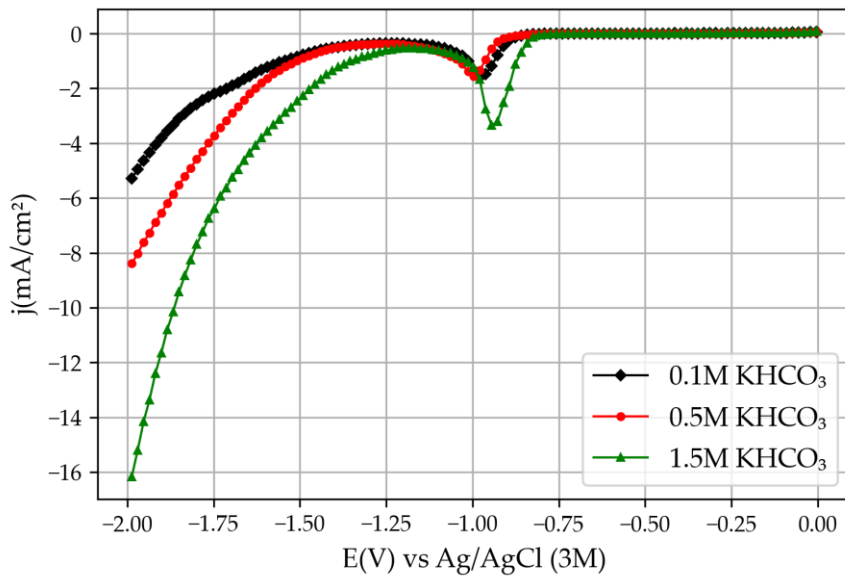


Figure 31: LSV at different potassium bicarbonate solutions (KHCO₃) concentrations.

KHCO₃/CO₂ electroreduction for fuel cell applications

Reaction and reactor optimization, prototyping with 3D printing and automatic testing.

5.3.2. Chronoamperometry

The working potential for electroreduction experiments was set at -1.6V to obtain the greatest current density without observing excessive formation of non-desired residual gasses. The current density should increase while augmenting KHCO₃ concentration, due to the improved conductivity of the solution and increased reaction rates. As expected, the results confirm a current density sixtimes higher for 1.5 M KHCO₃ solution respectively compared with 0.1 M KHCO₃ solution at -1.6 V (

Figure 32).

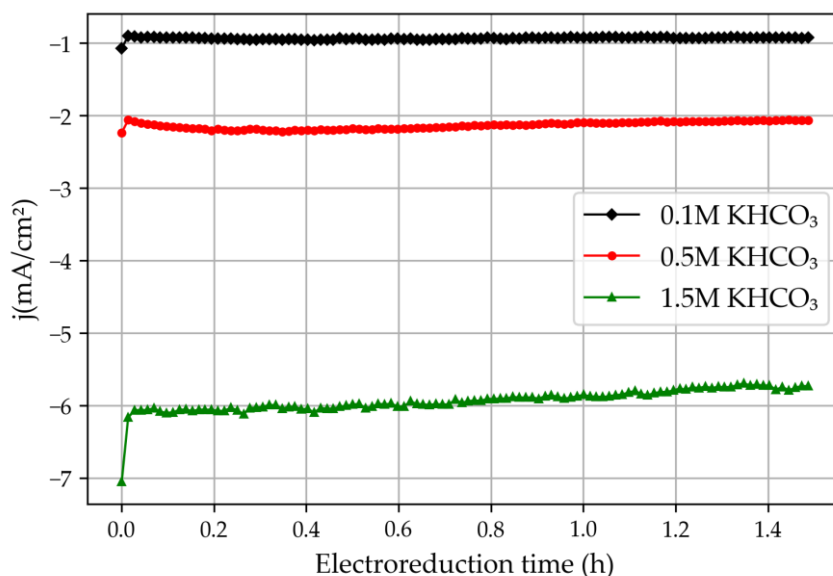


Figure 32: Chronoamperogram at -1.6V of bicarbonate solutions.

For the CO₂ saturated experiments, the same trend is observed with a 33% increase on the current density at -1.6 V for the saturated solution

5. Direct electrochemical reduction of bicarbonate

(Figure 33). The electroreduction current is stable during this interval of time for all experiments, slightly decreasing over time for experiments performed at 1.5 M KHCO₃. This could be due to a faster exhaustion of reactants, membrane poisoning, catalyst degradation or even a reduction of solution volume. A small amount of noise, most commonly present in experiments at higher currents, is due to gas bubbles formation, which attach and detach from the catalyst surface, affecting the active area.

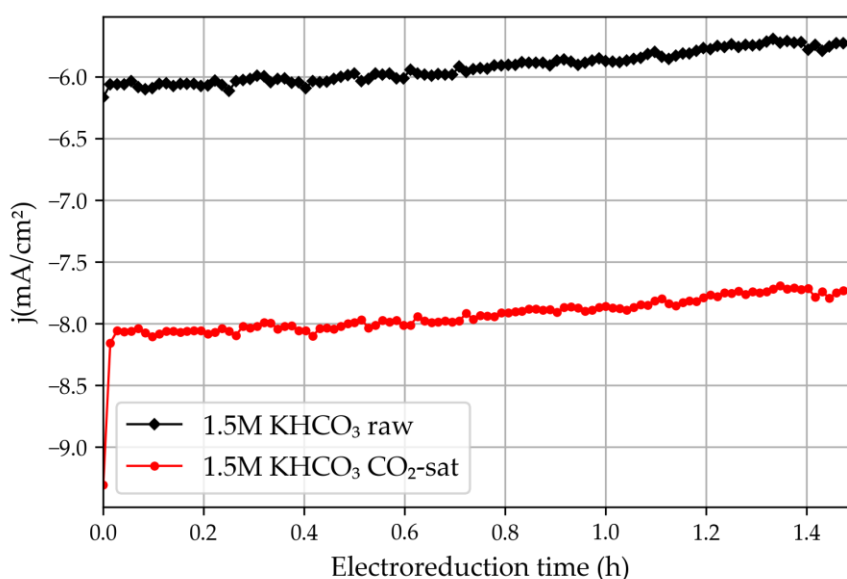


Figure 33: Chronoamperograms at -1.6V KHCO₃ solution compared non-CO₂ saturated solutions.

5.3.3. Analysis and quantification of products by ¹H NMR

The ¹H NMR spectra shows three singlets at around 8.44, 4.83 and 2.71 ppm, corresponding to HCOOK, DMSO, and H₂O respectively

KHCO₃/CO₂ electroreduction for fuel cell applications*Reaction and reactor optimization, prototyping with 3D printing and automatic testing.*

(Figure 34). The slightly basic media (~pH 9) of the potassium bicarbonate solution, including the non-observation of an O-H bond of formic acid around 11 ppm, confirms that potassium formate (HCOOK) is the main product, and the acid form is not present in reaction conditions. The observation of only one product in the liquid phase indicates a high selectivity of tin foil towards formate production.

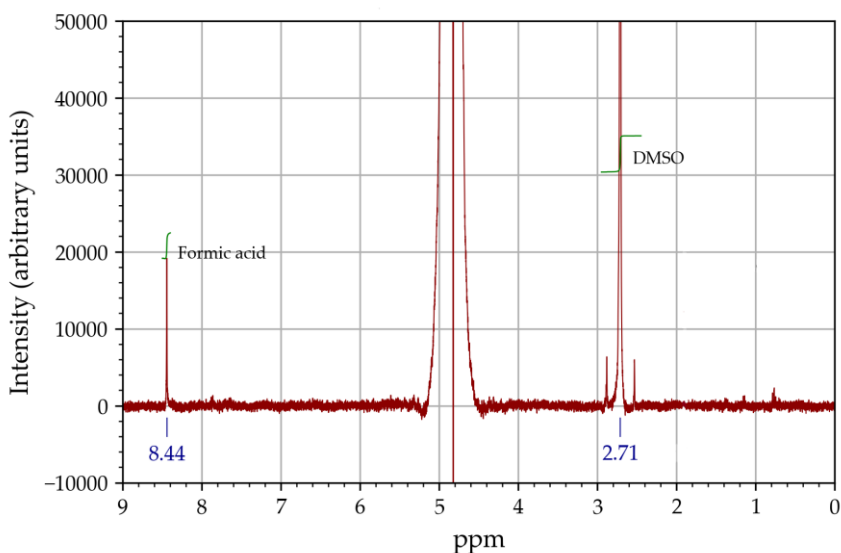


Figure 34: ¹H NMR spectra of the products in cathodic compartment.

The faradaic efficiency towards formate shows a significant increase from 0% to 18% in 0.1 M and 1.5 M solutions as summarized in **Table 5**. With the saturation of CO₂, the efficiency increases from 18% to 47%, noting the importance of pre-saturating the solution with pure CO₂.

5. Direct electrochemical reduction of bicarbonate

Table 5: Summary of the effects of the potassium bicarbonate (KHCO₃) concentration and the CO₂ pre-saturation on the faradaic efficiency of the electroreduction to formate.

KHCO₃ (aq) Concentration (M)	0.1 M	0.5 M	1.5 M	1.5 M
CO₂ pre-saturation	No	No	No	Yes
Faradaic efficiency (%)	not detected	8	18	47

As we can see in **Table 6**, bulk Sn seems to have the highest efficiency towards HCOOK/HCOOH compared with other similar bulk catalysts working in similar conditions.

Table 6: Summary of CO₂ electroreduction efficiencies towards HCOOH/HCOOK of similar bulk catalysts.

Catalyst (Working electrode)	Reference electrode	Electrolyte (Reactant)	CO₂ sat- uration	Faradaic effi- ciency	Ref.
Ag (99.98%) electrode	Ag/AgCl saturated with KCl	0.1M KHCO ₃ aqueous solution	No	not de- tected.	[83]
Au (99.95%) electrode			No	6	
Pd Metal			No	4.4	[84]
Cu-Based catalysts	Ag/Ag+ with 0.01 M	0.5M KHCO ₃ aqueous solution	Yes	3-15	[85]
Tin (99.98%) electrode	-1.6V vs Ag/AgCl saturated with KCl	1.5M KHCO ₃ aqueous solution	No	18	[15]
			Yes	47	

KHCO₃/CO₂ electroreduction for fuel cell applications*Reaction and reactor optimization, prototyping with 3D printing and automatic testing.***5.4. Conclusions**

During this study we confirmed the possibility to reduce bicarbonate solutions to formate without using pure CO₂, with significant amounts for non-CO₂ saturated solutions (18%) and almost 50% for saturated ones.

Bicarbonate can be easily obtained from atmospheric air by CO₂ capture, and there is an unlimited stock of it. In addition, CO₂ pollutes the atmosphere and increases the greenhouse effect, with serious consequences for our planet and society, so pulling it out of the atmosphere will contribute to mitigate its negative consequences. The direct conversion of atmospheric CO₂ stored as bicarbonate can make this technology more competitive in the market, and to have an alternative for formic acid/formate production which is currently obtained by a non-renewable and very contaminating process. Another great attribute of formic acid is fuel cells is that they have a theoretical higher energy density than lithium batteries and are safer than hydrogen fuel cells. Then, the possibility to have more competitive fuel cells with much higher energy density than current lithium batteries can also increase the competitiveness of renewable energies allowing the possibility to store more energy during its normally irregular energy production peaks.

To conclude, we can affirm that increasing the electroreduction efficiency and selectivity of bicarbonate to formate will become a great advance in energy storage systems, thus making renewable energies even more competitive. Investing in this technology is a great way to fight climate change and take economical profit at the same time.

5. Direct electrochemical reduction of bicarbonate

KHCO₃/CO₂ electroreduction for fuel cell applications

Reaction and reactor optimization, prototyping with 3D printing and automatic testing.

6. DESIGN AND FABRICATION OF RE- ACTOR WITH 3D PRINTING

6. Design of reactor with 3D printing

In this section will be described how a 3D printed reactor was designed and printed with SLA technique, evaluating advantages and disadvantages of this technique against conventional ones.

KHCO₃/CO₂ electroreduction for fuel cell applications

Reaction and reactor optimization, prototyping with 3D printing and automatic testing.

6.1. Module design with SolidWorks

The first module used for electroreduction was a workshop-made reactor manufactured with CNC machines, as described in **section 5.2.2**. The reactor was relatively big (30 ml in each compartment), and we wanted to decrease the volume to increase the concentration of produced products during the electroreduction experiments. Furthermore, the reactor was very heavy, and consisted of a lot of pieces and bolts, therefore it was hard to assembly and disassembly, hindering the cleaning between experiments, together with high manufacturing time and costs, making it hard to improve it or modify for new applications. To overcome this challenges, we designed a new module using SolidWorks (CAD software) considering that this time, the manufacturing technique will be SLA 3D printing, to have the following characteristics while maintaining the volume and the complexity (number of parts) of the reactor as low as possible **Figure 35** and **Figure 36**:

- The module should consist of two separated and symmetric compartments, the cathodic and the anodic, with the membrane assembled in between.
- The module should have one hole to assembly the counter electrode on the anodic compartment, and another one in the cathodic compartment for the working electrode.
- Each compartment should have two additional holes for a mini reference electrode and pH meter electrode from NTSensors specially bought for this.
- Each compartment should have two input entrances, one for automatic injection cleaning water and reagents using a pump.
- Each compartment should have one output hole for the evacuation of reagents and residual cleaning water.

6. Design of reactor with 3D printing

- The compartments also should have two holes for fitting thermometers, one in each compartment.
- The compartment should have 2 input holes for injecting pure CO₂ gas.
- The compartments should have enough space to fit a magnet for stirring.

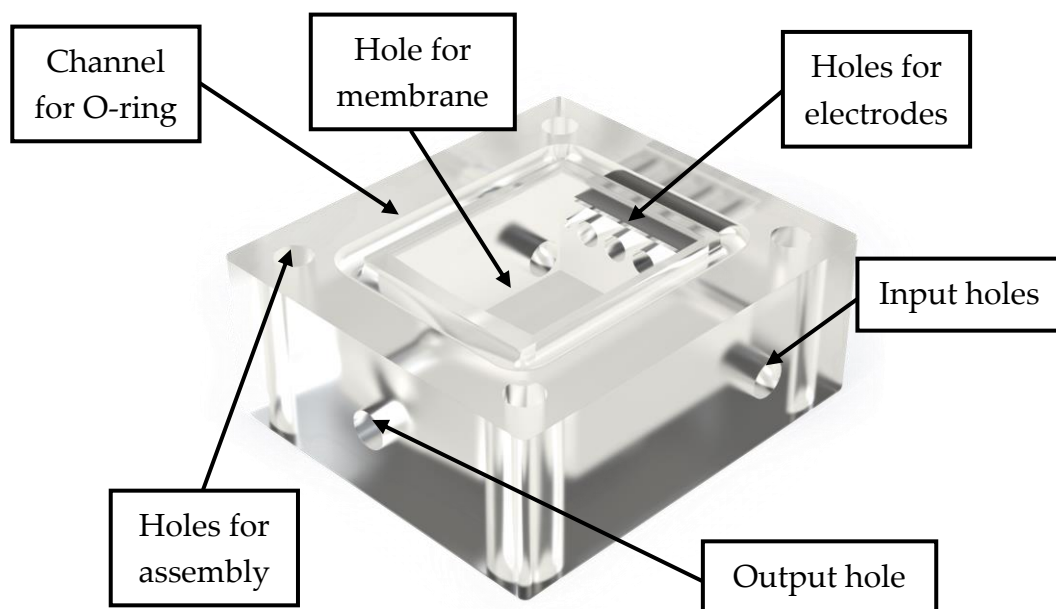


Figure 35: Rendered design of one compartment of the first prototype of reactor.

KHCO₃/CO₂ electroreduction for fuel cell applications

Reaction and reactor optimization, prototyping with 3D printing and automatic testing.

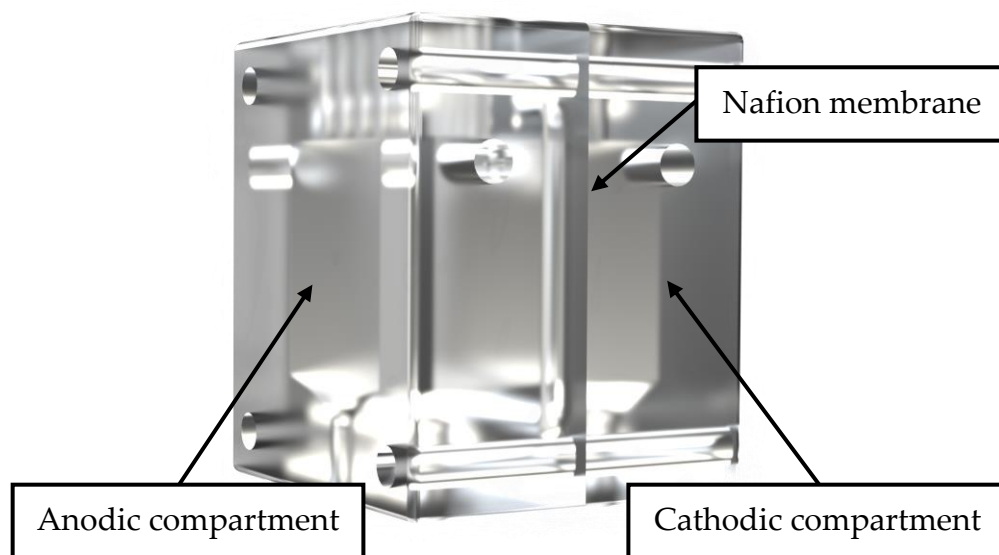


Figure 36: Rendered design of first prototype of reactor.

After the first design, the module was 3D printed and tested within the same day, and with the module on hand we decided that was necessary to improve some points and to implement a structure to support standard D.C. motors, as you can see in **Figure 37**. This was the first fast modification that 3D printing, and CAD software allowed us to perform, inside a design-test-new design iterative process.

6. Design of reactor with 3D printing

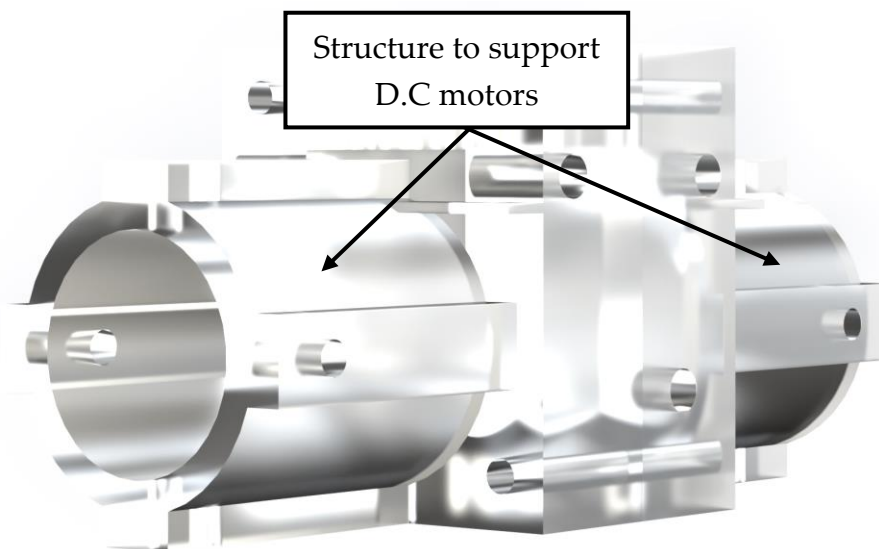


Figure 37: Rendered design of first prototype of reactor with supporting parts for D.C. stirring motors.

With this first prototype printed, and after testing it on real experiments we could identify the following points to improve.

- The volume can be even more reduced, in order to use a lesser amount of reagents and increase sensitivity.
- The original sealing was done using an O-ring technique and was not very robust, therefore we decided to implement another sealing technique using a silicon sheet.
- It would be good for the module to have holes for supporting it with bolts in order to make it more stable and robust to vibrations and movements.
- It is also necessary to design supporting accessories for the counter and working electrode, in order to make them more stable and robust.

KHCO₃/CO₂ electroreduction for fuel cell applications*Reaction and reactor optimization, prototyping with 3D printing and automatic testing.*

Between the first designed module and the final version, a total of 10 prototypes were designed, printed and tested, with considerably reduced times and prices, thanks to 3D printing iteration.

After all the improvements explained above, the final prototype has the characteristics described in **Table 7**.

Table 7: Comparison between first and final prototypes of reactors.

Points to improve	First prototype	Final prototype
Volume	6.5ml	1.5ml
Sealing	O-ring (Bad)	Silicone sheet (Good)
Supporting parts	None	Yes
Supports for electrodes	None	Yes

The parts of the reactor characteristics and can be seen in **Figure 38** and **Figure 39**:

- Two holes for working and counter electrodes.
- Two holes for pH meter and reference electrode in each compartment.
- Two holes for Thermometer and CO₂ gas injection in each compartment.
- Two holes for supporting the reactor with bolts.
- Space for magnetic stirrer
- One liquid output in each compartment
- Two liquid inputs in each compartment, one for reagents and the other for cleaning water.

6. Design of reactor with 3D printing

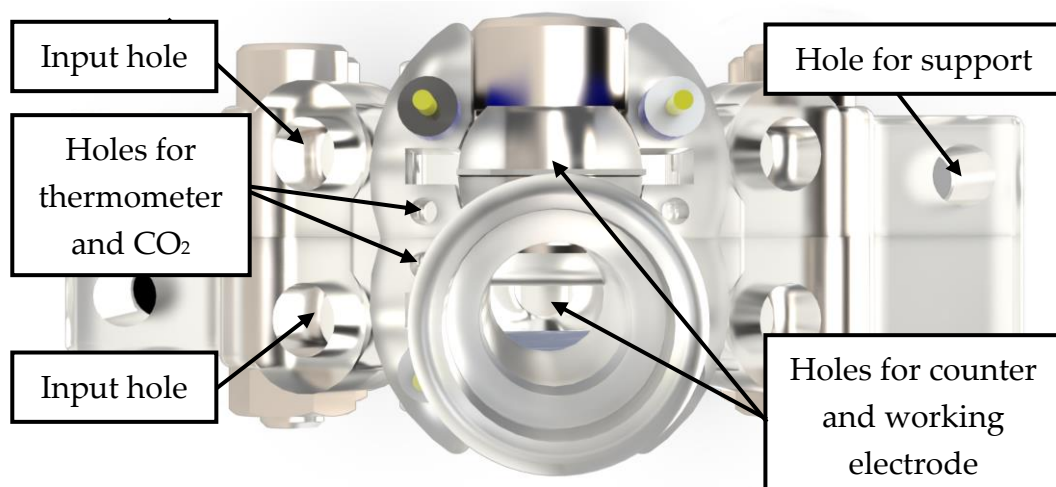


Figure 38: Top view of a rendered design of the final prototype of the reactor.

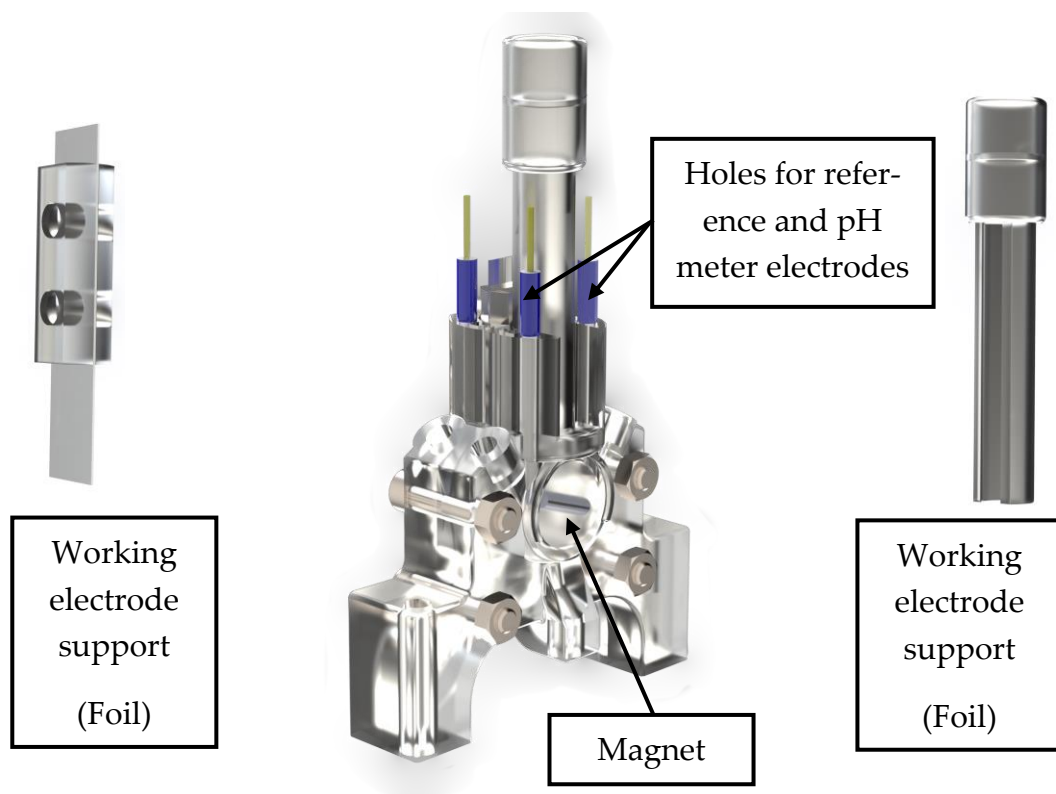


Figure 39: General view of a rendered design of the final prototype of the reactor.

KHCO₃/CO₂ electroreduction for fuel cell applications

Reaction and reactor optimization, prototyping with 3D printing and automatic testing.

Eventually, a reactor with more functionalities, better sealing, reduced volumes, and size was obtained as can be seen in figures

Figure 40. Figure 41 and Figure 42.

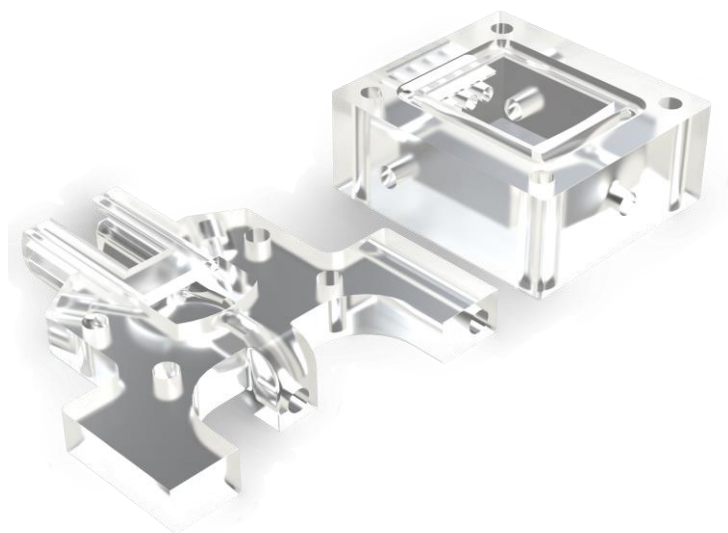


Figure 40: Comparison of a 3D render design of the first module prototype (right) against the final one (left).

6. Design of reactor with 3D printing

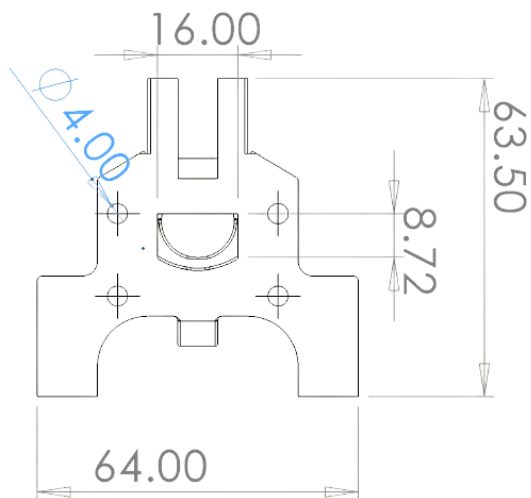


Figure 41: 2D sketch of the final reactor prototype with its main measures.

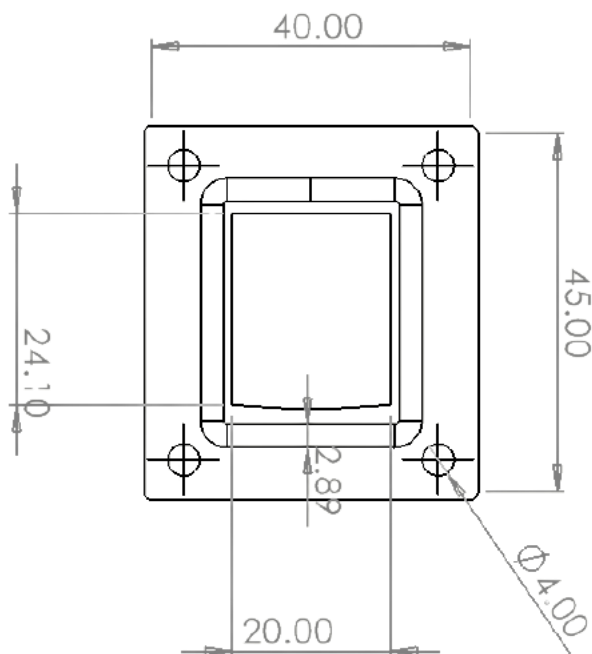


Figure 42: 2D drawing of the first reactor prototype with its main measures.

KHCO₃/CO₂ electroreduction for fuel cell applications

Reaction and reactor optimization, prototyping with 3D printing and automatic testing.

6.2. Reactor printing with SLA technology and assembly

The reactor with its supports for the electrodes were manufactured using SLA 3D printing technology. The printer was a Form 3 from Formlabs, charged with the “Standard clear resin”, also from Formlabs. The 3D designs from SolidWorks were sliced using Preform software. The reactor compartments were both printed at an angle of around 45° to obtain the best printing quality [86], and the supports were set mainly on the edges for better removal and cleaner walls, while avoiding the defects of support parts as much as possible, as you can see in **Figure 43**. The cost of the material used to print the reactor and the support for the electrodes is less than 6 euros and the printing time around 21h.

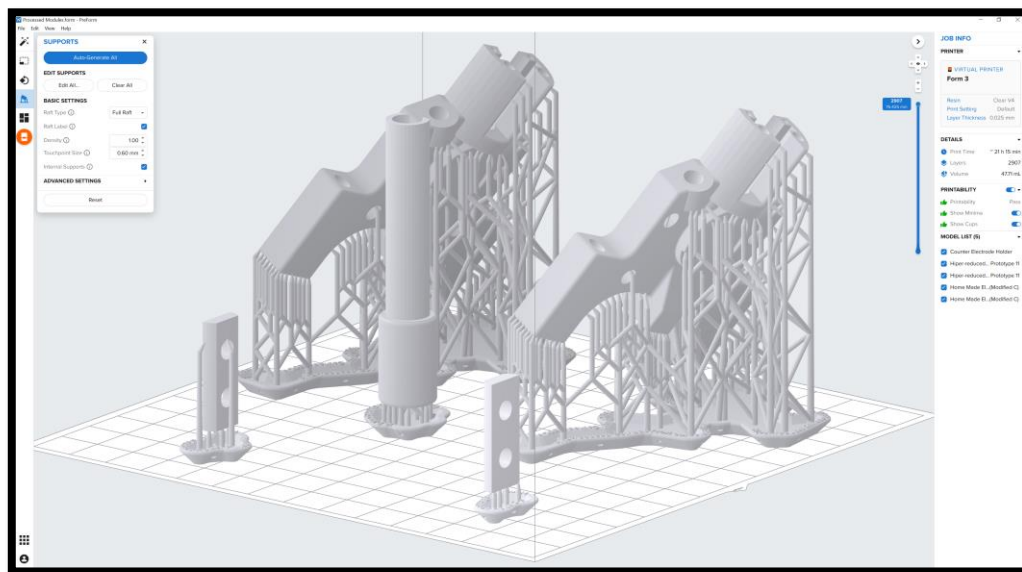


Figure 43: Preview of all the components of the reactor of the slicing program Preform.

6. Design of reactor with 3D printing

After printing the piece, the uncured resin is removed by using isopropanol as described in and post-cured with UV light lamp obtaining the final product (see **Figure 44**).

Both reactor compartments are attached together and the Nafion membrane is put in between. To ensure proper sealing, two silicon sheets (**Figure 45**) are put also on both sides of the membrane. When we screw the four bolts with low torque (2.5N/m^2 in order to not break the reactor), following a cross order, the reactor is sealed and ready for the experiments **Figure 46**.

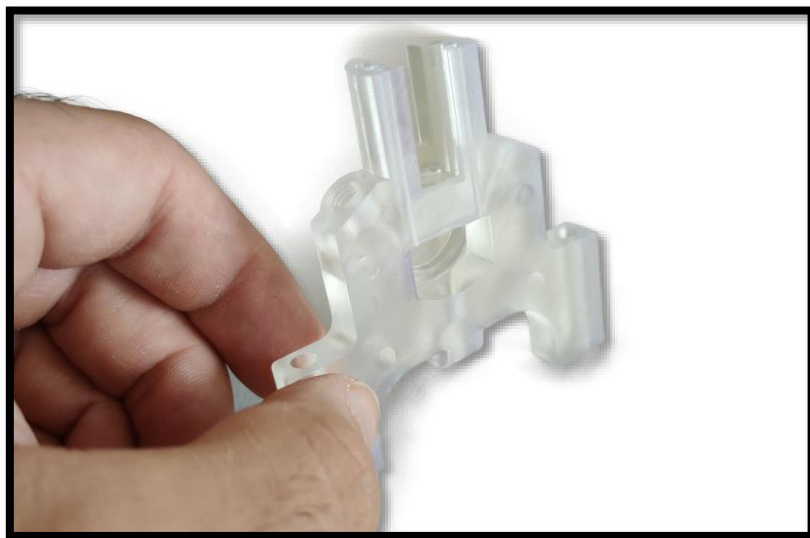


Figure 44: Photo of one of the final reactor compartments after post-curing.

KHCO₃/CO₂ electroreduction for fuel cell applications

Reaction and reactor optimization, prototyping with 3D printing and automatic testing.

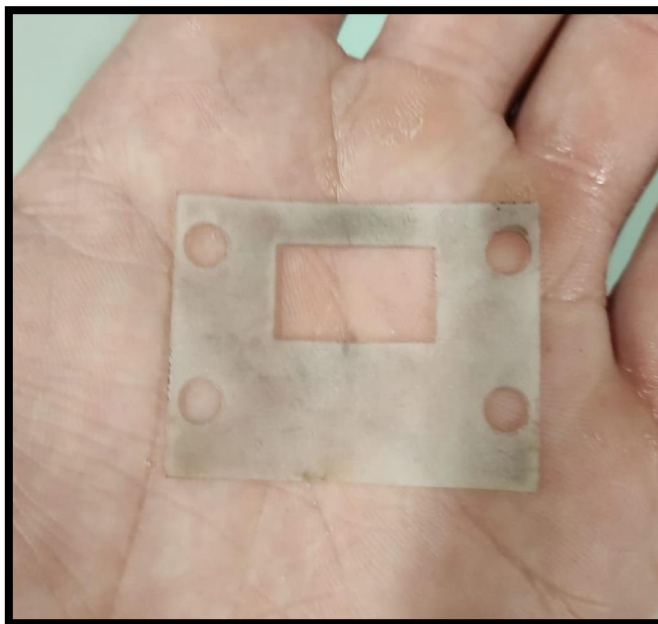


Figure 45: Silicone sheet cut with CO₂ laser used to seal both reactor compartments.

6. Design of reactor with 3D printing



Figure 46: Photo of the final prototype assembled.

6.3. Workshop-made reactor vs 3D printed

In this section, the 3D printed reactor is compared with the one used in the preliminary electroreduction experiments in **section 5**. In general, the advantages and disadvantages (Summarized in **Table 8**) of the 3D printed

KHCO₃/CO₂ electroreduction for fuel cell applications*Reaction and reactor optimization, prototyping with 3D printing and automatic testing.*

are the possibility to construct more complicated shapes, and therefore the possibility to reduce the volume (**Figure 47**), weight (**Figure 48**) and number of total parts composing the final module. That makes the 3D printed module easier to modify and clean. 3D printing is a technique that is characteristic for its fast-prototyping times and reduced prices, which allows to reduce by 10 the manufacture prices. On the other side, the workshop-made reactors can be manufactured with a wider variety of materials, therefore it can be more tolerant to aggressive products. Finally, the 3D printed reactor manufactured here is not gas-thigh, contrary to the workshop manufactured one, but is possible to make the 3D printed reactor completely sealed to the air.

Table 8: Comparison of the workshop-made reactor against 3D printed one.

Characteristics	Workshop reactor	3D printed reactor
Reaction volume	30ml	1.5ml
Transparency	No	Yes
Cleanability	Hard	Easy
Modifiability	Hard	Easy
Manufacture time	Weeks	1 day
Manufacturing price	500€	5€
Material tolerance	High	Low
Material variety	High	Low
Number of parts	More than 10	2
Number of bolts	30	4
Weight	1780g	47g
Gas-thigh	Yes	No

6. Design of reactor with 3D printing

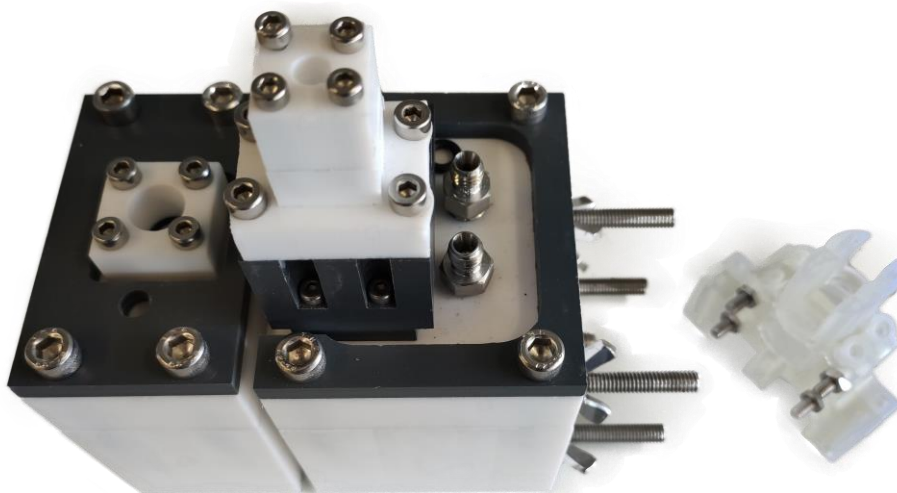


Figure 47: Size comparison of the workshop manufactured reactor (on the left) against 3D printed reactor (on the right).



Figure 48: Weight in grams of the workshop manufactured reactor (on the left) against 3D printed reactor (on the right).

KHCO₃/CO₂ electroreduction for fuel cell applications*Reaction and reactor optimization, prototyping with 3D printing and automatic testing.***6.4. Conclusions**

In general 3D printing shows great capabilities to substitute the classic workshop techniques for prototyping, mainly because its low costs, fast manufacture, and the possibility to obtain more complex parts, without the need to have a very expensive and specialized workshop and technicians. However, as said before, 3D printing is mainly for prototyping because the stability and the quality of the used materials is relatively low yet. Therefore, most of the times when a final prototype is achieved and ready to be commercialized or used in large scale production, the classic workshop manufacture techniques show a great advantage. Thus, these techniques are complementary and each one has its own applications.

7. Automatic and remote testing system

KHCO₃/CO₂ electroreduction for fuel cell applications

Reaction and reactor optimization, prototyping with 3D printing and automatic testing.

7. AUTOMATIC AND REMOTE TESTING SYSTEM

7. Automatic and remote testing system

Most of the necessary procedures to perform electroreduction experiments, such as filling the reactor, cleaning it, and sampling, are very simple and repetitive and can be automated. With this goal, a semi-autonomous testing system was designed and constructed to increase repeatability, testing capacity and scalability, while decreasing the price of the experiment and helping the researcher to work more efficiently and obtain more and better data.

KHCO₃/CO₂ electroreduction for fuel cell applications

Reaction and reactor optimization, prototyping with 3D printing and automatic testing.

7.1. Introduction

The physical parts of the testing system have been built mainly using 3D printing, due to the advantages commented in **section 3.5**.

Nowadays, and thanks to the emerging of low-cost 3D printers and Arduino, the movement Open Source is growing, and thanks to that almost everyone can build whatever is on their minds at a very reduced price. Due to that, during this thesis it was possible to design and assembly a functional semi-automated system for electroreduction testing at a very affordable price, demonstrating that most of the rutinary laboratory procedures can be automated to improve testing capacity, reproducibility, efficiency and decrease human and methodological errors, while liberating the researchers from rutinary and repetitive work allowing them to work on more challenging things.

The first step was to design a schema of how the system will be structured, followed by the design of all the parts and components of the system. The second step was the design all the system, done by using SolidWorks. During this phase, the disposition of all the mechanical components such as the reactor, the autosampler, syringe pump, supporting parts and was set. The third, was to assembly all the 3D printed supporting parts for the components to test if everything worked. During that process some components were redesigned to improve or correct non-fitting parts and iterating over that until reaching the final working device. The fourth step was the design of the electronic system to control the motors and solenoid valves. Finally, we implemented remote control of the system using Wi-Fi to control and monitor the experiment remotely.

7.2. Schematic design of the automated system

The first question to solve was the injection of the reagents and the cleaning water inside the reactor, and the most cost-efficient way to do that was by gravity, using solenoid valves. The problem with this method was the low precision and exactitude of the volume introduced. Also, this was not a very robust method because the flow of the water or reagents change in function of the level of tanks. Therefore, it was better to use pumps for the introduction of reagents as shown on figure **Figure 49**.

For the cleaning water pumping there were two main options: using a syringe pump or a peristaltic pump. The peristaltic pump was finally chosen due to the possibility to connect it with a water tank with no need to be recharged during long periods of time and relatively higher flow, which makes the water pumping faster, and its reduced price compared to pumps. But for the injection of reagents, we needed something more precise to control the injected volume, hence, we used a home-made injection pump (**section 7.3.6**) for the injection of reagents.

Once the reaction is finished, we need to collect the products. To do that and knowing that no precision is needed because we just take a part of the sample to analyse it, solenoid valves were used. The valves will be assembled at the bottom of the reactor to let the reagents fall by gravity to a home-made autosampler (**Section 7.3.4**).

The distribution of the instrumentation for data acquisition was done as shown in **Figure 50**. In addition to the basic three-electrode system used to monitor current and voltage during electroreduction experiments, a pH meter was introduced on both compartments to monitor the pH in real time. All the data was collected by the used instrumentation described

KHCO₃/CO₂ electroreduction for fuel cell applications

Reaction and reactor optimization, prototyping with 3D printing and automatic testing.

in **section 5** and transferred to a computer. That computer will act as an internet server for the remote monitoring and control of the experiment as will be described in the following sections.

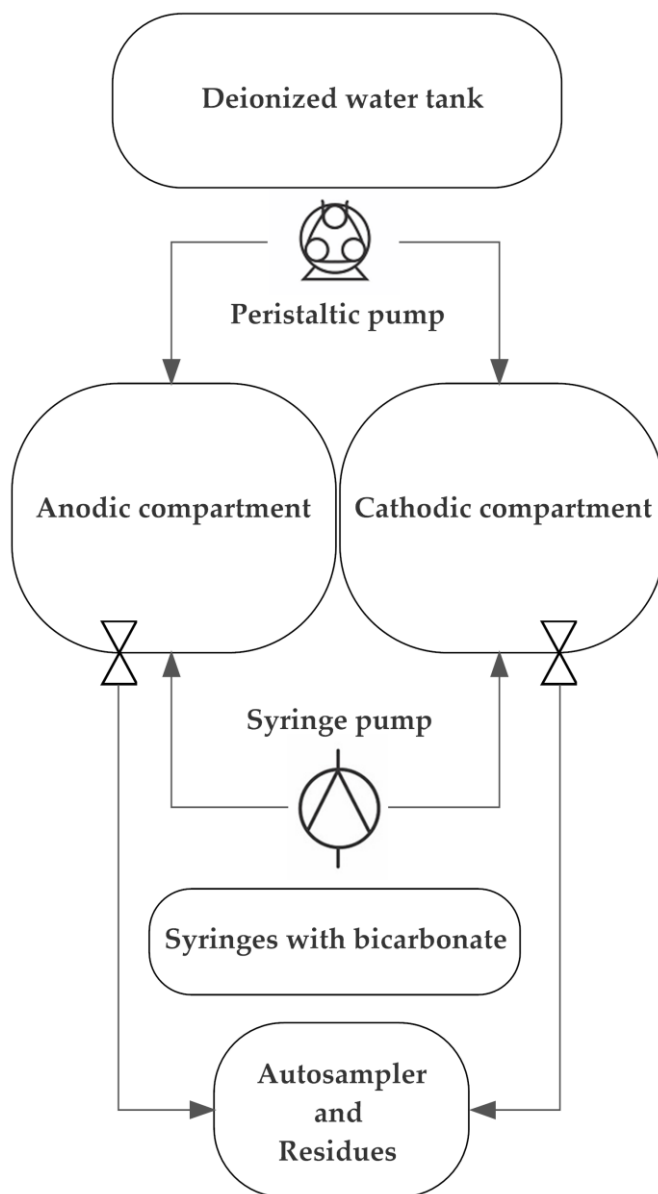


Figure 49: Flow diagram of the automatic cleaning and reagents injection of the system

7. Automatic and remote testing system

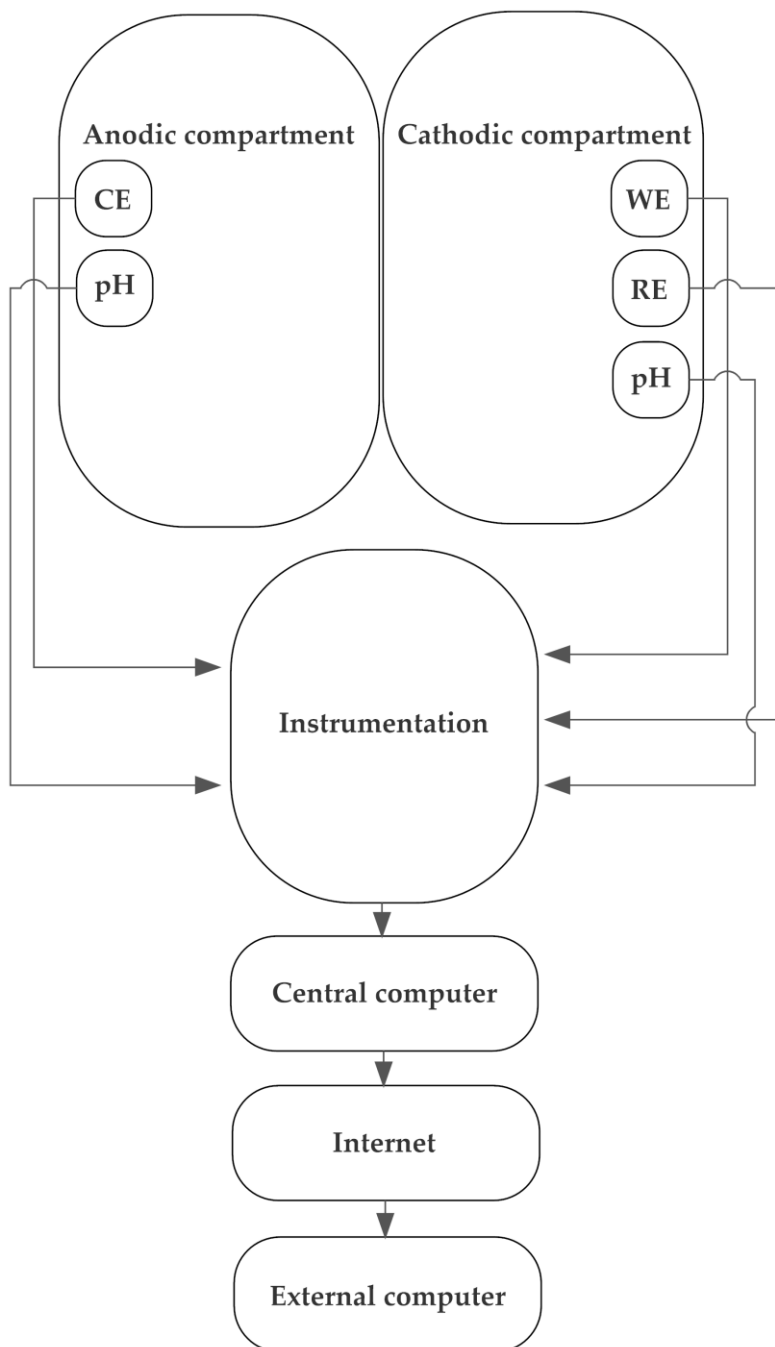


Figure 50: Diagram of the different sensors inside the reactor.

KHCO₃/CO₂ electroreduction for fuel cell applications

Reaction and reactor optimization, prototyping with 3D printing and automatic testing.

7.3. Design of the system with SolidWorks

For the prototyping and designing of all the system components SolidWorks was used to facilitate the choosing of final components and assembly.

7.3.1. Support for the reactor

The support is fixed on two PCV plates on a 90-degree disposition by 4 bolts, as you can see in **Figure 51**. To support the reactor, 2 bolts are inserted on the 2 predesigned holes (one for the anodic compartment and another for the cathodic compartment) as you can see in **Figure 52**, then these bolts are screwed on the support rails. Thanks to the length of these 2 rails, the reactor position is adjustable horizontally and vertically if spacers are added. There is also another hole on the centre to create space for the output solenoid valves.

7.3.2. Solenoid valves

To evacuate the products and the cleaning water, two solenoid valves are installed at the bottom of the reactor, as you can see on **Figure 53**. For this step is not necessary to have precision on the sampling, because we just take a portion for analysing, and this is the cheapest and most simple way to achieve that while maintaining functionality.

7.3.3. Stirring Motors

To generate agitation inside the reactor, two stepper motors are used (see **Figure 54**). They are supported using a 3D printed piece (in green) and screwed on the reactor for support. The stepper motors are more expensive and can't reach very high speeds compared with conventional DC motors,

7. Automatic and remote testing system

but as we need to monitor the agitation speed in a precise way, those motors are the best option for that, as explained in section 3.7.1. The stirring is generated using a cylindrical magnet introduced inside the reaction chamber, as you can see in **Figure 55**. The movement of the motors is transferred magnetically with the magnet contained inside and two nickel magnets supported by a 3D printed support (in yellow) show in **Figure 54**.

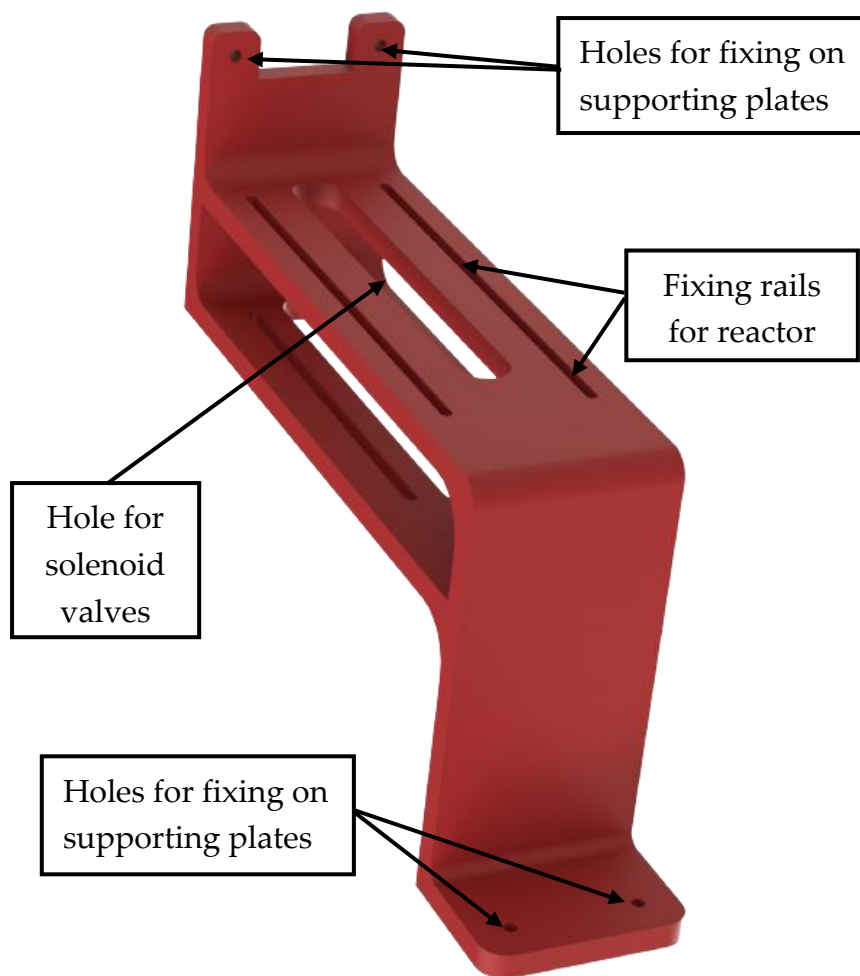


Figure 51: 3D render view of the designed support for the electrochemical reactor.

KHCO₃/CO₂ electroreduction for fuel cell applications

Reaction and reactor optimization, prototyping with 3D printing and automatic testing.

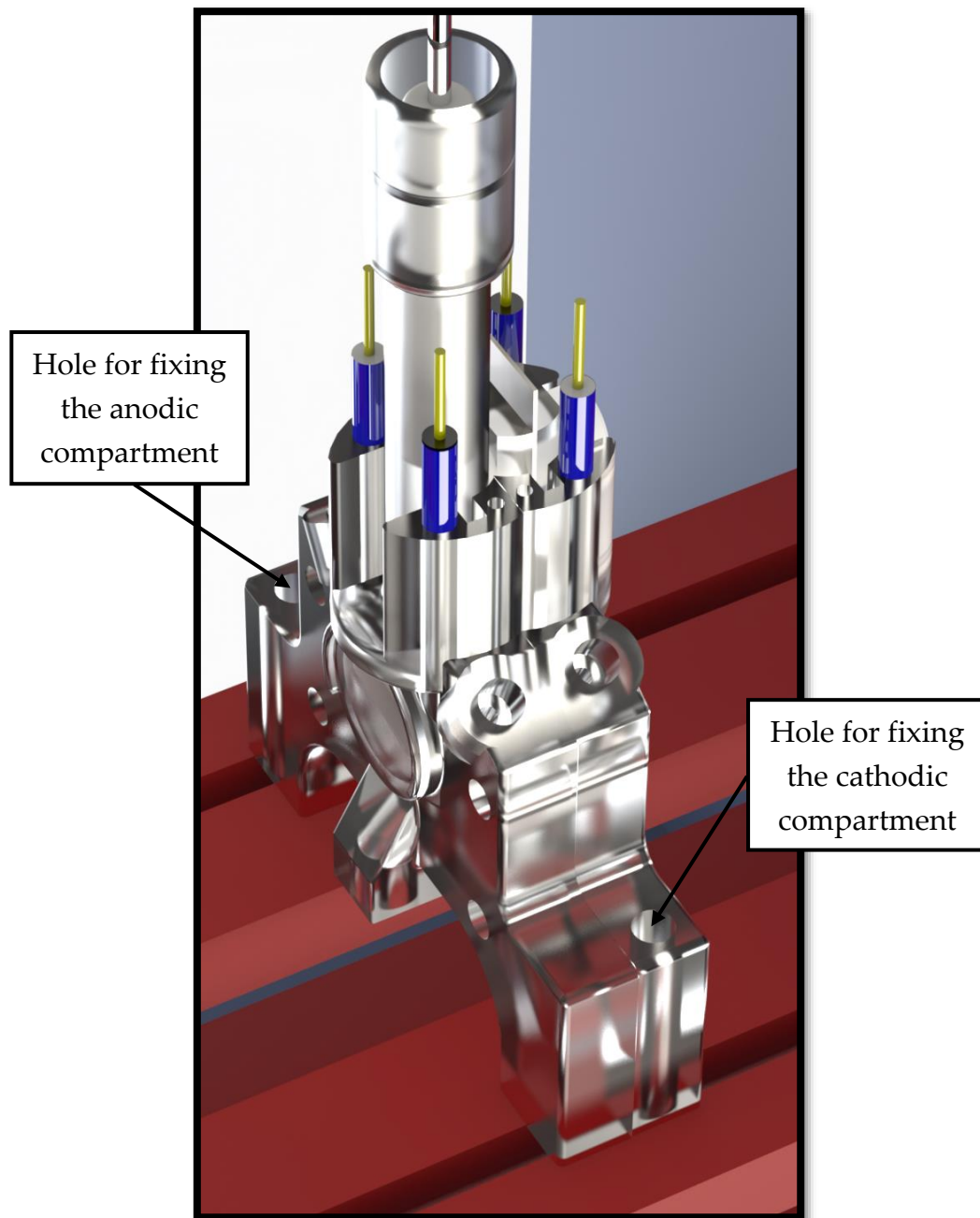


Figure 52: 3D render view of the designed reactor on the designed support (without screwed bolts).

7. Automatic and remote testing system

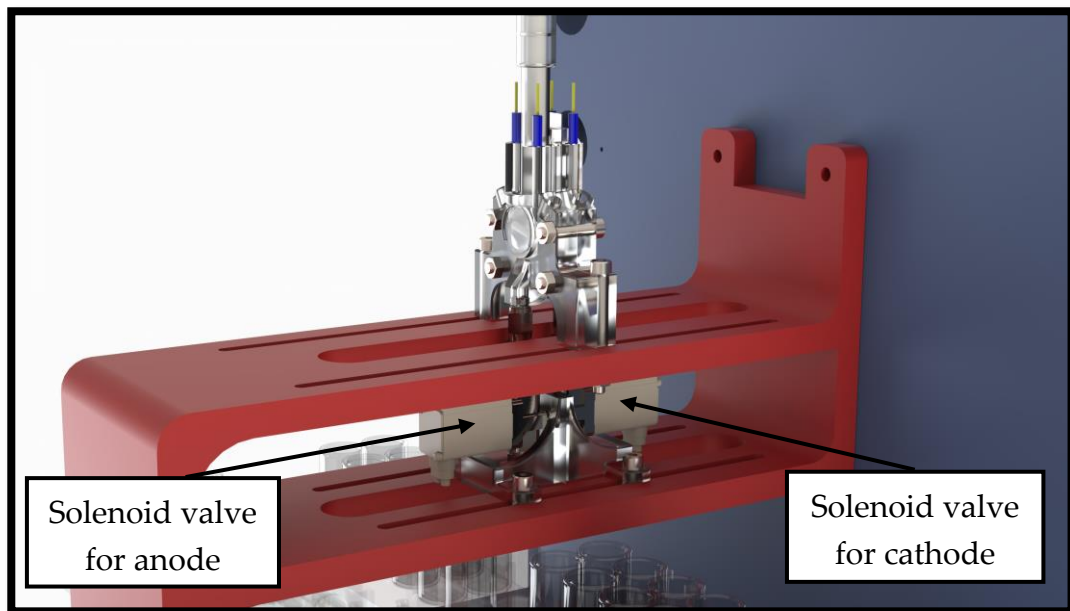


Figure 53: 3D render view with the solenoid valves at the bottom of the reactor.

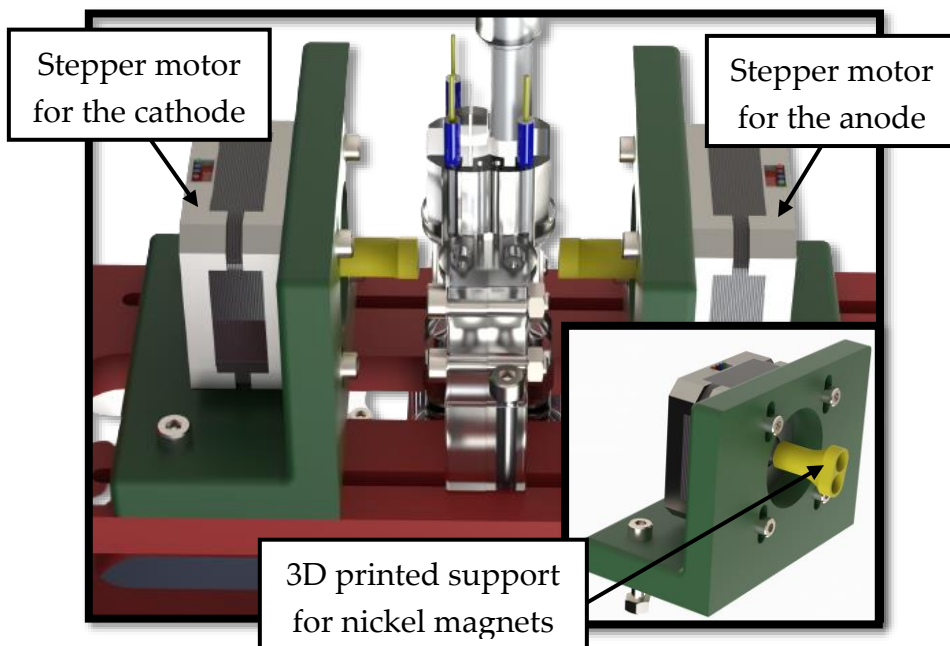


Figure 54: 3D render view of the system with the stirring motors for tuneable agitation.

KHCO₃/CO₂ electroreduction for fuel cell applications

Reaction and reactor optimization, prototyping with 3D printing and automatic testing.

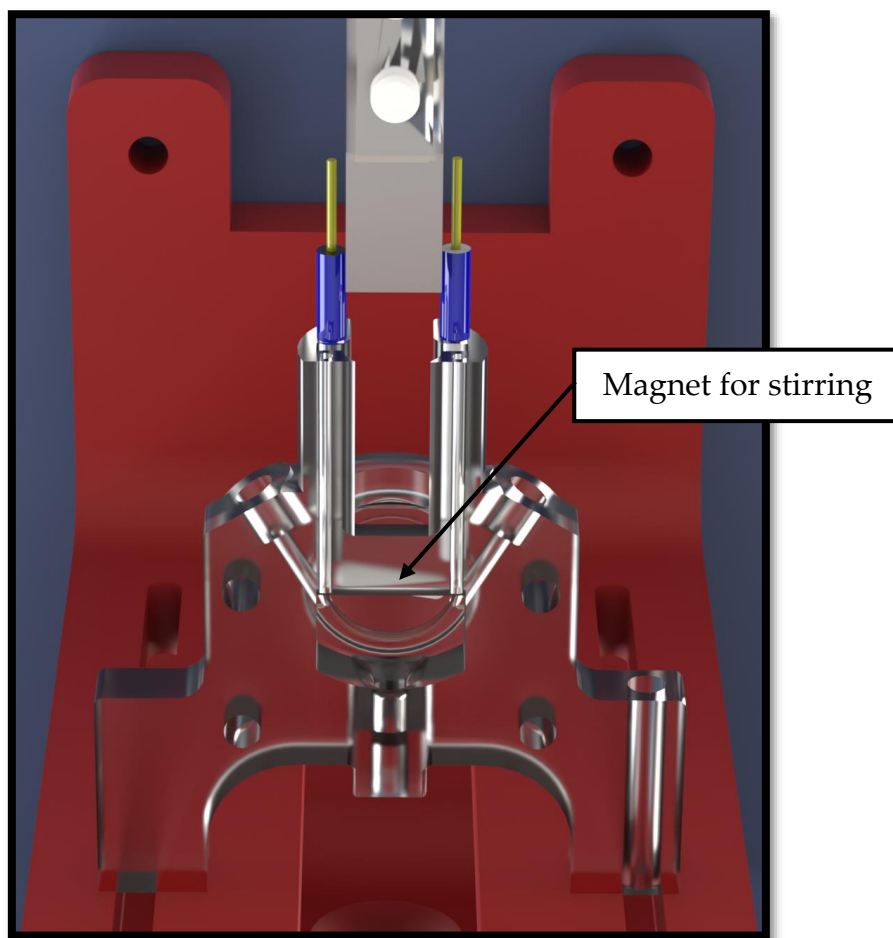


Figure 55: 3D render view of the system with the magnet for stirring on the wall of the reactor.

7.3.4. Autosampler

For the automatic sampling between experiments, a linear autosampler consisting of a linear two simple rail system was designed, as

7. Automatic and remote testing system

depicted in **Figure 56** and **Figure 57**. This application doesn't require extremely precise movements; therefore, this system is used instead of the linear guided ones used for industry and CNC machines, because of its lower price. A 3D printed support consisting of 12 × 2 cartridges was printed (one for the cathodic compartment and another for the anodic compartment, 24 in total) to support the vials where the reaction products are stored. The stepper motor used to move the linear axis is also supported using a 3D printed support (coloured in green in **Figure 57**). To evacuate the residues and cleaning water, an evacuation channel was located on the centre of the autosampler. An endstop was used to automatically calibrate the autosampler.

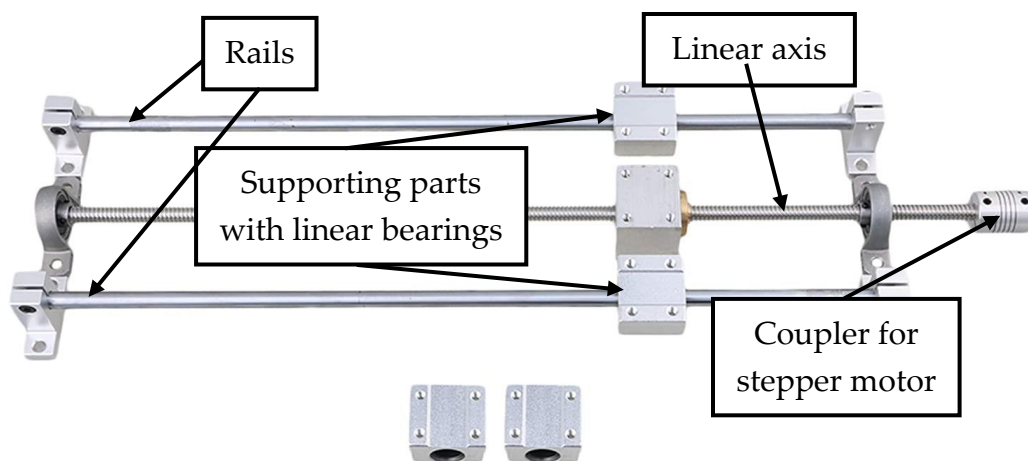


Figure 56: Photo of the real linear two simple rail system used for the home-made autosampler.

KHCO₃/CO₂ electroreduction for fuel cell applications

Reaction and reactor optimization, prototyping with 3D printing and automatic testing.

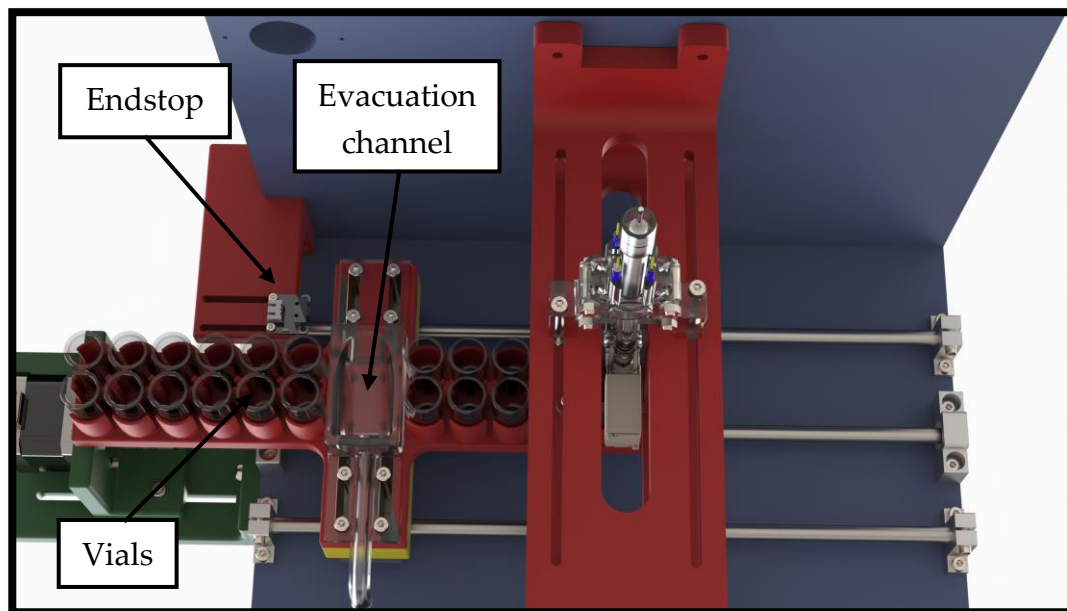


Figure 57: 3D render of the system with the autosampler, *endstop* and evacuation channel.

7.3.5. Peristaltic Pump

To clean the reactor between the experiments, deionized water was pumped from a 5L tank by a peristaltic pump for each compartment (see

Figure 58). Those pumps ensure a good flow at a very reduced price. To ensure good sealing and fast and easy manipulation of the tubes, a straight fitting – threaded tube is used to connect the with the reactor.

7. Automatic and remote testing system

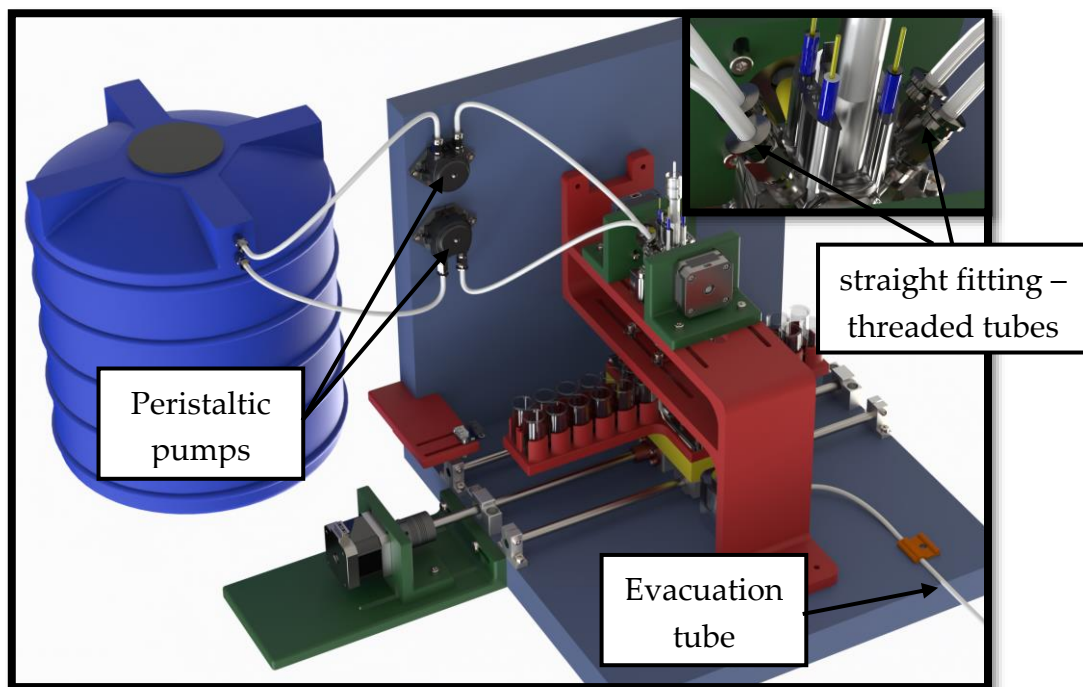


Figure 58: 3D render of the system with the two peristaltic pumps.

7.3.6. Syringe Pump

The home-made syringe pump was designed using 3D printed parts and a linear two rail system, moved using a stepper motor, shown in **Figure 59**. The rails are assembled and supported by the red 3D printed parts. For this application, the 3D printed parts were designed to accommodate 2 syringes at the same time to inject the same volume to the two reactor compartments. For the connections with the reactor a straight fitting – threaded tube is used as for the peristaltic pumps.

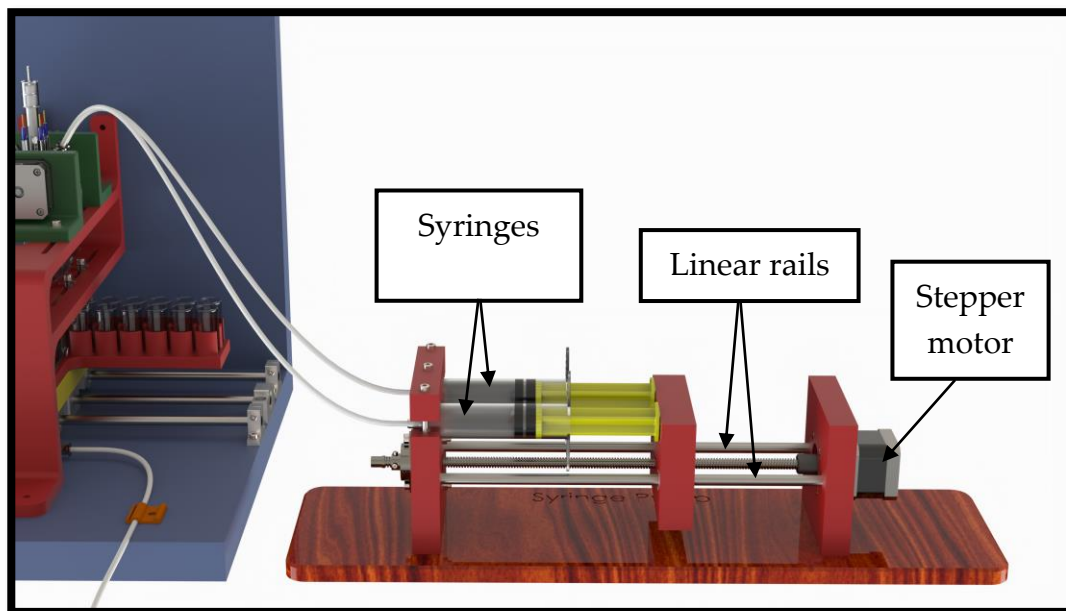
KHCO₃/CO₂ electroreduction for fuel cell applications*Reaction and reactor optimization, prototyping with 3D printing and automatic testing.*

Figure 59: 3D render of the system with the home-made syringe pump.

A visualization of all the rendered system is on **Figure 60** for better visualization of how all the following parts are arranged. There is also a 3D animation video of the assembly of the system in the following link (<https://youtu.be/D1LTHAsbfE4>)

- 1.- Support for the reactor.
- 2.- Solenoid valves.
- 3.- Stirring motors.
- 4.-Autosampler.
- 5.-Peristaltic pumps.
- 6.-Syringe pumps.

7. Automatic and remote testing system

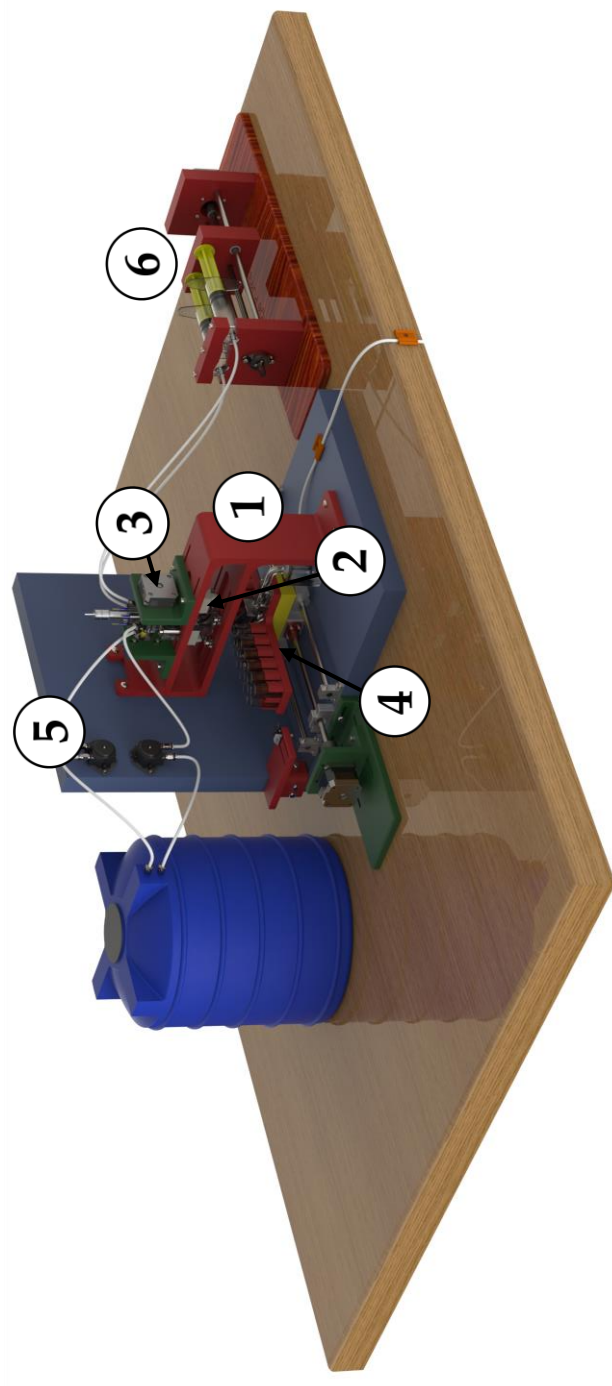


Figure 60: Rendered design of all the system.

KHCO₃/CO₂ electroreduction for fuel cell applications*Reaction and reactor optimization, prototyping with 3D printing and automatic testing.***7.4. Printing of the system**

In this section the costs of the system and all the components will be analysed.

The supporting parts, as not very high quality and resolution is needed, were printed with FDM technology, and using PLA due to its extremely low price and good mechanical properties. As you can see in **Table 9** the total price of all the supporting parts, with the home-made syringe included, do not exceed the 35 euros. Also, the printing time of all the pieces is relatively low, considering that they are printed individually, it's around 70h, but if multiple ones are printed on the same batch this time could be much lower.

Table 9: Summary of all the 3D printed parts with FDM technology used for the automatic system (**Table 10** for the 3D printed parts used in the syringe pump)

FDM printed parts	Printing time (h)	Plastic weight (g)	Quantity	Material cost (€)
Support for reactor	24	330	1	11.5
Support for autosampler	7	80	1	3
Support for cables	1	15	1	0.5
Support for endpoint	3	32	1	1.5
Support for stirring	3	33	2	3.2
Support for solenoid valves	1	9	2	0.6
Support autosampler	3	33	1	1.6
Support for vials	9	100	1	3.4
Spacer for residues	4	50	1	1.7
Total	55	682	11	27

7. Automatic and remote testing system

Table 10: Summary of all the 3D printed parts with FDM technology used for the syringe pump.

FDM printed parts	Printing time (h)	Plastic weight (g)	Quantity	Material cost (€)
Support for syringes	6	80	1	3
Support for motor	5	60	1	2
Central part	4	55	1	1.92
Clamp	2	18	1	0.6
Total	17	213	4	7.52

The parts printed with SLA technology were the reactor compartments, the supports for the catalysts and the evacuation channel. The evacuation channel is in contact with the solutions and the PLA is not as stable as the resin, therefore this part was printed with SLA. The costs of all these parts are less than 24 euros **Table 11**, which is also very low. And the printing time is around 60h considering that they were printed individually at the highest resolution possible. However, scarifying a little bit the resolution, increasing the layer height from 25 μm to 100 μm , and printing all together the time can be reduced to less than 10h.

Table 11: Summary of all the 3D printed parts cost in time and price with SLA technology.

SLA 3D printed parts	Printing time (h)	Material volume (ml)	Quantity	Material cost (€)
Reactor compartments	18	37	1	4.995
Catalyst holder	1	3.5	2	0.945
Counter electrode holder	4	5	1	0.675
Residues Output	37	125	1	16.875
Total	60	170.5	5	23.49

KHCO₃/CO₂ electroreduction for fuel cell applications

Reaction and reactor optimization, prototyping with 3D printing and automatic testing.

7.5. Electronic circuit design.

The electronic components were previously tested with a basic protoboard (**Figure 61**). Once all the electronic components were tested and their good functionality confirmed, a PCB was designed using EasyEDA software and manufactured by JLCPCB company. In the **Figure 62** you can check the electric scheme to know how the connections are set and which pins are used. In **Figure 63** there is a realistic render of the final PCB and in **Figure 64** the real image with all components soldered.

The electronic circuit is over dimensioned to accommodate future modifications of the system, and designed to accommodate the following electronic components:

- ESP32 microcontroller
- Five stepper motor drivers (two for the steppers for the stirring motors, one for the stepper used in autosampler, one for the stepper used in syringe pump, one extra slot for possible ampliation of the system, for example automatic injection of the samples)
- Four Transistors (MOSFET), two used to actuate the solenoid valves, and two extras for future ampliation.
- Inputs for the peristaltic pump.
- Three Inputs for endpoints.
- Jumpers at the input of micro-stepping pins of the stepper motor drivers to be able to change manually the micro-stepping modes.

7. Automatic and remote testing system

The power supply feeds the electronics with 24V, which is the recommended voltage for the solenoid valves, but since that voltage is too high for the ESP32 and peristaltic pump, a voltage regulator from 24V to 5V is put in between power supply and peristaltic pump and another one from 24V to 3.3V in between ESP32 and power supply. The optimal voltage for the stepper motors is normally 12V, but they can also work fine at 24V therefore it was not necessary to add regulators here. To improve and homogenize the signal some components were added:

- At the input of the solenoid valves, diodes are set to protect the rest of the components from electronic rebounds, together with the recommended resistances in the datasheet.
- Capacitors are also put in between the power supply and stepper motor drivers to homogenize the current and correct current peaks.

All the used electronic components are listed in **Table 12**.

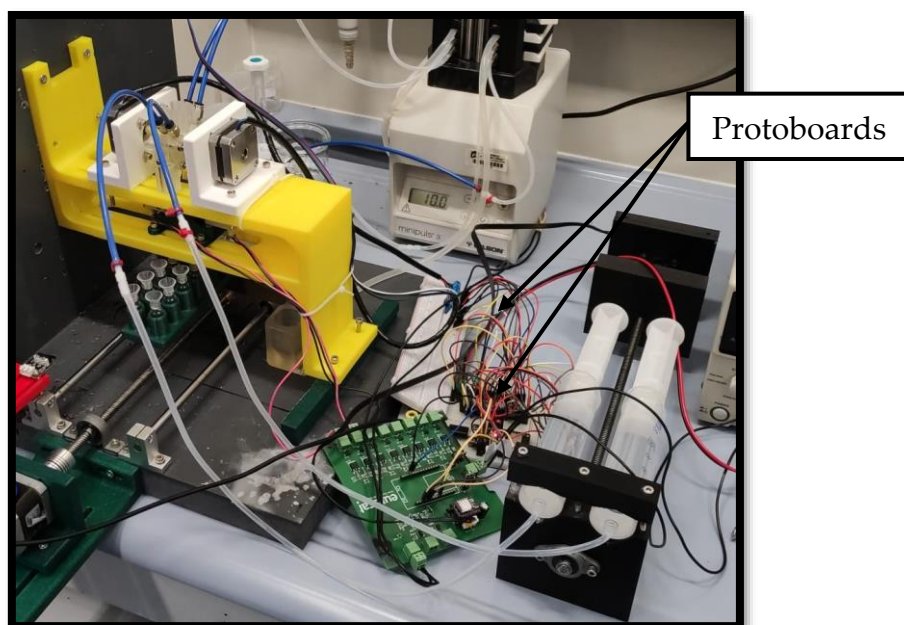


Figure 61: Photo of the system with the protoboard.

KHCO₃/CO₂ electroreduction for fuel cell applications
Reaction and reactor optimization, prototyping with 3D printing and automatic testing.

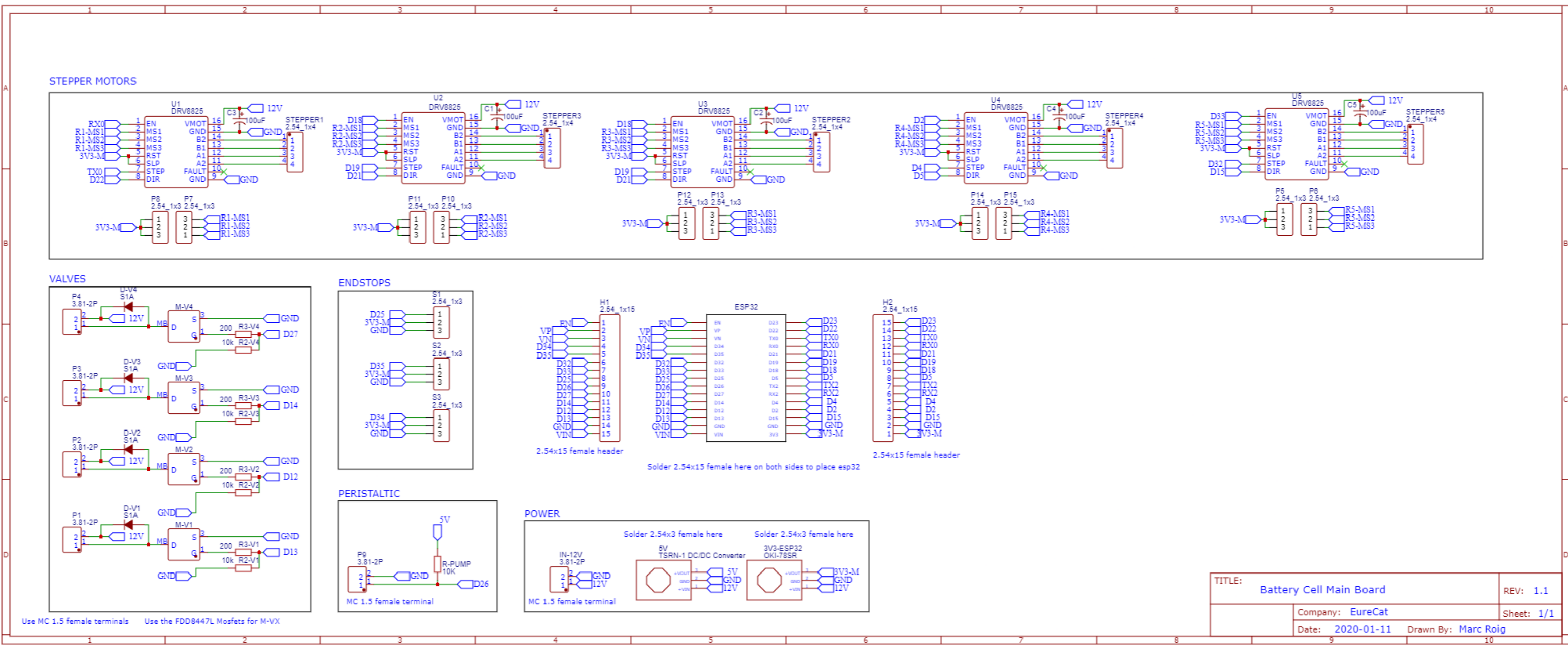


Figure 62: Scheme of electronic circuit used to control all the electronic components for the experiments.

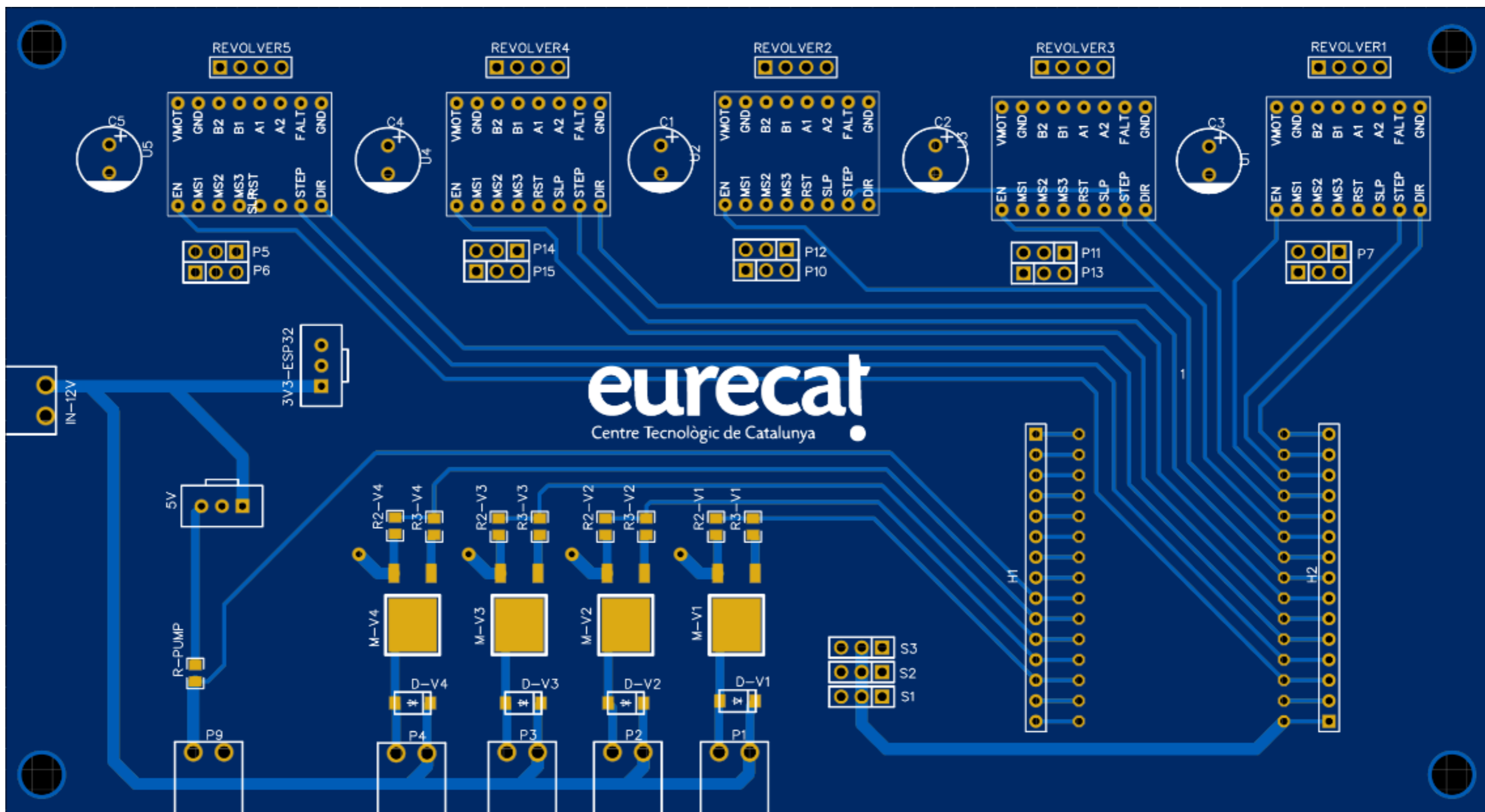


Figure 63: Realistic render of the final PCB.

KHCO₃/CO₂ electroreduction for fuel cell applications
Reaction and reactor optimization, prototyping with 3D printing and automatic testing.

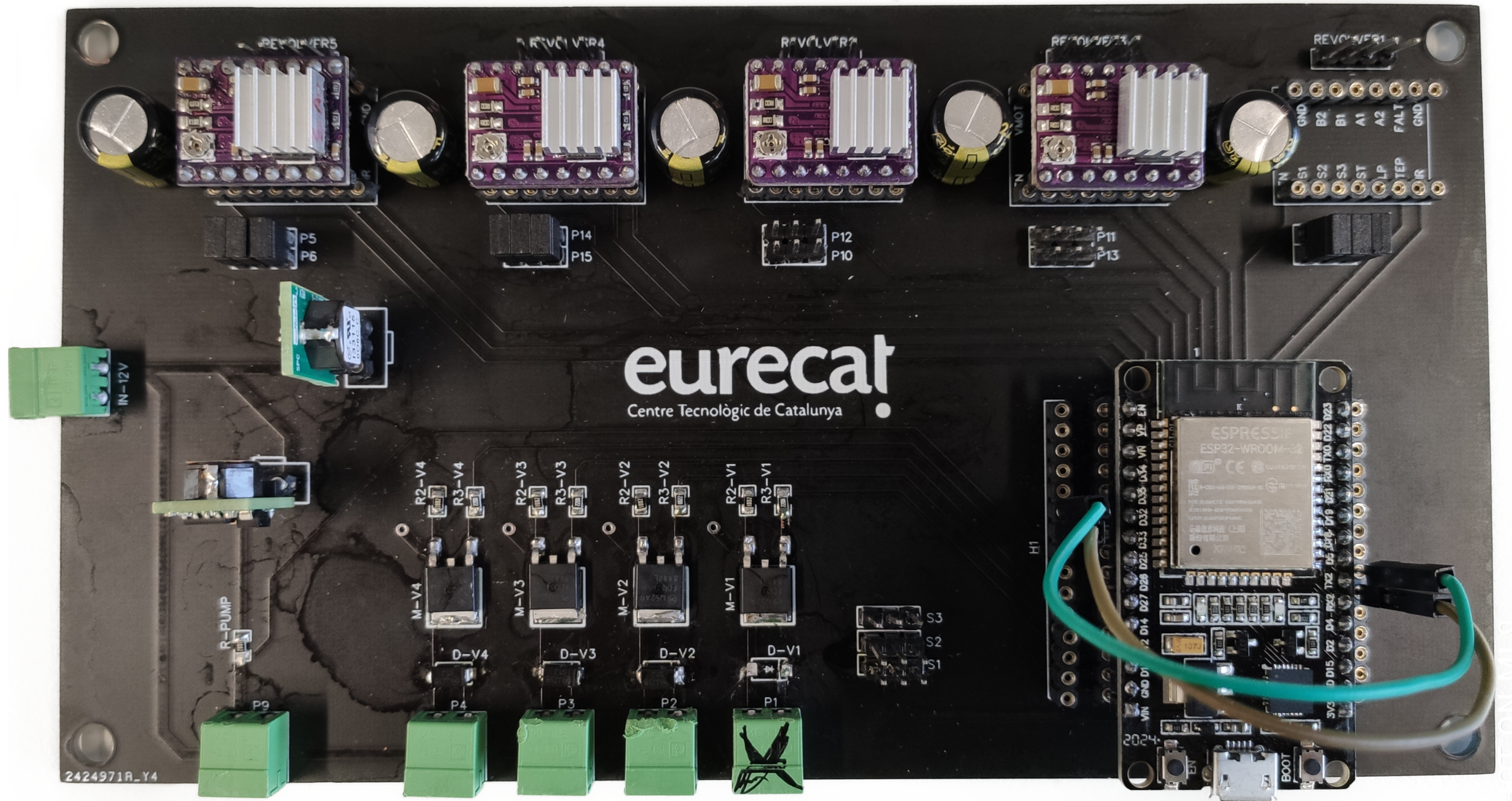


Figure 64: Photo of the final PCB with all the components soldered.

8. Results obtained with automatic system

Table 12: Summary table of all the electronic components soldered on the designed PCB.

Electronics Components				
Type	Image	Uds	€/u	€
Switching Diode (S1A)		100	0.05	5.10
SMD Resistor (10k)		20	0.27	5.30
SMD Resistor (220)		5000	0.00	10.00
Logic Level MOSFET SMD (FDD8447L)		5	0.46	2.31
Male terminal 2 contacts (MC 1.5/ 2-G-3.81)		20	0.72	14.32
Female terminal 2 contacts (MC 1.5/ 2-G-3.81)		20	0.46	9.14
DC-DC Step Down (3.3V dc, 1.5A, 4.95W)		1	4.23	4.23
DC-DC Step Down (5V dc)		1	15.94	15.94
Aluminium capacitor (68uF)		10	1.15	11.52
Female Header 2.54mm		10	0.51	5.08
Male Header 2.54mm		10	0.27	2.66
Jumper		30	0.03	0.78
Total cost				86.38

KHCO₃/CO₂ electroreduction for fuel cell applications

Reaction and reactor optimization, prototyping with 3D printing and automatic testing.

7.6. System assembly

The final system was assembled as follows, but a high-quality multi-channel peristaltic pump was used instead of two standard single channel peristaltic pumps, because we already had it, but is not necessary to use high precision pumps for this application. Following the **Figure 65** and **Figure 66**. The reactor **(1)** was screwed on the yellow support using the bolts described in the previous section, between the stirring motors and with the solenoid valves at the bottom. At the front with the is the syringe pump **(2)** connected to the reactor with flexible tubing. The multichannel peristaltic pump **(3)** at the bottom is used for both pumping the cleaning water from the water tank **(4)** and pumping the residual water coming from the residual channel. The autosampler **(5)** attached to the PVC table and below the reactor for sampling. There are also 3 cameras on the top of the system **(6)** used for remotely monitoring the system. The electronic PCB **(7)** is attached at the back of the system to avoid contact with possible liquid leakages and to have the system cleaner with less possible number of cables visible. Outside of the fume hood, the power supply **(8)** and potentiostat **(9)** are found.

The total cost of the system is calculated by the sum of FDM 3D printed parts, SLA 3D printed parts, computer used to run the programs, all the hardware and electronic components used, reaching a value of about 1000 € (**Table 13**). Considering that this was the cost of just the prototype, it is possible to obtain even lower values if scale production is achieved in the future. Therefore, once these systems are produced, it can be very cost effective and help to increase the productivity of our researchers.

The cost of the electrodes and potentiostat can vary a lot depending on the quality, but the price of all would be between 1700 and 12000 euros, as you can be seen in **Table 14**. As they are not part of the automatic system

8. Results obtained with automatic system

they are accounted separately. The application of real time measurement of pH and temperature described in section 6.1 was not achieved due to lack of time, but the prices of all those sensors needed for that are considered.

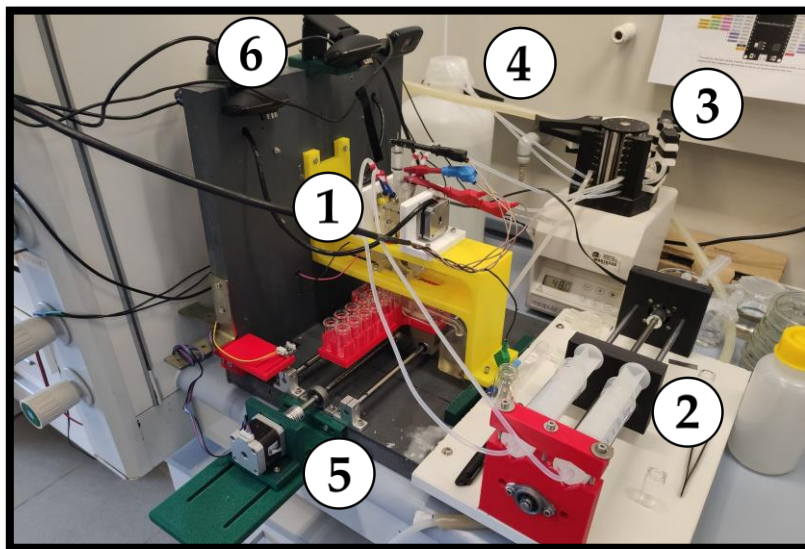


Figure 65: Photo of a general view of the system.

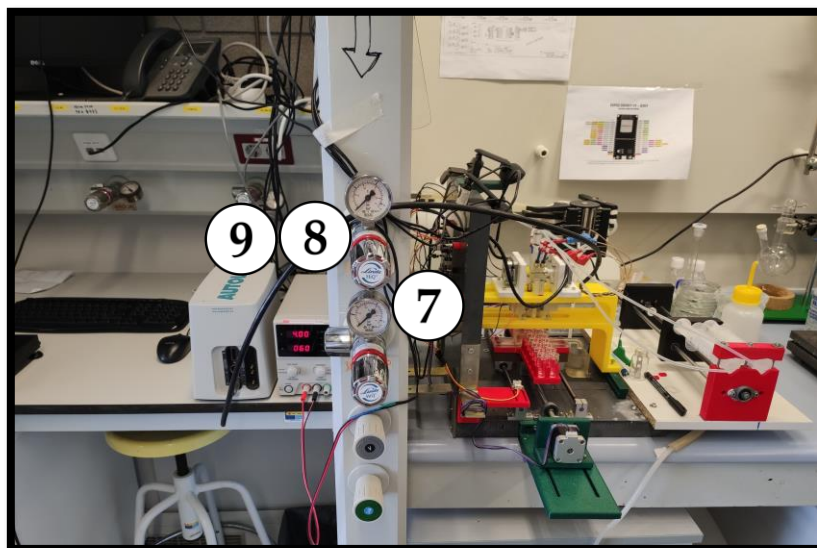


Figure 66: Photo of a general view of the system.

KHCO₃/CO₂ electroreduction for fuel cell applications*Reaction and reactor optimization, prototyping with 3D printing and automatic testing.***Table 13:** Summary of the price of components used for the automatic system.

Price of components	Quantity	PPU (€)	Total price (€)
Printed components	1	-	58.01
Electronic circuit (PCB)	5	3.2	16
Electronic components	1	-	86.38
Linear rail (Autosampler)	2	47	94
Stainless steel solenoid valve	2	20.28	40.56
Screws	-	-	20
Tubing	-	-	20
Wiring	-	-	10
Peristaltic pumps	2	13.69	27.38
Webcams	3	23.98	71.94
Tube connections	-	-	10
Stirring motors	2	10	20
Autosampler and syringe motors	2	15	30
Basic computer	1	300	300
Regulable power supply	1	100	100
Others	1	-	100
-	-	-	1004.27

Table 14: Summary of the price of components related to electroreduction.

Price of components	Quantity	PPU (€)	Total price (€)
Potentiostat	1	-	500 to 10000
Electrodes	4	160	640
Tin foil	1	150	150
Platinum wire	1	168	168
Thermometers	2	100	200
-	-	-	1658 to 11158

7.7. MicroPython programming for control

For programming the electronic components, both Python and C++ were on the table [87]. Despite C++ being a compiled language, therefore it is executed faster and more efficiently by computers, it is less readable for humans, thus it is harder to make changes and iterate over different prototypes of codes. Therefore Python, which is an interpreted language, was used due to its simplicity, that works very well for simple prototype applications where non-efficient and low-level code like C++ is required.

ESP32 Micropython code

<https://github.com/eurebatt/remote-control> (Link to online repository of the code)

Define class for a stepper motor

```
class Stepper:
    def __init__(self, stp_pin, dir_pin, pow_pin, step_sleep_us=1000,
full_rev=360, step_angle=1.8, pitch_mm=8, microstepping=32):
```

KHCO₃/CO₂ electroreduction for fuel cell applications

Reaction and reactor optimization, prototyping with 3D printing and automatic testing.

```
self.stp = Pin(stp_pin, Pin.OUT)
self.dir = Pin(dir_pin, Pin.OUT)
self.pow = Pin(pow_pin, Pin.OUT, value=0)
self.step_sleep_us = step_sleep_us
self.steps_per_mm = ((full_rev / step_angle) / pitch_mm) * mi-
crostepping
```

Power on the stepper motor

```
def power_on(self):
    self.pow.value(0)
```

Power off the stepper motor

```
def power_off(self):
    self.pow.value(1)
```

Set direction for the stepper motor

```
def set_direction(self, direction):
    self.dir.value(direction)
```

Rotate the stepper motor for the given steps

```
def rotate_steps(self, steps):
    for i in range(abs(steps)):
        self.stp.value(1)
        sleep_us(self.step_sleep_us)
        self.stp.value(0)
        sleep_us(self.step_sleep_us)
```

Rotate the stepper motor for the given millimetres

```
def rotate_mm(self, mm):
    self.power_on()
    self.rotate_steps(mm * self.steps_per_mm)
    self.power_off()
```

8. Results obtained with automatic system

Define class for start and stop valves and peristaltic pump

class Single:

```
def __init__(self, pin, engage_value=0, disengage_value=1):  
    self.pin = Pin(pin, Pin.OUT)  
    self.engage_value = engage_value  
    self.disengage_value = disengage_value  
    self.disengage()
```

Return the status of the component

```
def status(self):  
    return self.pin.value
```

Start/open the component

```
def engage(self):  
    self.pin.value(self.engage_value)
```

Stop/close the component

```
def disengage(self):  
    self.pin.value(self.disengage_value)
```

Activate the component for the given milliseconds

```
def activate(self, duration_ms):  
    self.engage()  
    sleep_ms(duration_ms)  
    self.disengage()
```

Define class for Endpoint

class Endpoint:

Define pin for Endpoint

KHCO₃/CO₂ electroreduction for fuel cell applications*Reaction and reactor optimization, prototyping with 3D printing and automatic testing.*

```
def __init__(self, pin):
    self.pin = Pin(pin, Pin.IN)

# Return status of Endpoint

def status(self):
    return self.pin.value()

# Create instance for steppers used for stirring
stirrer_stepper = Stepper(stp_pin=19, dir_pin=21, pow_pin=18)

# Create instance for steppers used for the autosampler
sampler_stepper = Stepper(stp_pin= 2, dir_pin= 4, pow_pin=15, step_sleep_us=10)

# Create instance for steppers used for the syringe_pump
syringe_stepper = Stepper(stp_pin=32, dir_pin= 5, pow_pin=33)

# Create instance for the peristaltic pump
perist_pump = Single(pin=26, engage_value=0, disengage_value=1)

# Create instance for the solenoid valve in cathode
catho_valve = Single(pin=27, engage_value=1, disengage_value=0)

# Create instance for the solenoid valve in anode
anode_valve = Single(pin=14, engage_value=1, disengage_value=0)

# Create instance for the Endpoint
endpoint = Endpoint(pin=25)
```

Define function for zeroing the autosampler

```
def zeroing_sampler():  
    sampler_stepper.set_direction(1)  
    sampler_stepper.power_on()  
    while endpoint.status() == 1:  
        sampler_stepper.rotate_steps(1)  
    sampler_stepper.power_off()
```

Define setup function to switch off all the components before every experiment

```
def setup():  
    stirrer_stepper.power_off()  
    sampler_stepper.power_off()  
    syringe_stepper.power_off()  
    perist_pump.disengage()  
    catho_valve.disengage()  
    anode_valve.disengage()
```

Define function for the stirring duration

```
def stiring(duration_ms):  
    stirrer_stepper.power_on()  
    stirrer_stepper.set_direction(1)  
    deadline = ticks_add(ticks_ms(), duration_ms)  
    while ticks_diff(deadline, ticks_ms()) > 0:  
        stirrer_stepper.rotate_steps(1)  
    stirrer_stepper.power_off()
```

Define function for the stirring duration

```
def sleep_ms(ms):  
    deadline = ticks_add(ticks_ms(), ms)  
    while ticks_diff(deadline, ticks_ms()) > 0:  
        pass
```

Define function for connecting the ESP32 to the Wi-Fi

KHCO₃/CO₂ electroreduction for fuel cell applications

Reaction and reactor optimization, prototyping with 3D printing and automatic testing.

```
def wifiConnect(ssid, password):
    station = network.WLAN(network.STA_IF)

    if station.isconnected():
        return station.ifconfig()

    if not station.active():
        station.active(True)

    station.connect(ssid, password)

    while not station.isconnected():
        pass

    return station.ifconfig()

setup()

ifconfig = wifiConnect('Eurecat_Lab', 'Eureca2021!')

print(ifconfig)

# Open the socket used to perform the communication between the ESP32 and the
server

socket = usocket.socket(usocket.AF_INET, usocket.SOCK_STREAM)
socket.bind(('', 3000))
socket.listen(5)

while True:
    conn, addr = socket.accept()
    payload = conn.recv(1024).decode('utf-8')
    command = payload.split('\r\n')[-1].split(' ')

    print(command)
```


8. Results obtained with automatic system

```
if command[0] == 'stiring':
    stiring(int(command[1]))

elif command[0] == 'autosampler':
    sampler_stepper.set_direction(int(command[1]))
    sampler_stepper.rotate_mm(int(command[2]))

elif command[0] == 'syringepump':
    syringe_stepper.set_direction(int(command[1]))
    syringe_stepper.power_on()
    syringe_stepper.rotate_steps(int(command[2]))
    syringe_stepper.power_off()

elif command[0] == 'valvecathode':
    catho_valve.activate(int(command[1]))

elif command[0] == 'valveanode':
    anode_valve.activate(int(command[1]))

elif command[0] == 'peristalticpump':
    perist_pump.activate(int(command[1]))

elif command[0] == 'autosampler_zeroing':
    zeroing_sampler()

conn.send('HTTP/1.1 200 OK\n')
conn.send('Content-Type: text/plain\n')
conn.send('Connection: close\n\n')
conn.sendall('Done')
conn.close()
```

7.8. Web for remote control programming with node

We applied online remote control to the automatic testing system. To do that, the commands were sent using socket communication over TCP

KHCO₃/CO₂ electroreduction for fuel cell applications

Reaction and reactor optimization, prototyping with 3D printing and automatic testing.

(Transmission control protocol) to the ESP32, via Wi-Fi connection, with the information to execute the necessary functions to move or activate the desired electronic components. The commands we want to execute are sent from a website interface. In that website there are two panels, one for the control of each electronic component individually (**Figure 67**), and the other one to program entire sequences of experiments (**Figure 68**). To monitor that all the components of the experiments are working fine, 3 cameras were installed (**Figure 69**).

System set up sequence

- Move Autosampler to residues channel position.
- Power on the peristaltic pump during 7500 ms to prefill with deionized water the tubing and eliminate air bubbles.
- Power on cathodic valve during 15000 ms to eliminate excess off deionized water.
- Power on anodic valve during 15000 ms to eliminate excess off deionized water.
- Power the syringe pump to prefill tubes with bicarbonate and eliminate air bubbles.
- Power on cathodic valve during 15000 ms to eliminate excess of bicarbonate.
- Power on anodic valve during 15000 ms to eliminate excess of bicarbonate.
- Move Autosampler to vial 1 position.

Reaction sequence

- Power the syringe pump to fill the reactor with 1.5ml of bicarbonate.
- Auto-clicking for power on the potentiostat and set electroreduction conditions through its software.
- Power on stirring motors if stirring is desired to apply and start the experiment.
- Auto-clicking for store the data obtained during the experiment.
- Power on cathodic valve during 15000 ms to sample products in cathodic compartment.
- Power on anodic valve during 15000 ms to sample products in anodic compartment.
- Move Autosampler to residues channel position.

Cleaning Sequence (repeat 3 times)

- Power on the peristaltic pump during 8250 ms to fill reactor with deionized water for cleaning.
- Power on stirring motors during 10000 ms to agitate the solution for better cleaning.
- Power on cathodic valve during 15000 ms to eliminate dirty cleaning water.
- Power on anodic valve during 15000 ms to eliminate dirty cleaning water.
- Move autosampler to next vial.

Set up next experiment sequence

(All sequence starts again)

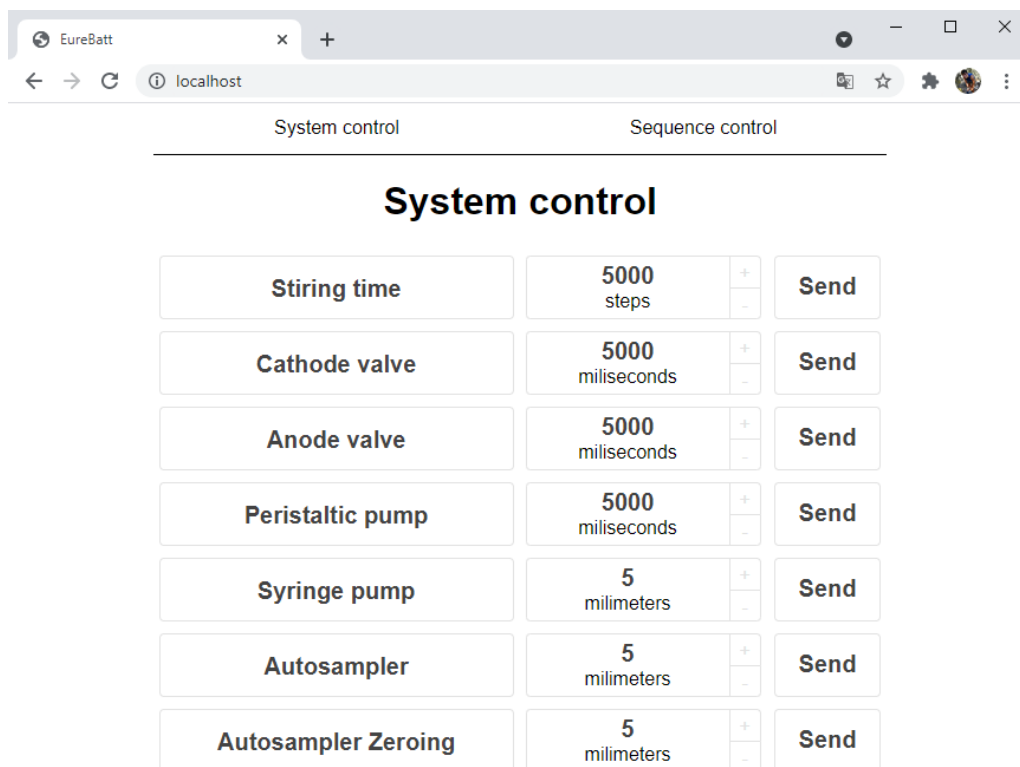
KHCO₃/CO₂ electroreduction for fuel cell applications*Reaction and reactor optimization, prototyping with 3D printing and automatic testing.*

Figure 67: Interface for individual control of the experiments.

8. Results obtained with automatic system

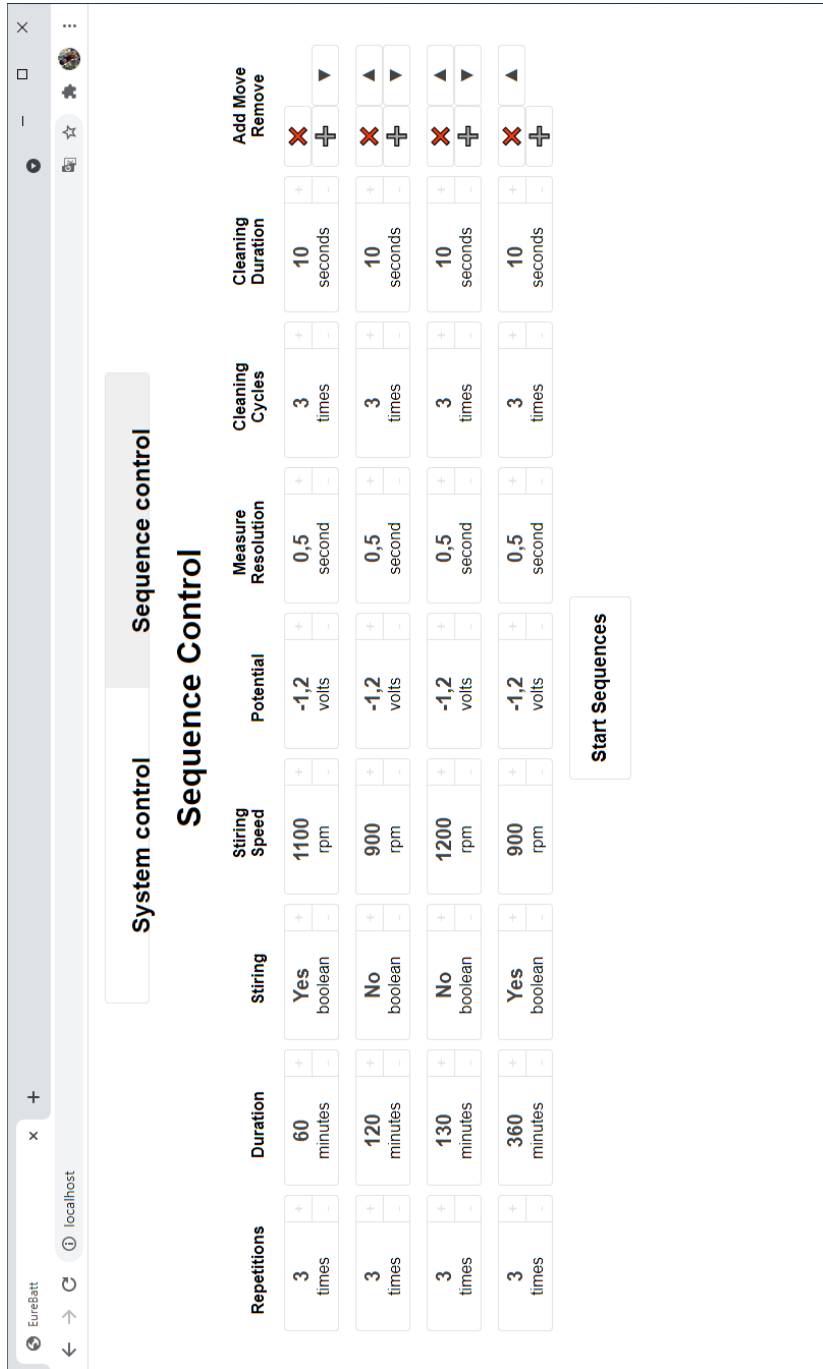


Figure 68: Interface for programming the sequences of the experiments.

KHCO₃/CO₂ electroreduction for fuel cell applications
Reaction and reactor optimization, prototyping with 3D printing and automatic testing.

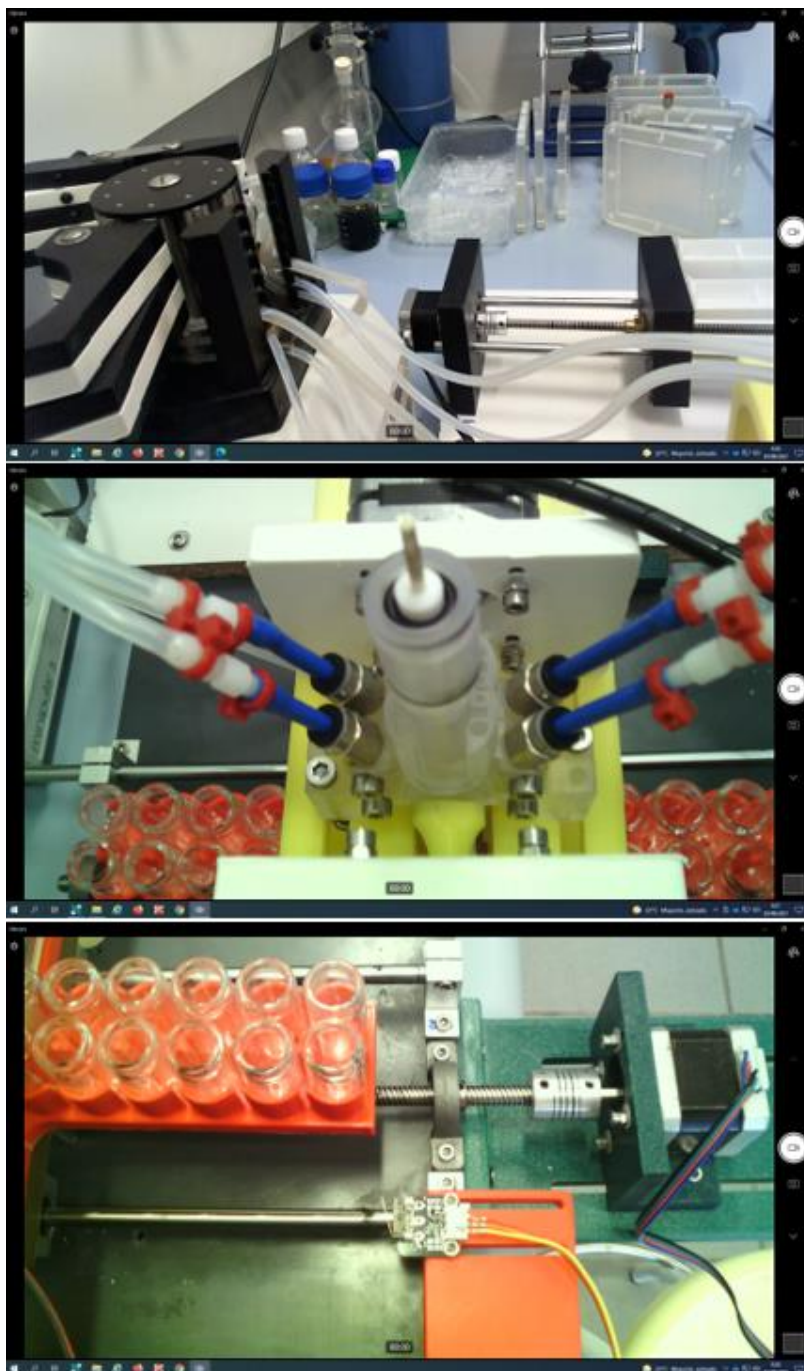


Figure 69: The 3 different real time views of the system using cameras.

7.9. Conclusions

In this section, we have demonstrated the possibility and the viability to automate some of the most repetitive and rutinary procedures in laboratory using simple 3D design/printing techniques, electronics, and programming. With that, the quality of the experimental data can be improved, by eliminating possible human error in repetitive actions, the rutinary work can done performed automatically and therefore we researchers can be concentrated in more intellectually demanding activities, and, finally, the productivity can be highly improved. Another important thing is the possibility to escalate this system to perform multiple experiments in parallel and obtain large quantities of data, necessary for a better interpretation of results and to apply machine learning and statistical models to get more insights.

KHCO₃/CO₂ electroreduction for fuel cell applications

Reaction and reactor optimization, prototyping with 3D printing and automatic testing.

8. AUTOMATIC SYSTEM TESTING

8. Results obtained with automatic system

This section contains the results for the electroreduction of bicarbonate using the designed automatic testing system on the tin (Sn) and Ceria based catalysts

KHCO₃/CO₂ electroreduction for fuel cell applications

Reaction and reactor optimization, prototyping with 3D printing and automatic testing.

8.1. Introduction

Nowadays we are starting to experience the fourth industrial revolution or also called automation revolution. A lot of different industries are trying to automate as much as possible the fabrication of products in order to increase their competitiveness in the market [88], obtaining great results [89].

In this section we want to demonstrate that it is possible to automate in a large extent some of the procedures used in laboratories by performing the electroreduction of bicarbonate using the automatic system described in **section 7**. Also, we are going to use the 3D printed reactor described in **section 6** to prove the viability and great advantages of 3D printed reactors in chemical and chemical engineering research. The data obtained in this experiment will be evaluated and compared to the data obtained using the home-made reactor without automation as described in **section 5**.

8.2. Experimental

8.2.1. Materials and Methods

In this section the same materials and bicarbonate as CO₂ source listed in **section 5** were used. As catalyst, tin (Sn) was also used, but, at the same time, a new ceria-based catalyst was evaluated. Those catalysts consisted of Cerium Oxide (CeO₂) ink coated on a carbon paper using a sprayer, that were doped with Copper and Nickel with different percentages as shown in **Table 15**.

8. Results obtained with automatic system

Table 15: List of ceria-based catalyst used.

Name of the sample	Abbreviation
CeO ₂ dopped with copper in 1 to 3 ratio	CeO ₂ -Cu(1/3)
CeO ₂ dopped with copper in 1 to 1 ratio	CeO ₂ -Cu(1/1)
CeO ₂ dopped with copper in 3 to 3 ratio	CeO ₂ -Cu(3/1)
CeO ₂ dopped with Nickel in 1 to 3 ratio	CeO ₂ -Ni(1/3)
CeO ₂ dopped with Nickel in 1 to 1 ratio	CeO ₂ -Ni(1/1)
CeO ₂ dopped with Nickel in 3 to 1 ratio	CeO ₂ -Ni(3/1)

For electroreduction experiments, the reference electrodes, a mini reference electrode for small volumes from NTS sensors was used, with a potential in front of the Ag/AgCl (3M KCl) of -0.045V. The counter electrode consisted in a platinum wire of 0.5mm of diameter and with 1cm length in contact with the solution. The working electrodes were in form of foil, supported in a 3D printed support as described in **section 6**.

Cyclic voltammetry was used to characterize the catalyst's electrochemical behaviour and was performed with the same conditions described in **Figure 30** and **Figure 31** in **section 5**. Also, the chronoamperometries were used to analyse the products obtained from the bicarbonate electroreduction as was done in **section 5**.

The reactor used is the final prototype presented in **section 6**, and the electroreduction conditions were the following:

- **Bicarbonate concentration:** 1.5 M
- **Catalyst 1:** Tin foil (Bulk), thickness: 0.5mm, reactive surface: 1cm²
- **Catalyst 2:** Ceria-based catalysts described in **Table 15**.
- **Stirring:** No

KHCO₃/CO₂ electroreduction for fuel cell applications*Reaction and reactor optimization, prototyping with 3D printing and automatic testing.*

- **Electroreduction time:** 1 h
- **CO₂ saturation:** No
- **Potential:** -1.2 V
- **Scan rate:** 0.1 V/s

8.3. Results and discussion

8.3.1. Electroreduction with Tin catalysts

The cyclic voltammetry performed with the new 3D printed mini reactor is like the one obtained with the workshop-made reactor, but with higher current densities **Figure 70**. This is due the reduced resistance between the counter and working electrode.

The first set of experiments were performed with a Tin foil pre-oxidated on atmospheric air during 24h. The chronoamperometries show that the first experiments present significantly higher current density than the later repetitions of the same experiment (**Figure 71**). This is due to the oxide layer generated on the tin foil when it is exposed to air. On the contrary, the catalyst in later experiments, due the automatic cleaning, is not exposed to the air, because it remains into the reactor, which is filled by cleaning water between experiments. Therefore, they are not in contact with atmospheric air and can't regenerate this oxide layer. This observation highlights the importance of the tin oxide layer for increasing the current density during electroreduction reactions [80]. Without the automatic system, this factor was not observed, as the catalyst was removed by hand from the reactor in order to clean the reactor between the experiments. This was generating repetitions of experiments with a lot of different current densities due to

8. Results obtained with automatic system

the difficulty of controlling the quantity of oxide regenerated during the manual cleaning procedure.

To confirm the possibility that this higher current density obtained in repetition 1 is due the oxide layer, we performed another set of experiments with a new non-treated and non-peroxidised Tin foil. The results obtained (**Figure 72**), show that the first experiment presents only slightly higher intensity than the later consecutive repetitions, possibly due to oxidation residues, but is still significantly lower than the ones obtained when the foil is pre-oxidated during 24h.

To test the regeneration of the oxide layer in between experiments, another set of experiments was performed. These experiments consisted in applying a positive potential (+0.5 V) during 5min to the electrodes in between experiments to re-oxidize the Tin. However, the chronoamperometries showed that the oxide layer was barely regenerated, as shown in **Figure 73**. This could be due that the oxide produced is not the same as the one that is spontaneously produced by atmospheric oxygen or because the oxide is getting detached from the foil. Nevertheless, there was no oxide dust observed in the bottom of the reactor. The other option is that 5 min of oxidation is not enough to significantly regenerate the oxide layer. Larger times and different oxidative potentials would need to be tested.

These results show that is not possible to perform repetitions of the same experiment because the oxide layer is reduced during the electroreduction, and consequently, the catalytic activity of the catalyst decreases over time. Therefore, it is necessary to perform experiments at potential values higher than -0.9 V because it's important to not damage this layer.

KHCO₃/CO₂ electroreduction for fuel cell applications

Reaction and reactor optimization, prototyping with 3D printing and automatic testing.

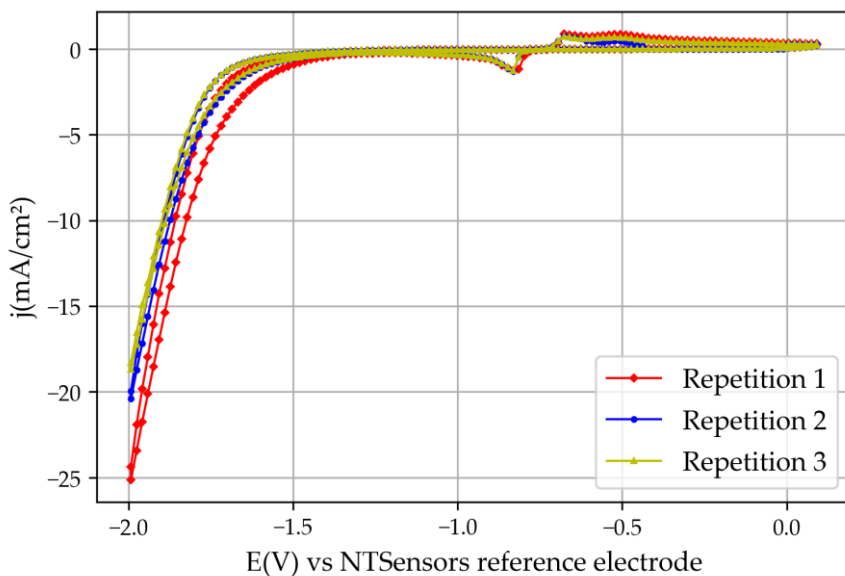


Figure 70: Three repetitions of CV's using Tin catalysts and automatic system.

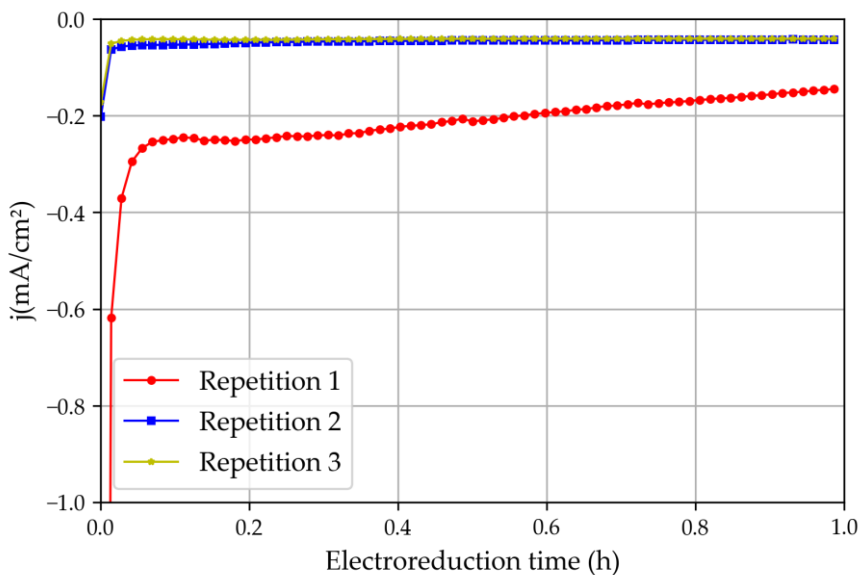


Figure 71: Three repetitions of chronoamperometries using non-treated Tin catalysts oxidized in atmosphere and the automated system.

8. Results obtained with automatic system

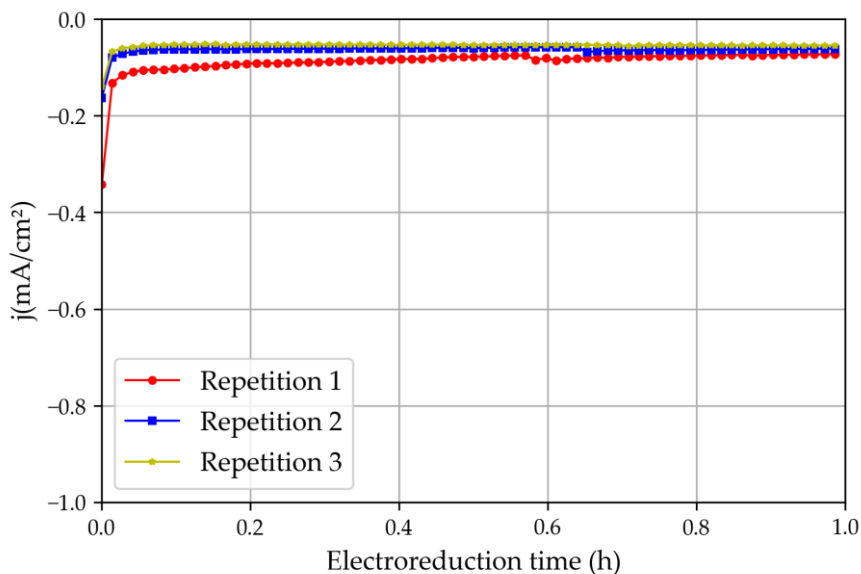


Figure 72: Three repetitions of chronoamperometries using new Tin catalysts non-oxidized in atmosphere and automatic system.

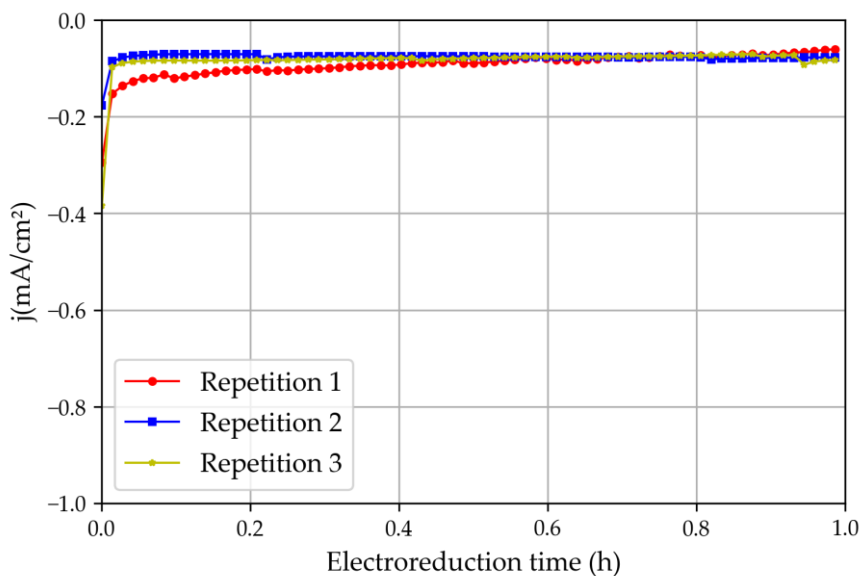


Figure 73: Three repetitions of chronoamperometries using pre-treated Tin catalysts and automatic system.

KHCO₃/CO₂ electroreduction for fuel cell applications

Reaction and reactor optimization, prototyping with 3D printing and automatic testing.

8.3.2. ESEM characterization of ceria-based catalysts

The ESEM with elemental mapping characterization of those catalysts can be seen in **Figure 74**, where different dispersions of the elements can be observed. The nickel penetrates more into the carbon paper while copper remains on the surface. That may be due the larger atom radius of copper in front of nickel.

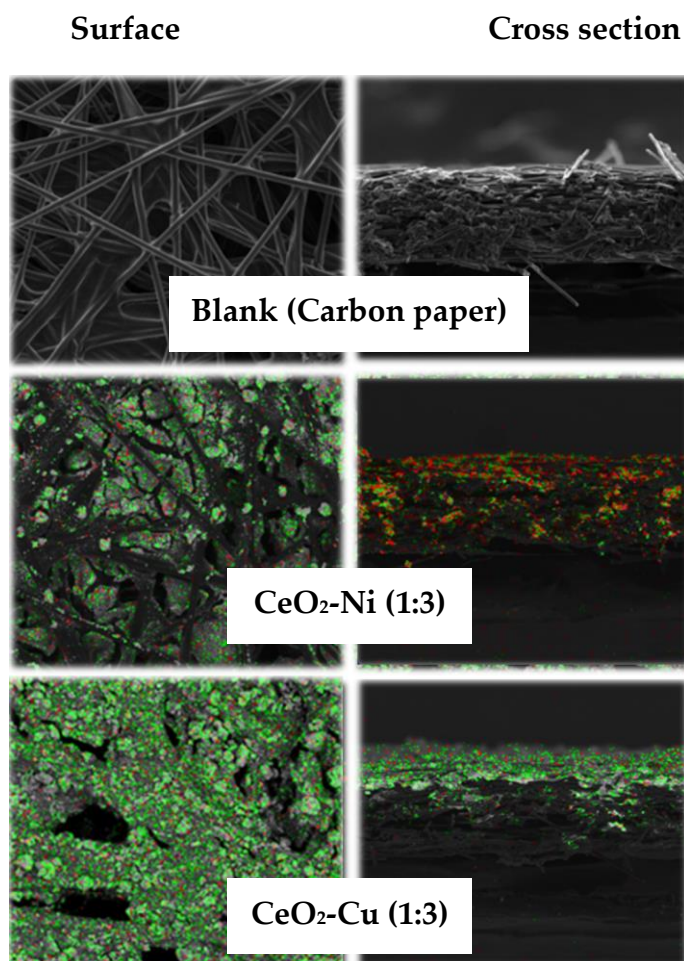


Figure 74: ESEM images of Ceria catalysts doped with Ni, Cu and blank. The green dots correspond to the CeO₂ while red dots represent the Ni and Cu atoms respectively.

8.3.3. Electroreduction with Ceria catalysts

Experiments with Ceria-based catalyst listed in **Table 15** were performed using the same reactor and the same conditions as the experiments performed with tin catalysts. The CVs shows lower current density for the raw CeO₂ (Blank) but significantly higher ones for the doped one (**Figure 75** and **Figure 76**). The current density increases directly with the percentage of copper (**Figure 75**), similarly to the nickel doped catalysts (**Figure 76**), obtaining quite equivalent results between them.

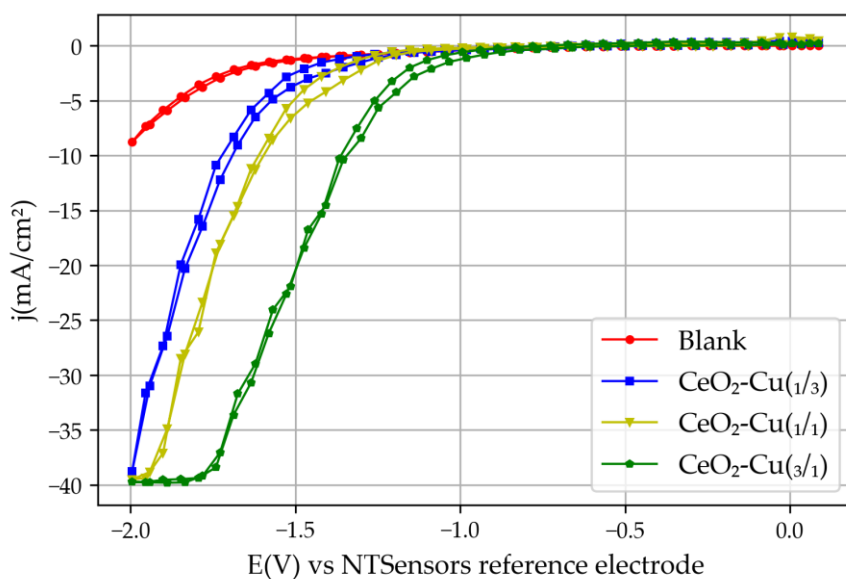


Figure 75: Cyclic voltammety of using copper doped Ceria catalysts performed with automatic system.

KHCO₃/CO₂ electroreduction for fuel cell applications

Reaction and reactor optimization, prototyping with 3D printing and automatic testing.

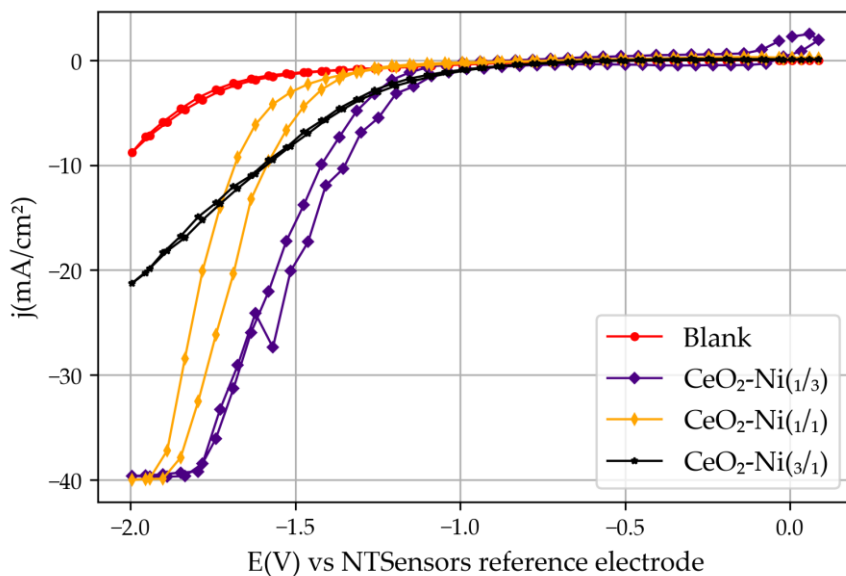


Figure 76: Cyclic voltammometry of using Nickel doped Ceria catalysts performed with automatic system.

The electroreduction of bicarbonate using Ceria-based catalysts was also performed in the same conditions as for the Tin catalysts. The chronoamperometries show an irregular current intensity due to the high number of bubbles formed (**Figure 77**). This irregularity makes difficult to analyse which one is more active. Therefore, is necessary to perform experiments at lower electrical potential in the future, to avoid bubble formation. The high number of bubbles formed suggest that most products are gases.

8. Results obtained with automatic system

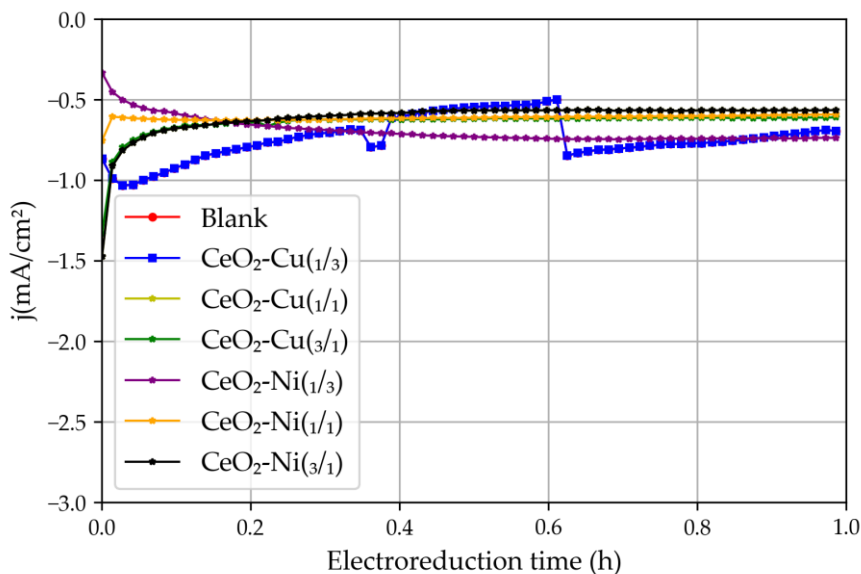


Figure 77: Chronoamperometry of all the Ceria-based catalysts performed with automatic system.

8.3.4. Characterization of products using NMR

For the characterization of the products, NMR was used, as described in **section 5**. The NMR analysis of the products obtained in the cathodic compartment for the experiments performed with tin catalyst show three visible peaks at the following positions **8.44**, **2.71** and **1.9 ppm**, corresponding to formate proton, DMSO (internal standard) and acetic proton (**Figure 78**). The integration of the peaks and its corresponding comparison with the internal standard gives a faradaic efficiency between 20 to 25 % towards formic acid, which is slightly higher than the one obtained in experiments performed with workshop made reactor in **section 5**. Moreover, here the potential used was slightly lower, -1.2 V instead of the -1.6 V used in previous experiments. Differently from the previous experiments, at this point a small amount of acetic acid was obtained, with an efficiency

KHCO₃/CO₂ electroreduction for fuel cell applications*Reaction and reactor optimization, prototyping with 3D printing and automatic testing.*

of around 7 %. As expected, the proton NMR for the last repetition of experiments (**Figure**) shows that there is much lower concentration of formic acid and acetic acid (below the detection limit) due the reduction of the oxide layer as we commented in the previous section.

The proton NMR analysis for the anodic compartment shows that there is small amount of formic acid and acetic acid there **Figure 79**. Therefore, it indicates that small those products are crossing the Nafion membrane as expected [90].

Finally, the proton NMR analysis of the samples obtained with Ce-ria-based catalysts shows that no liquid products are obtained using those catalysts **Figure 80**. Reinforcing the previous hypothesis, that most of the produced products are gases.

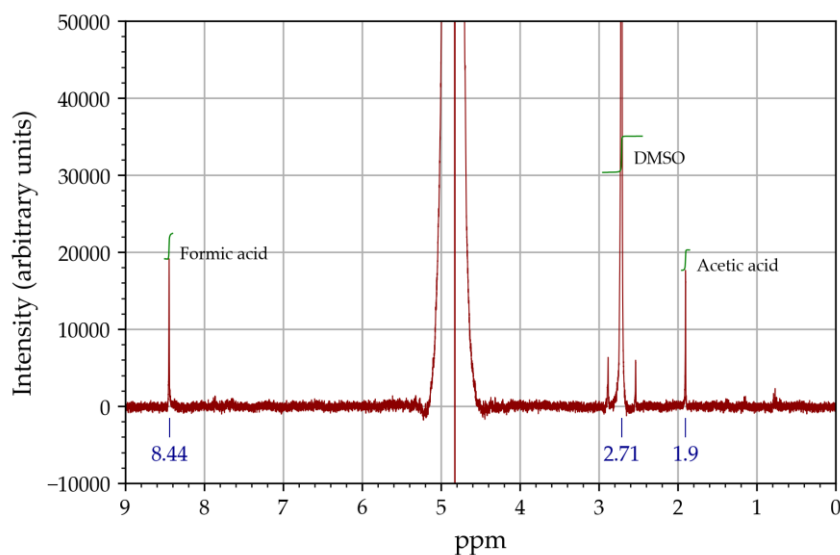


Figure 78: NMR spectra of the products obtained in the first repetition of electroreduction experiments using tin catalyst in cathodic compartment.

8. Results obtained with automatic system

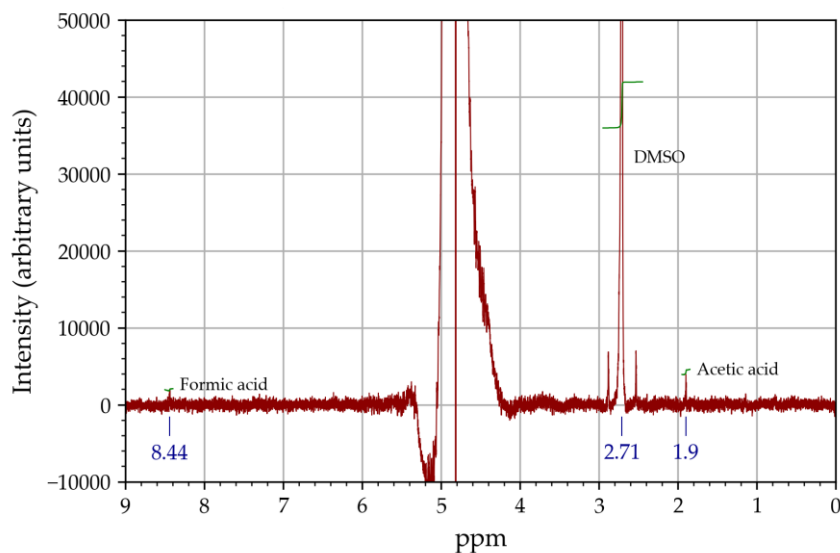


Figure 79: NMR spectra of the products obtained in the third repetition of electroreduction experiments using tin catalyst in cathodic compartment.

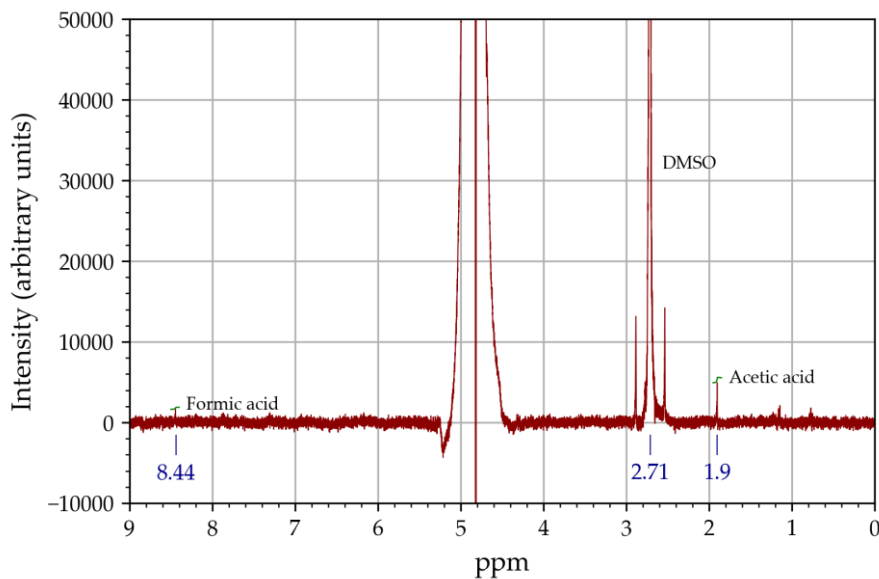


Figure 79: NMR spectra of the products obtained in the first repetition of electroreduction experiments using tin catalyst in anodic compartment.

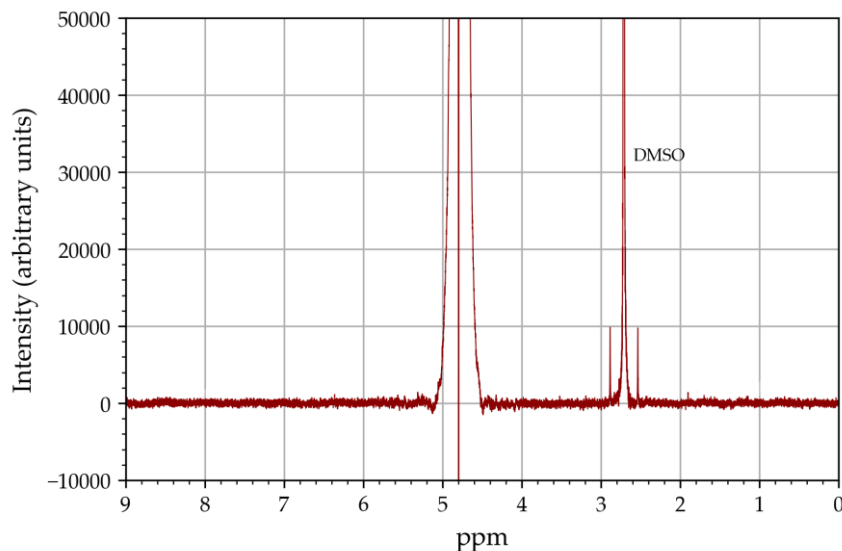
KHCO₃/CO₂ electroreduction for fuel cell applications*Reaction and reactor optimization, prototyping with 3D printing and automatic testing.*

Figure 80: NMR spectra of the products obtained for the electroreduction experiments using Ceria-based catalysts in cathodic compartment.

8.5. Conclusions

The automatic testing of electroreduction catalysts is possible, obtaining results similar or even better than non-automated experiments. This opens a door to the massive testing of electrocatalysts, the real time monitoring of parameters and the implementation of machine learning to get more insights.

8. Results obtained with automatic system

KHCO₃/CO₂ electroreduction for fuel cell applications

Reaction and reactor optimization, prototyping with 3D printing and automatic testing.

9. DIRECT FORMATE/FORMIC ACID FUEL CELL

***Based on:** Adrianna Nogalska, Andreu Bonet Navarro, Ricard Garcia-Valls, *MEA Preparation for Direct Formate/Formic Acid Fuel Cell – Comparison of Palladium Black and Palladium Supported on Activated Carbon Performance on Power Generation in Passive Fuel Cell*, *Electrochem 2* (20201) 64-70.

9. Results obtained with automatic system

In this section, the performance of membrane electrode assemblies (MEA's) using supported palladium on activated carbon (PdC) and unsupported palladium black (PdB) as catalyst with HCOOH and HCOOK solutions is tested.

KHCO₃/CO₂ electroreduction for fuel cell applications

Reaction and reactor optimization, prototyping with 3D printing and automatic testing.

9.1. Introduction

Nowadays, the capture and conversion of CO₂ has become a main social, economic, and technologic priority due to the climate change emergency. For CO₂ removal to become cost-effective, it is necessary to develop strategies to convert it into usable products. One of the simplest and arguably less energy-demanding CO₂ reduction paths involves its conversion to formic acid. This way, renewable energy, which is intermittent and unpredictable, could be stored as formic acid without any additional CO₂ released into the atmosphere. Despite being easy to transport and store for long times, the use of formic acid in fuel cells has rarely been investigated as compared to hydrogen and direct alcohol fuel cells, probably due to its energy density (2.1 kWh/L) which is lower than that of methanol (5.9 kWh/L). However, formic acid has numerous advantages: (i) it is a non-flammable liquid at ambient temperature, (ii) allows for easy storage and (iii) the formic acid cross over the proton exchange membrane is six times lower compared to methanol [91], that means that it provides better mass transport improving energy density [90]. The disadvantage of the acid over its salt is its corrosive nature. This can be overcome by use of salt, such as potassium formate, with the same high theoretical cell potential (1.45 V) and fast oxidation kinetics. Thus, the potential use of formate salt in fuel cells has gained a lot of attention in the scientific community [92].

The heart of the fuel cell, specifically the proton exchange membrane fuel cell, is the membrane-electrode assembly. It is a combination of the gas diffusion layers and catalysts for redox reactions on the anode and cathode with a proton exchange membrane in a sandwich structure [93]. The selection of the catalyst is crucial and mainly depends on the fuel used in the system.

9. Results obtained with automatic system

Gao et al. [94] studied the possible use of a blended fuel of formate and formic acid on platinum. The authors show that the mechanism of the oxidation of mixed fuel is through direct oxidation, while HCOOH alone undergoes oxidation through an indirect mechanism that can lead to poisoning. Still, they reported achieving higher current densities when using formate compared to the acid alone. Initially, researchers were using platinum catalyst for the formate/formic acid oxidation, as it is used in direct alcohol fuel cells, yet studies show that palladium has better performance, it is cheaper (according to prices of metal catalysts in Sigma Aldrich on October 2020) and it is rarely poisoned by CO, increasing the stability of the catalytic reaction. Bartrom et al. [95] found that formate oxidizes rather efficiently and with no strong bound intermediate on palladium. Catalysts are often supported on activated carbon providing a high contact area, excellent electron conductivity, and improved mass transfer allowing lowering of noble metal usage [96]. Palladium, when supported on activated carbon, can give high reactivity with highly concentrated HCOOH [97].

The main objective of this work is to compare the performance of passive, air breathing formate/formic acid fuel cells using two catalysts, palladium black and palladium supported on activated carbon, with two different fuels, HCOOH and HCOOK, at ambient conditions (25° C, 1 bar) using low fuel concentration (1 M) to demonstrate which catalyst is most efficient for future commercialization under those conditions. The performance towards formate/formic acid oxidation in a fuel cell system was evaluated by polarization curves followed by constant current discharge. Moreover, X-ray diffraction of the catalysts was performed to describe their crystalline structure, size and to understand the catalysis mechanism.

KHCO₃/CO₂ electroreduction for fuel cell applications

Reaction and reactor optimization, prototyping with 3D printing and automatic testing.

9.2. Experimental

9.2.1. Materials

Parts of membrane electrode assembly (MEA), such as: Toray paper 060, TGP-H-060, as gas diffusion layer (GDL); Nafion membrane 117; and cathode, cloth gas diffusion electrode (GDE) 4 mg/cm² PtB; were purchased from Fuel Cell Store (<https://www.fuelcellstore.com/>, College Station, TX, USA). Both catalysts, palladium black (surface area 40–60 m²/g, 99.95% trace metals basis) and palladium on carbon (extent of labelling: 30 wt.% loading, matrix activated carbon support), and Nafion glue (Nafion 117 solution 5% in a mixture of lower aliphatic alcohols and water) were purchased from Sigma Aldrich (Madrid, Spain). Isopropanol used in catalytic ink preparation was purchased from Scharlau (Barcelona, Spain). Hydrogen peroxide 30% (*v/v*) (Sigma-Aldrich, Madrid, Spain) and 95–97% H₂SO₄ (Serviquimia, Tarragona, Spain) were used to prepare cleaning solutions for the Nafion membrane. Potassium formate (reagent plus 99%) and formic acid (for synthesis) used as fuels were purchased from Sigma Aldrich (Madrid, Spain).

9.2.2. Methods and reagents

Figure 81 shows a schematic description of the membrane electrode assembly preparation starting from the catalyst application. The anode was prepared by air brushing (3 bar) of Pd-based catalyst, PdB or PdC, on 9 cm² of a 16 cm² previously cleaned Nafion membrane, following the procedure described in section 5.2.2, to create a catalyst coated membrane (CCM). The catalytic ink was composed of palladium catalyst wetted by Milli-Q water, 2-propanol and Nafion glue. The solid part was 6% wt of the total ink while the catalyst to Nafion proportion was 10:1.

9. Results obtained with automatic system

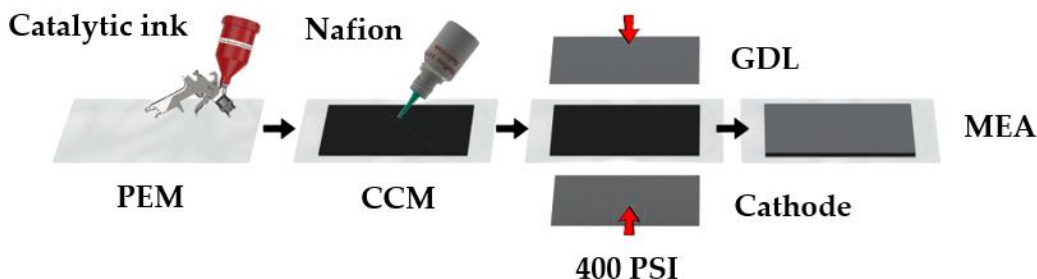


Figure 81: Schematic illustration of membrane electrode assembly (MEA) fabrication.

Before the deposition, the ink was sonicated (Ultrasons Selecta 3000683 (Selecta, Barcelona, Spain), 50/60 kHz, 110 W) for 30 min. For the MEA preparation, (i) Toray carbon paper (9 cm² GDL), (ii) anode CCM (Nafion membrane 16 cm² containing sprayed catalyst of 9 cm²) and (iii) commercial cathode (cathode cloth GDE 4 mg/cm² PtB) were glued with (iv) 100 μL of Nafion 117 solution 5% and pressed for 2 h with 400 psi. The pressure was applied by a manual home-made system (**Figure 82**) which consisted of two plates of high hardness material, held by treated rods in through holes at four opposite points (1). Inside the two plates is the load cell (2) with the flat-surface lug (3), and an additional part (4) of the same dimensions as the lug. The MEA placed between the additional piece and the stud is compressed by adjusting the screws always in cross and measuring the value of the force exerted through the compression SENSING, S.L (AEP transducers, Modena, Italy) device connected in port (5). Once the required value is reached, the cell display can be disconnected.

KHCO₃/CO₂ electroreduction for fuel cell applications

Reaction and reactor optimization, prototyping with 3D printing and automatic testing.

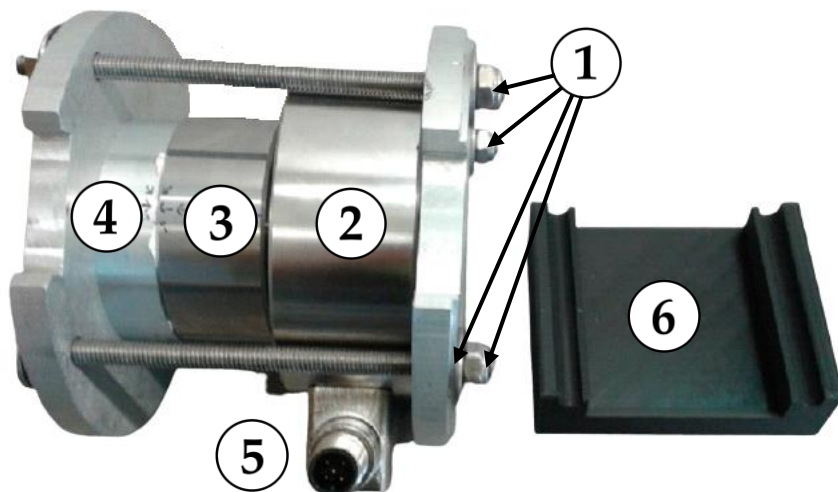


Figure 82: Home-made system for MEA fabrication.

In all measurements, either 1.0 M formic acid or 1.0 M potassium formate were used as fuel source on the anode side with capacity of 7.2 mL in the passive fuel cell (**Figure 83**), consisting of a cathodic compartment (**1**) (PMMA) with air entrance, stainless steel current collectors (**2**) covered with silicon gasket, anodic compartment (**3**) and MEA (**4**) (PMMA). Ambient air was used as oxygen source for the cathodic compartment. Fuel cell Monitor 3.0 (<https://www.fuelcellstore.com>) was used for the electrochemical characterization of fuel cells. Polarization and corresponding power generation curves were obtained through automatic mode starting from open circuit potential (OCP), whereas the constant-current discharge was measured in manual mode. The working current in galvanostatic conditions was chosen at maximum power point based on the characteristic polarization curves of each system. Additionally, we performed measurements on 20 mA in all systems (3 mA/mg for PdB; 10 mA/mg for PdC). The galvanostatic tests were stopped when cell voltage reached 0.00 V. All measurements were performed at 25°C and 1013 hPa. The cells were cleaned with Milli-Q

9. Results obtained with automatic system

water and 1% H₂SO₄ between experiments. Current and power density were normalized by weight of palladium for better interpretation of results.

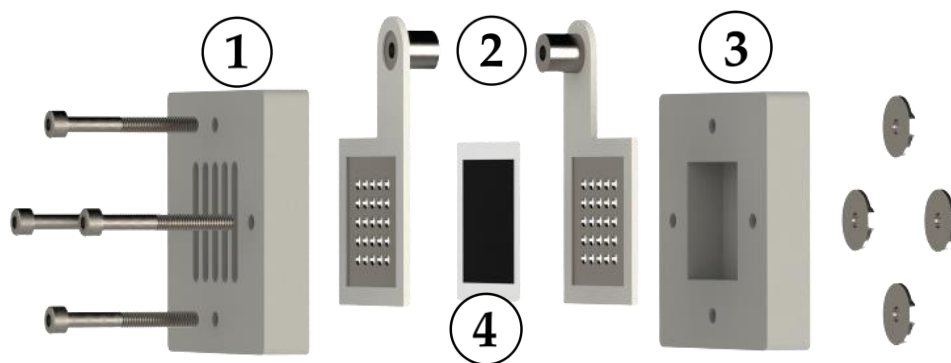


Figure 83: 3D render of an exploded view of fuel cell.

The power production efficiency was calculated based on the theoretical faradic efficiency of conversion and experimental results from galvanostatic measurements by integration of the power vs. time function. Theoretically, the maximum energy our cells could produce was 0.5092 Wh with 100% efficiency. As the fuel cell (FC) system is passive, air breathing and functioning under ambient conditions, the faradic efficiency of conversion is equal to the overall energy efficiency [98]. The characterization of palladium catalysts crystalline structures was done by X-ray diffraction (XRD) (Siemens D5000 diffractometer; Bragg-Brentano para focusing geometry and vertical θ - θ goniometer, Aubrey, Texas, USA). The angular 2θ diffraction range was between 5 and 70°. Data was collected with an angular step of 0.05° at 3 s/step and sample rotation. CuK α radiation was obtained from a copper X-ray tube operated at 40 kV and 30 mA. Obtained spectra were analysed with High Score Plus software. Based on the obtained diffractograms, particles size was calculated with TOPAS 6.1 software.

KHCO₃/CO₂ electroreduction for fuel cell applications*Reaction and reactor optimization, prototyping with 3D printing and automatic testing.***9.3. Results and discussion**

All the parameters of the fuel cell tests are gathered in **Table 16**. The experiments were performed in passive mode and ambient conditions with no additional energy consumption. Moreover, the use of Nafion glue for the MEA preparation and use of home-made manual pressing system allowed not using heat, contributing to the decrease in the energy consumption.

Table 16: Fuel cell parameters

Parameter	Value
Fuel cell nature	Passive
Anode	PdC or PdB, 1 mg/cm ²
PEM	Nafion 117
Cathode	PtB, 4 mg/cm ²
Catalyst effective area	9 cm ²
Fuel	HCOOH/HCOOK 1 M, 7.2 mL
Oxygen source	Ambient air
Conditions	25°C, 1013 hPa

Palladium black (PdB), was just precipitated palladium, while PdC corresponds to 30% of palladium supported on activated carbon. **Figure 84** presents the X-ray diffractograms of the two commercial catalysts. The analysis confirmed the typical face centred cubic structure of crystalline palladium particles [99]. Diffraction peaks at $2\Theta = 40.2, 46.6$ and 67.9 , which represent the Bragg reflections from the (111), (200) and (220) planes, which are present in the diffraction patterns of both diffractograms. PdB gives higher intensity, probably because of its purity. Activated carbon was found to have a highly amorphous state and low crystallinity [100], thus it

9. Results obtained with automatic system

was not detected with XRD. Furthermore, the size of the catalyst's particles was calculated to be 7.8 ± 0.2 and 7.1 ± 0.1 nm for PdB and PdC, respectively, thus larger size and the same larger surface area should have a positive impact on the PdB performance.

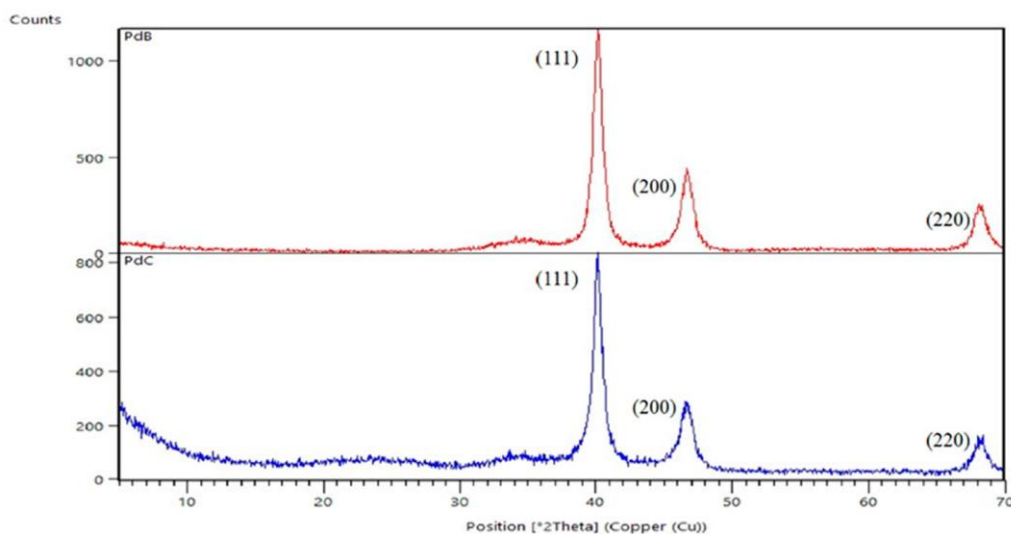


Figure 84: Diffractograms of catalysts.

Elnabawy et al. [101] studied the selectivity of platinum and palladium catalysts towards formic acid oxidation to CO₂. The suggested anodic reaction mechanisms are depicted in Figure 85: direct via formate (**blue**), direct via carboxyl (**black**) and indirect via carboxyl (**red**) through CO*. Pd (100) is mainly catalysing the reaction through carboxyl and might get slightly poisoned by CO* but it does not lead to permanent deactivation due to its easy removal from the surface. Pd anodes generally offer lower tendency to get poisoned by CO* than Pt anodes. On the other hand, Pd (111) can catalyse the reaction through both paths, formate and carboxyl; however,

KHCO₃/CO₂ electroreduction for fuel cell applications

Reaction and reactor optimization, prototyping with 3D printing and automatic testing.

the formate group becomes stabilized and, as result, the HCOO* path has a higher contribution to the overall activity on Pd (111).

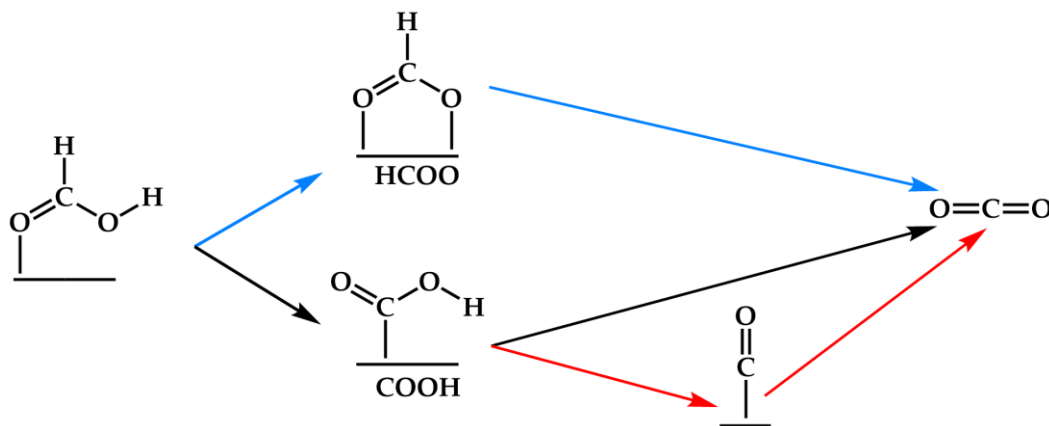


Figure 85: A general formic acid oxidation mechanism on Pd and Pt anodes of direct formic acid fuel cells (DFAFCs) by Elnabawy et al. Reproduced from [101].

Performance results of the prepared MEAs with different fuels in terms of polarization curves are shown in **Figure 86** based on the polarization curves we can say that PdC performs better in OCP and gives higher current density as well. This might be ascribable to the better gas transport properties of PdC. The use of activated carbon for the Pd support provides a high contact area between catalyst and reagents. Additionally, PdC particles are much smaller than PdB and they contain only 30% of palladium on their surfaces. When we sprayed unsupported palladium, we noticed that it tends to agglomerate, and to confirm that, the suspensions were sonicated an exaggerated time (2h) to be able to appreciate the aggregation of particles of unsupported catalyst with naked eye (**Figure 87**). That aggregation may cause an increase in the mass transfer resistance of gasses and fuels, which agrees with the literature [102] [103].

9. Results obtained with automatic system

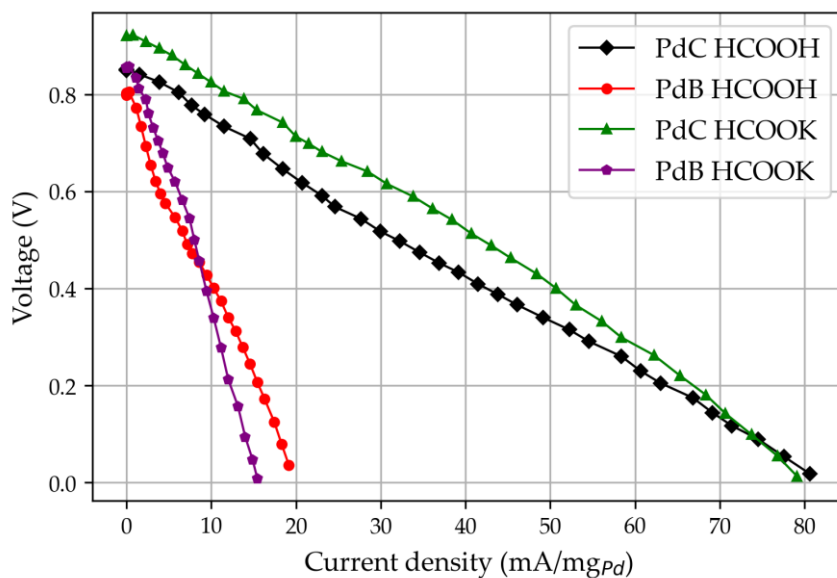


Figure 86: Polarization curves of the developed formate/formic acid fuel cells.



Figure 87: Comparison of homogeneous dispersion of catalyst in inks.

KHCO₃/CO₂ electroreduction for fuel cell applications*Reaction and reactor optimization, prototyping with 3D printing and automatic testing.*

Table 17 includes the open circuit potential values of all studied cases derived from **Figure 84**.

The electrochemical potential of formic acid (or formate salt) oxidation reaction (*Eq. 6*) in **section 3** is 1.45 V

Table 17. Theoretical reaction potential and measured open circuit potentials of the studied cells.

Theoretical Potential (V)	PdC OCP (V)		PdB OCP (V)	
	HCOOH 1 M	HCOOK 1 M	HCOOH 1 M	HCOOK 1 M
1.45	0.85	0.92	0.8	0.85

Despite the theoretical OCP being 1.45 V, according to the net reaction of formate/formic acid oxidation (*Eq. 6*), the experimental results were lower. This difference between the theoretical potential value and the measured value is imputable to the use of air as oxygen source instead of pure oxygen as the catalyst type should not influence the OCP. Moreover, HCOOK has a slightly higher OCP compared to the acid for both studied catalysts. The better performance of the salt might be a result of its higher dissociation. Indeed, the dissociation constant for HCOOK is 0.19 mol/dm³, while for HCOOH it is only 1.46×10^{-4} mol/dm³ [104]. Based on XRD analysis we state that both catalysts used in this study are Pd (111) where formate anions are precursors for the oxidation reaction.

Figure 88 includes the values of power density as a function of current density for all studied FC configurations. Additionally, in **Table 18** all

9. Results obtained with automatic system

data of maximum power peak is gathered based on the cell performances from *Figure 88*. Once again, the use of PdC results in better performance and higher power density compared to PdB. The maximum power peak with PdC appears at similar current density for both fuels, with the peak being higher for HCOOK. Thus, from a kinetic standpoint, its oxidation reaction is clearly more favourable. PdB reveals the opposite tendency: the maximum power density is almost equal for both studied fuels, but the current density on the peak is higher for HCOOH.

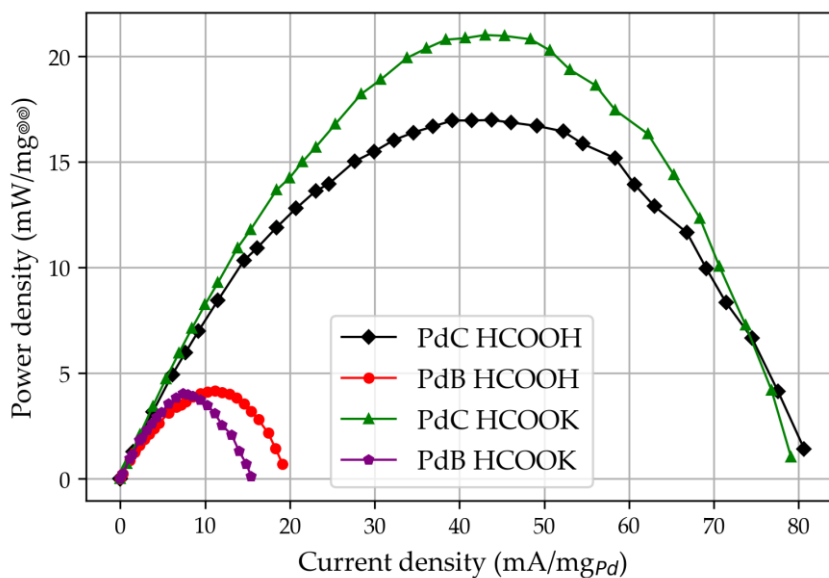


Figure 88: Formate/Formic acid fuel cells performance.

KHCO₃/CO₂ electroreduction for fuel cell applications*Reaction and reactor optimization, prototyping with 3D printing and automatic testing.***Table 18:** Formate/formic acid fuel cells' maximum power peak data.

Catalyst	PdC		PdB	
	HCOOH	HCOOK	HCOOH	HCOOK
Fuel (7.2 mL, 1 M)				
Power max (mW/mgPd)	16.99	21.01	4.17	4.04
Current at PM (mA/mgPd)	36.87	43.01	11.15	7.43

Table 19 represents the comparison of obtained results of power density normalized to catalyst area with literature findings. It summarizes the results of the formate/formic acid fuel cells working in different conditions, such as temperature, oxygen source or fuel concentration and addition of supporting electrolyte in the form of an alkaline solution. In our system, we are evaluating the performance of an FC in very mild and ambient conditions using a fuel of low molarity without an electrolyte, and we could still detect power even with an amount of catalyst as low as 1 mg/cm². Considering that no additional energy was used for solution circulation, pure oxygen pumping or heating it is a promising start for development of self-sufficient fuel cells for CO₂ recycling.

9. Results obtained with automatic system

Table 19: Comparison of obtained results with literature findings.

Cathode	Anode (mg/cm ₂)	Membrane	Max. Power Density (mW/cm ₂)	T (°C)	Fuel and C (M)	O ₂ Source	Ref
Fe-Co	Nano-Pd/C, 4	Commercial anion-	258	60	4M HCOOK / 4M KOH	Pure O ₂	[98]
Fe-Co	PdC, 2	Quaternized polysulfone	130	80	5 M HCOOK	Pure O ₂	[104]
PtB	PdB, 4	Polymer anion ex-	105	60	1 M HCOOK	Air (21%)	[95]
PtC	PdC, 4	Cation-exchange	300	25	1 M HCOONa /3 M NaOH	H ₂ O ₂	[105]
PtC	PdC, 2	Nafion mem-	103	45	3 M HCOOH	Pure O ₂	[106]
PtC	PdC, 2	Nafion mem-	5.6	25	1 HCOOK	Air (21%)	This work

KHCO₃/CO₂ electroreduction for fuel cell applications*Reaction and reactor optimization, prototyping with 3D printing and automatic testing.*

Moreover, power generation experiments were carried out to assess the performance of developed FCs in time. Performing the power generation experiments in constant current discharge, at maximum power peak, leads to unstable measurements due to fast potential losses [107]. Mikolajczuk et al., proved the hypothesis that in high current densities the reaction never reaches the steady state, and the CO₂ bubble production is very fast, which leads to blocking of access of fuel to catalyst and deactivates the catalyst. To verify this assumption, in addition to the measurements at maximum power current, we performed experiments at 20 mA and indeed we observed higher efficiency in all studied cases (*Figure 89*).

Figure 89 reports the values obtained for all studied fuel cells' configurations in power generation studies. As expected, based on polarization curves (**Figure 88** and **Figure 87**), PdB has an overall lower efficiency of constant current discharge compared to PdC. On the other hand, the salt had high power density and current density but the energy production efficiency in constant current discharge was much lower. The FC efficiency is limited by the catalyst's activity, fuel dissociation state and by the solute conductivity. Above we showed that the dissociation of the salt is higher than the acid's, thus these differences can be assigned to the conductivity of cations. Indeed, limiting ion conductivity at 298.15 K of K⁺ is 73.50 S·cm²/mol, which is much lower than the one of H⁺ which is 349.85 S·cm²/mol [108]. Thus, even though the salt can be dissociated more easily, the overall power generation in time will be lower. Boncina et al. [108] observed that the molar conductivity of the salt does not change with its concentration, while for acid it exponentially decreases with the increase of molarity. This means that lower energy generation of salt could be compensated with a higher concentration.

9. Results obtained with automatic system

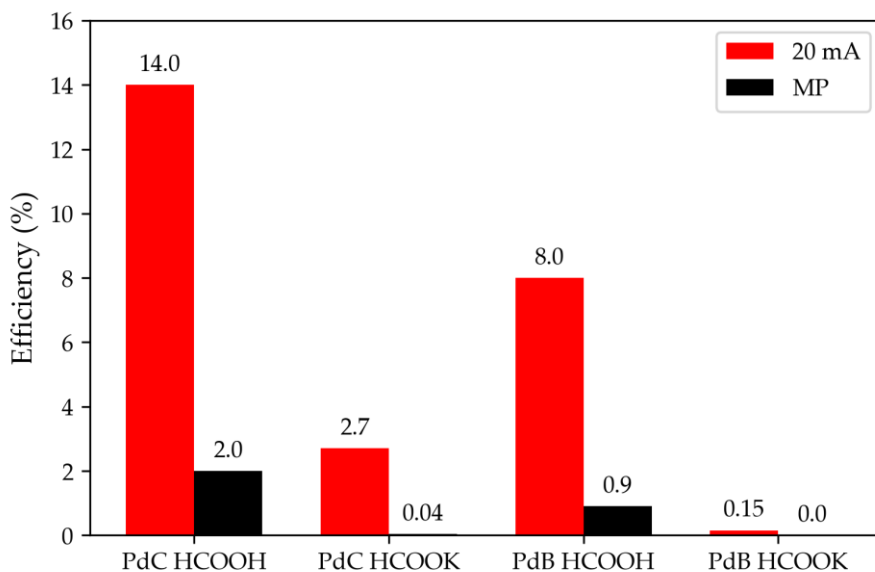


Figure 89: Constant current discharging efficiency at 20 mA and maximum power current (MP).

Moreover, Nafion is a proton exchange membrane; therefore, protons would pass through it easily. Yet, potassium ions might contribute to the membrane clogging, ultimately poisoning it. These assumptions are supported by studies reported by Bogdanowicz et al. [109]. In their article, the authors studied the selectivity of cation permeability through Nafion 117 membranes and reported a higher transport resistance of K^+ over H^+ , but it did not block the entrance.

KHCO₃/CO₂ electroreduction for fuel cell applications*Reaction and reactor optimization, prototyping with 3D printing and automatic testing.***9.4. Conclusions**

MEA preparation with a home-made manual pressing system without heating with the Nafion glue application contributed to decrease the additional energy consumption. XRD analysis showed that palladium black and palladium on carbon are (111) face centred cubic structures, which makes them appropriate for formate/formic acid oxidation through HCOO* adsorption. PdB revealed low performance in polarization curves and exhibited a lower energy generation efficiency compared to PdC. Unsupported palladium agglomerated during the MEA preparation which caused decreases in mass transfer. Carbon supported Pd catalysts demonstrate good activity providing high contact area along with the potential for a more efficient Pd metal utilization with lower metal loadings.

Simple characterization in terms of the polarization curve does give us information about the capability of the system towards power generation. In this case, HCOOK gave better results due to higher dissociation constant over HCOOH. However, in the long term constant current discharge we observed a faster FC efficiency decrease when using potassium formate compared to formic acid. Based on the literature research it can be attributed to two possibilities, **i)** lower conductivity of potassium ion and **ii)** membrane clogging caused by K⁺. Hence, we proved the potential use of formate salt in passive, air breathing fuel cells, through HCOO* oxidation.

9. Results obtained with automatic system

KHCO₃/CO₂ electroreduction for fuel cell applications

Reaction and reactor optimization, prototyping with 3D printing and automatic testing.

10. GENERAL CONCLUSIONS AND FUTURE WORK

10. General conclusions and future work

KHCO₃/CO₂ electroreduction for fuel cell applications

Reaction and reactor optimization, prototyping with 3D printing and automatic testing.

Main conclusions

- The electroreduction of bicarbonate performs with good efficiencies towards formic acid, up to 20% when no CO₂ pre-saturation of the bicarbonate solution is performed, and up to 50% when pre-saturation is applied. But is necessary to increase it, together with the reaction rates for large scale production and to become competitive against conventional methods of formic acid production
- 3D printing techniques such as FDM and SLA are great techniques for prototyping chemical reactors, decreasing the size, complexity, weight, and price, together with the increased manufacturing time and prototyping. However, even knowing that the number of printable materials has increased drastically in the last decade, it's necessary to increase it and create materials also compatible with reagents and conditions.
- Thanks to 3D Design, 3D printing, Open-Source world, and the decrease of price of electronic components, it is very cost effective to prototype automatic systems to increase productivity and repeatability in the laboratory.
- It is also possible to control the automatic system remotely, increasing repetitively while avoiding human error and increasing researcher's efficiency, together with more flexibility and the possibility to work outside of the lab, decreasing the risk of accidents.
- The produced formic acid can be used to power a fuel cell, and therefore, it will be possible to use it as an energy carrier.

Future work

- It is necessary to test more catalysts at different conditions using multiple automatic systems in parallel, to increase the testing capacity.
- It is necessary to couple the gas phase products to a GC to characterise the gases produced during the reaction.
- The 3D printed reactor must be redesigned to be completely gas tight.
- Apply the real time control of pH and temperature to get more insights about the reaction.
- The large quantity data obtained with the multi-automatic analysis system can be coupled with an AI to get more insights about the reaction.
- The formic acid is slightly permeable to Nafion, therefore it's possible to design a membrane to overcome this problem.
- The system can be automated even more, by design an automatic injection of the liquid sample into the vials or to pump directly to a HPLC to characterize the sample automatically.
- The possibility to automatically change the catalyst and membrane must be evaluated, but it may require high precision and advanced robotic arms that may not be cost efficient at the moment.

KHCO₃/CO₂ electroreduction for fuel cell applications

Reaction and reactor optimization, prototyping with 3D printing and automatic testing.

REFERENCES

- [1] “global warming - Causes of global warming | Britannica.”
- [2] T. R. Anderson, E. Hawkins, and P. D. Jones, “CO₂, the greenhouse effect and global warming: from the pioneering work of Arrhenius and Callendar to today’s Earth System Models,” *Endeavour*, vol. 40, no. 3, pp. 178–187, 2016, doi: 10.1016/j.endeavour.2016.07.002.
- [3] “CO₂ Levels: Current & Historic Atmospheric Carbon Dioxide / Global Temperature Graph & Widget.”
- [4] “Global Temperature | Vital Signs – Climate Change: Vital Signs of the Planet.”
- [5] D. I. Stern and R. K. Kaufmann, “Anthropogenic and natural causes of climate change,” *Clim. Change*, vol. 122, no. 1–2, pp. 257–269, 2014, doi: 10.1007/s10584-013-1007-x.
- [6] Y. Malhi *et al.*, “Climate change and ecosystems: Threats, opportunities and solutions,” *Philos. Trans. R. Soc. B Biol. Sci.*, vol. 375, no. 1794, 2020, doi: 10.1098/rstb.2019.0104.
- [7] A. E. Cahill *et al.*, “How does climate change cause extinction?,” *Proc. R. Soc. B Biol. Sci.*, vol. 280, no. 1750, 2013, doi: 10.1098/rspb.2012.1890.
- [8] P. Bierwirth, “Carbon Dioxide Toxicity and Climate Change: A Serious Unapprehended Risk for Human Health,” *Aust. Natl. Univ.*, no. October 2017, pp. 1–19, 2014, doi: 10.13140/RG.2.2.16787.48168.
- [9] D. Lüthi *et al.*, “High-resolution carbon dioxide concentration record 650,000-800,000 years before present,” *Nature*, vol. 453, no. 7193, pp. 379–382, 2008, doi: 10.1038/nature06949.
- [10] A. Haines and J. A. Patz, “CLINICIAN ’ S CORNER Health Effects of Climate Change,” *Victoria*, vol. 291, no. 1, pp. 99–103, 2004.

- [11] Richard S. J. Tol, “The Economic Effects of Climate,” *J. Econ. Perspect. J. Econ. Perspect.*, vol. 23, no. 2, pp. 29–51, 2009.
- [12] Z. Wang, C. Shi, Q. Li, and G. Wang, “Impact of heavy industrialization on the carbon emissions: An empirical study of China,” *Energy Procedia*, vol. 5, pp. 2610–2616, 2011, doi: 10.1016/j.egypro.2011.03.324.
- [13] H. Catalán, “Curva ambiental de Kuznets: implicaciones para un crecimiento sustentable,” *Econ. Inf.*, vol. 389, pp. 19–37, 2014, doi: 10.1016/s0185-0849(14)72172-3.
- [14] A. Nogalska, A. Zukowska, and R. Garcia-valls, “Atmospheric CO₂ capture for the artificial photosynthetic system,” vol. 00125, 2017, doi: 10.1051/e3sconf/20172200125.
- [15] A. Bonet Navarro, A. Nogalska, and R. Garcia-Valls, “Direct Electrochemical Reduction of Bicarbonate to Formate Using Tin Catalyst,” *Electrochem*, vol. 2, no. 1, pp. 64–70, 2021, doi: 10.3390/electrochem2010006.
- [16] A. Nogalska, A. B. Navarro, and R. Garcia-Valls, “Mea preparation for direct formate/formic acid fuel cell—comparison of palladium black and palladium supported on activated carbon performance on power generation in passive fuel cell,” *Membranes (Basel)*, vol. 10, no. 11, pp. 1–10, 2020, doi: 10.3390/membranes10110355.
- [17] “Hydrogen Fuel Cells vs. Battery Electrics: Why Fuel Cells are a Major Contender - Garrett Motion.”
- [18] I. Tsiropoulos, W. Nijs, D. Tarvydas, and P. Ruiz Castillo, *Towards net-zero emissions in the EU energy system by 2050*. 2020. doi: 10.2760/081488.
- [19] C. M. Quintella, S. A. Hatimondi, A. P. S. Musse, S. F. Miyazaki, G. S. Cerqueira, and A. De Araujo Moreira, “CO₂ capture technologies: An overview with technology assessment based on patents and articles,” *Energy Procedia*, vol. 4, pp. 2050–2057, 2011, doi: 10.1016/j.egypro.2011.02.087.

KHCO₃/CO₂ electroreduction for fuel cell applications*Reaction and reactor optimization, prototyping with 3D printing and automatic testing.*

- [20] B. R. J. Pearson *et al.*, “Energy Storage via Carbon-Neutral Fuels Made From CO₂, Water, and Renewable Energy This paper highlights how a versatile energy carrier can be produced by recycling,” vol. 100, no. 2, 2012.
- [21] A. K. Singh, J. H. Montoya, J. M. Gregoire, and K. A. Persson, “Robust and synthesizable photocatalysts for CO₂ reduction: a data-driven materials discovery,” *Nat. Commun.*, vol. 10, no. 1, 2019, doi: 10.1038/s41467-019-08356-1.
- [22] H. Yuan, B. Cheng, J. Lei, L. Jiang, and Z. Han, “Promoting photocatalytic CO₂ reduction with a molecular copper purpurin chromophore,” *Nat. Commun.*, vol. 12, no. 1, pp. 1–9, 2021, doi: 10.1038/s41467-021-21923-9.
- [23] U. Ulmer *et al.*, “Fundamentals and applications of photocatalytic CO₂ methanation,” *Nat. Commun.*, vol. 10, no. 1, pp. 1–12, 2019, doi: 10.1038/s41467-019-10996-2.
- [24] J. Albero, Y. Peng, and H. García, “Photocatalytic CO₂ Reduction to C₂+ Products,” *ACS Catal.*, vol. 10, no. 10, pp. 5734–5749, 2020, doi: 10.1021/acscatal.0c00478.
- [25] M. Abdinejad, M. N. Hossain, and H. B. Kraatz, “Homogeneous and heterogeneous molecular catalysts for electrochemical reduction of carbon dioxide,” *RSC Adv.*, vol. 10, no. 62, pp. 38013–38023, 2020, doi: 10.1039/d0ra07973a.
- [26] S. Fukuzumi, Y. M. Lee, H. S. Ahn, and W. Nam, “Mechanisms of catalytic reduction of CO₂ with heme and nonheme metal complexes,” *Chem. Sci.*, vol. 9, no. 28, pp. 6017–6034, 2018, doi: 10.1039/c8sc02220h.
- [27] J. Qiao, Y. Liu, F. Hong, and J. Zhang, “A review of catalysts for the electroreduction of carbon dioxide to produce low-carbon fuels,” *Chem. Soc. Rev.*, vol. 43, no. 2, pp. 631–675, 2014, doi: 10.1039/c3cs60323g.
- [28] L. Lü, J. Y. H. Fuh, and Y. S. Wong, *Laser-Induced Materials and Processes for Rapid Prototyping*. 2001. doi: 10.1007/978-1-

- 4615-1469-5.
- [29] T. Grzegorz Gawel, “Review of additive manufacturing methods,” *Solid State Phenom.*, vol. 308, no. July, pp. 1–20, 2020, doi: 10.4028/www.scientific.net/SSP.308.1.
- [30] T. Pereira, J. V. Kennedy, and J. Potgieter, “A comparison of traditional manufacturing vs additive manufacturing, the best method for the job,” *Procedia Manuf.*, vol. 30, pp. 11–18, 2019, doi: 10.1016/j.promfg.2019.02.003.
- [31] T. Suntharalingam, B. Nagaratnam, P. Keerthan, and P. Hackney, “Evolution Of Additive Manufacturing Technology In Construction Industry & Challenges On Implementation : A Construction Industry & Challenges On Implementation,” no. November, 2019.
- [32] S. Vyavahare, S. Teraiya, D. Panghal, and S. Kumar, “Fused deposition modelling: a review,” *Rapid Prototyp. J.*, vol. 26, no. 1, pp. 176–201, 2020, doi: 10.1108/RPJ-04-2019-0106.
- [33] J. Huang, Q. Qin, and J. Wang, “A review of stereolithography: Processes and systems,” *Processes*, vol. 8, no. 9, 2020, doi: 10.3390/PR8091138.
- [34] “3D Printing Questions - www.the3dprintingspecialist.com.”
- [35] “How to design parts for SLA 3D printing | Hubs.”
- [36] H. K. Mohajan, “The First Industrial Revolution : Creation of a New Global Human Era The First Industrial Revolution : Creation of a New Global Human Era,” no. October, 2019.
- [37] H. K. Mohajan, “The Second Industrial Revolution has Brought Modern Social and Economic Developments,” no. January, 2020.
- [38] B. H. Roberts, “The Third Industrial Revolution : Implications for Planning Cities and Regions The Third Industrial Revolution : Implications for Planning Cities and Regions,” no. June, 2015.
- [39] J. Min, Y. Kim, S. Lee, T. W. Jang, I. Kim, and J. Song, “The Fourth Industrial Revolution and Its Impact on Occupational

KHCO₃/CO₂ electroreduction for fuel cell applications*Reaction and reactor optimization, prototyping with 3D printing and automatic testing.*

Health and Safety, Worker's Compensation and Labor Conditions," *Saf. Health Work*, vol. 10, no. 4, pp. 400–408, 2019, doi: 10.1016/j.shaw.2019.09.005.

- [40] D. Özkiziltan and A. Hassel, "Humans versus Machines: An Overview of Research on the Effects of Automation of Work," *SSRN Electron. J.*, no. January 2021, 2021, doi: 10.2139/ssrn.3789992.
- [41] "Future Skills You'll Need In Your Career By 2030 | Top Universities."
- [42] "7 Job Skills Of The Future (That AIs And Robots Can't Do Better Than Humans)."
- [43] "Stepper Motors: Types, Uses and Working Principle | Article | MPS."
- [44] "Solenoid Valve - How They Work | tameson.com."
- [45] "ABOUT SOLENOID VALVES | Jaksa Solenoid Valves."
- [46] "Motion Techniques For Improved Liquid Handling."
- [47] "Medical Grade Tubing and Compounds for Peristaltic Pumps - Tekni-Plex."
- [48] "Mechanical Endstop - RepRap."
- [49] "What Is a Breadboard and How Does It Work? A Quick Crash Course."
- [50] "What is a PCB or Printed Circuit Board? - Technical Terms by Eurocircuits."
- [51] "How Transistors Work (BJT and MOSFET) - The Simple Explanation."
- [52] "What is a Diode? | Fluke."
- [53] "Introduction to DC-DC Converters."
- [54] "How Capacitors Work | HowStuffWorks."

- [55] M. R. Smith and S. S. Myers, "Impact of anthropogenic CO₂ emissions on global human nutrition," *Nat. Clim. Chang.*, vol. 8, no. 9, pp. 834–839, 2018, doi: 10.1038/s41558-018-0253-3.
- [56] M. Workman, N. McGlashan, H. Chalmers, and N. Shah, "An assessment of options for CO₂ removal from the atmosphere," *Energy Procedia*, vol. 4, no. November 2015, pp. 2877–2884, 2011, doi: 10.1016/j.egypro.2011.02.194.
- [57] A. Nogalska, A. Zukowska, and R. Garcia-Valls, "Atmospheric CO₂ capture for the artificial photosynthetic system," *E3S Web Conf.*, vol. 22, 2017, doi: 10.1051/e3sconf/20172200125.
- [58] S. Nitopi *et al.*, "Progress and Perspectives of Electrochemical CO₂ Reduction on Copper in Aqueous Electrolyte," *Chem. Rev.*, vol. 119, no. 12, pp. 7610–7672, 2019, doi: 10.1021/acs.chemrev.8b00705.
- [59] S. Hosseini, S. Kheawhom, S. M. Soltani, and M. K. Aroua, "Electrochemical reduction of bicarbonate on carbon nanotube-supported silver oxide: An electrochemical impedance spectroscopy study," *J. Environ. Chem. Eng.*, vol. 6, no. 1, pp. 1033–1043, 2018, doi: 10.1016/j.jece.2017.12.036.
- [60] M. Spichiger-Ulmann and J. Augustynski, "Electrochemical reduction of bicarbonate ions at a bright palladium cathode," *J. Chem. Soc. Faraday Trans. 1 Phys. Chem. Condens. Phases*, vol. 81, no. 3, pp. 713–716, 1985, doi: 10.1039/F19858100713.
- [61] T. Li, E. W. Lees, M. Goldman, D. A. Salvatore, D. M. Weekes, and C. P. Berlinguette, "Electrolytic Conversion of Bicarbonate into CO in a Flow Cell," *Joule*, vol. 3, no. 6, pp. 1487–1497, 2019, doi: 10.1016/j.joule.2019.05.021.
- [62] X. Min and M. W. Kanan, "Pd-Catalyzed Electrohydrogenation of Carbon Dioxide to Formate: High Mass Activity at Low Overpotential and Identification of the Deactivation Pathway," *J. Am. Chem. Soc.*, vol. 137, no. 14, pp. 4701–4708, 2015, doi: 10.1021/ja511890h.

KHCO₃/CO₂ electroreduction for fuel cell applications*Reaction and reactor optimization, prototyping with 3D printing and automatic testing.*

- [63] H. Zhong, K. Fujii, Y. Nakano, and F. Jin, "Effect of CO₂ bubbling into aqueous solutions used for electrochemical reduction of CO₂ for energy conversion and storage," *J. Phys. Chem. C*, vol. 119, no. 1, pp. 55–61, 2015, doi: 10.1021/jp509043h.
- [64] R. Kortlever, K. H. Tan, Y. Kwon, and M. T. M. Koper, "Electrochemical carbon dioxide and bicarbonate reduction on copper in weakly alkaline media," *J. Solid State Electrochem.*, vol. 17, no. 7, pp. 1843–1849, 2013, doi: 10.1007/s10008-013-2100-9.
- [65] S. OBARA and T. SEKINE, "Electrolytic Reduction of Dichromate Ion at a Mercury Cathode," *J. Electrochem. Soc. Japan*, vol. 32, no. 1, pp. 41–46, 1964, doi: 10.5796/jesj.32.1.41.
- [66] N. Sreekanth and K. L. Phani, "Selective reduction of co₂ to formate through bicarbonate reduction on metal electrodes: New insights gained from sg/tc mode of secm," *Chem. Commun.*, vol. 50, no. 76, pp. 11143–11146, 2014, doi: 10.1039/c4cc03099k.
- [67] L. R. L. Ting and B. S. Yeo, "Recent advances in understanding mechanisms for the electrochemical reduction of carbon dioxide," *Curr. Opin. Electrochem.*, vol. 8, pp. 126–134, 2018, doi: 10.1016/j.coelec.2018.04.011.
- [68] P. Isa Amos, H. Louis, K. Adesina Adegoke, E. Akpan Eno, A. Ozioma Udochukwu, and T. Odey Magu, "Understanding the Mechanism of Electrochemical Reduction of CO₂ Using Cu/Cu-Based Electrodes: A Review Asian Journal of Nanoscience and Materials," *Asian J. Nanosci. Mater.*, vol. 1, no. 4, pp. 183–224, 2018.
- [69] A. J. Garza, A. T. Bell, and M. Head-Gordon, "Mechanism of CO₂ Reduction at Copper Surfaces: Pathways to C₂ Products," *ACS Catal.*, vol. 8, no. 2, pp. 1490–1499, 2018, doi: 10.1021/acscatal.7b03477.
- [70] J. Hussain, E. Skúlason, and H. Jónsson, "Computational study of electrochemical CO₂ reduction at transition metal electrodes," *Procedia Comput. Sci.*, vol. 51, no. 1, pp. 1865–1871, 2015, doi:

- 10.1016/j.procs.2015.05.419.
- [71] K. Lum, K. Kamarudi, and W. R. W. Daud, "Overview w on Dir rect Form ic Acid d Fuel Cells (DF FAFCs) as an En nergy So ource s," vol. 3, pp. 33–39, 2012, doi: 10.1016/j.apcbee.2012.06.042.
- [72] N. V. Rees and R. G. Compton, "Sustainable energy: A review of formic acid electrochemical fuel cells," *J. Solid State Electrochem.*, vol. 15, no. 10, pp. 2095–2100, 2011, doi: 10.1007/s10008-011-1398-4.
- [73] O. Z. Sharaf and M. F. Orhan, "An overview of fuel cell technology: Fundamentals and applications," *Renew. Sustain. Energy Rev.*, vol. 32, pp. 810–853, 2014, doi: 10.1016/j.rser.2014.01.012.
- [74] A. Mohapatra and S. Tripathy, "A Critical Review of the use of Fuel Cells Towards Sustainable Management of Resources," *IOP Conf. Ser. Mater. Sci. Eng.*, vol. 377, no. 1, 2018, doi: 10.1088/1757-899X/377/1/012135.
- [75] G. K. S. Prakash, F. A. Viva, and G. A. Olah, "Electrochemical reduction of CO₂ over Sn-Nafion[®] coated electrode for a fuel-cell-like device," *J. Power Sources*, vol. 223, pp. 68–73, 2013, doi: 10.1016/j.jpowsour.2012.09.036.
- [76] C. Cui, H. Wang, X. Zhu, J. Han, and Q. Ge, "A DFT study of CO₂ electrochemical reduction on Pb(211) and Sn(112)," *Sci. China Chem.*, vol. 58, no. 4, pp. 607–613, 2015, doi: 10.1007/s11426-015-5323-z.
- [77] P. Bumroongsakulsawat and G. H. Kelsall, "Effect of solution pH on CO: Formate formation rates during electrochemical reduction of aqueous CO₂ at Sn cathodes," *Electrochim. Acta*, vol. 141, pp. 216–225, 2014, doi: 10.1016/j.electacta.2014.07.057.
- [78] K. Saravanan, Y. Basdogan, J. Dean, and J. A. Keith, "Computational investigation of CO₂ electroreduction on tin oxide and predictions of Ti, V, Nb and Zr dopants for improved

KHCO₃/CO₂ electroreduction for fuel cell applications*Reaction and reactor optimization, prototyping with 3D printing and automatic testing.*

- catalysis,” *J. Mater. Chem. A*, vol. 5, no. 23, pp. 11756–11763, 2017, doi: 10.1039/c7ta00405b.
- [79] J. Medina-Ramos, R. C. Pupillo, T. P. Keane, J. L. Dimeglio, and J. Rosenthal, “Efficient conversion of CO₂ to CO using tin and other inexpensive and easily prepared post-transition metal catalysts,” *J. Am. Chem. Soc.*, vol. 137, no. 15, pp. 5021–5027, 2015, doi: 10.1021/ja5121088.
- [80] R. Zhang, W. Lv, and L. Lei, “Role of the oxide layer on Sn electrode in electrochemical reduction of CO₂ to formate,” *Appl. Surf. Sci.*, vol. 356, pp. 24–29, 2015, doi: 10.1016/j.apsusc.2015.08.006.
- [81] W. Sheng *et al.*, “Electrochemical reduction of CO₂ to synthesis gas with controlled CO/H₂ ratios,” *Energy Environ. Sci.*, vol. 10, no. 5, pp. 1180–1185, 2017, doi: 10.1039/c7ee00071e.
- [82] M. Rumayor, A. Dominguez-Ramos, and A. Irabien, “Formic Acid manufacture: Carbon dioxide utilization alternatives,” *Appl. Sci.*, vol. 8, no. 6, pp. 1–12, 2018, doi: 10.3390/app8060914.
- [83] H. Noda, S. Ikeda, Y. Oda, K. Imai, M. Maeda, and K. Ito, “Electrochemical Reduction of Carbon Dioxide at Various Metal Electrodes in Aqueous Potassium Hydrogen Carbonate Solution,” *Bulletin of the Chemical Society of Japan*, vol. 63, no. 9, pp. 2459–2462, 1990. doi: 10.1246/bcsj.63.2459.
- [84] S. Nakagawa, A. Kudo, M. Azuma, and T. Sakata, “Effect of pressure on the electrochemical reduction of CO₂ on Group VIII metal electrodes,” *J. Electroanal. Chem.*, vol. 308, no. 1–2, pp. 339–343, 1991, doi: 10.1016/0022-0728(91)85080-9.
- [85] D. Yang *et al.*, “Selective electroreduction of carbon dioxide to methanol on copper selenide nanocatalysts,” *Nat. Commun.*, vol. 10, no. 1, pp. 1–9, 2019, doi: 10.1038/s41467-019-08653-9.
- [86] “Model orientation best practices for SLA printing.”
- [87] “Python Vs C++ (Top 16 Differences Between C++ And Python).”

- [88] J. Frohm, V. Lindström, M. Winroth, and J. Stahre, “The industry’s view on automation in manufacturing,” *IFAC Proc. Vol.*, vol. 9, no. PART 1, pp. 453–458, 2006, doi: 10.3182/20060522-3-fr-2904.00073.
- [89] C. Coombs, D. Hislop, S. K. Taneva, and S. Barnard, “The strategic impacts of Intelligent Automation for knowledge and service work: An interdisciplinary review,” *Journal of Strategic Information Systems*, vol. 29, no. 4. 2020. doi: 10.1016/j.jsis.2020.101600.
- [90] S. Z. Rejal, M. S. Masdar, and S. K. Kamarudin, “A parametric study of the direct formic acid fuel cell (DFAFC) performance and fuel crossover,” *Int. J. Hydrogen Energy*, vol. 39, no. 19, pp. 10267–10274, 2014, doi: 10.1016/j.ijhydene.2014.04.149.
- [91] K. J. Jeong *et al.*, “Fuel crossover in direct formic acid fuel cells,” *J. Power Sources*, vol. 168, no. 1 SPEC. ISS., pp. 119–125, 2007, doi: 10.1016/j.jpowsour.2007.02.062.
- [92] L. An and R. Chen, “Direct formate fuel cells: A review,” *J. Power Sources*, vol. 320, pp. 127–139, 2016, doi: 10.1016/j.jpowsour.2016.04.082.
- [93] M. Chen, C. Zhao, F. Sun, J. Fan, H. Li, and H. Wang, “Research progress of catalyst layer and interlayer interface structures in membrane electrode assembly (MEA) for proton exchange membrane fuel cell (PEMFC) system,” *eTransportation*, vol. 5, p. 100075, 2020, doi: 10.1016/j.etrans.2020.100075.
- [94] Y. Y. Gao, C. H. Tan, Y. P. Li, J. Guo, and S. Y. Zhang, “Formic acid-Formate blended solution: A new fuel system with high oxidation activity,” *Int. J. Hydrogen Energy*, vol. 37, no. 4, pp. 3433–3437, 2012, doi: 10.1016/j.ijhydene.2011.11.077.
- [95] A. M. Bartrom, J. Ta, T. Q. Nguyen, J. Her, A. Donovan, and J. L. Haan, “Optimization of an anode fabrication method for the alkaline Direct Formate Fuel Cell,” *J. Power Sources*, vol. 229, pp. 234–238, 2013, doi: 10.1016/j.jpowsour.2012.12.007.

KHCO₃/CO₂ electroreduction for fuel cell applications*Reaction and reactor optimization, prototyping with 3D printing and automatic testing.*

- [96] E. Lam and J. H. T. Luong, "Carbon materials as catalyst supports and catalysts in the transformation of biomass to fuels and chemicals," *ACS Catal.*, vol. 4, no. 10, pp. 3393–3410, 2014, doi: 10.1021/cs5008393.
- [97] R. Larsen, S. Ha, J. Zakzeski, and R. I. Masel, "Unusually active palladium-based catalysts for the electrooxidation of formic acid," *J. Power Sources*, vol. 157, no. 1, pp. 78–84, 2006, doi: 10.1016/j.jpowsour.2005.07.066.
- [98] L. Q. Wang *et al.*, "Energy efficiency of platinum-free alkaline direct formate fuel cells," *Appl. Energy*, vol. 175, pp. 479–487, 2016, doi: 10.1016/j.apenergy.2016.02.129.
- [99] B. Qi, L. Di, W. Xu, and X. Zhang, "Dry plasma reduction to prepare a high performance Pd/C catalyst at atmospheric pressure for CO oxidation," *J. Mater. Chem. A*, vol. 2, no. 30, pp. 11885–11890, 2014, doi: 10.1039/c4ta02155j.
- [100] N. H. ABDULLAH *et al.*, "Effect of Acidic and Alkaline Treatments to Methylene Blue Adsorption from Aqueous Solution by Coconut Shell Activated Carbon," *Int. J. Curr. Res. Sci. Eng. Technol.*, vol. 1, no. Spl-1, p. 319, 2018, doi: 10.30967/ijcrset.1.s1.2018.319-324.
- [101] A. O. Elnabawy, J. A. Herron, J. Scaranto, and M. Mavrikakis, "Structure Sensitivity of Formic Acid Electrooxidation on Transition Metal Surfaces: A First-Principles Study," *J. Electrochem. Soc.*, vol. 165, no. 15, pp. J3109–J3121, 2018, doi: 10.1149/2.0161815jes.
- [102] F. Paquin, J. Rivnay, A. Salleo, N. Stingelin, and C. Silva, "Multi-phase semicrystalline microstructures drive exciton dissociation in neat plastic semiconductors," *J. Mater. Chem. C*, vol. 3, pp. 10715–10722, 2015, doi: 10.1039/b000000x.
- [103] V. R. K. Velpula, T. Ketike, G. Paleti, S. R. R. Kamaraju, and D. R. Burri, "A Facile Synthesis of Pd–C₃N₄@Titanate Nanotube Catalyst: Highly Efficient in Mizoroki–Heck, Suzuki–Miyaura C–C Couplings," *Catal. Letters*, vol. 150, no. 1, pp. 95–105, 2020,

- doi: 10.1007/s10562-019-02955-9.
- [104] L. Zeng, Z. K. Tang, and T. S. Zhao, "A high-performance alkaline exchange membrane direct formate fuel cell," *Appl. Energy*, vol. 115, pp. 405–410, 2014, doi: 10.1016/j.apenergy.2013.11.039.
- [105] Y. Li, H. Wu, Y. He, Y. Liu, and L. Jin, "Performance of direct formate-peroxide fuel cells," *J. Power Sources*, vol. 287, pp. 75–80, 2015, doi: 10.1016/j.jpowsour.2015.04.014.
- [106] S. D. Han, J. H. Choi, S. Y. Noh, K. Park, S. K. Yoon, and Y. W. Rhee, "Performance characterization of direct formic acid fuel cell using porous carbon-supported palladium anode catalysts," *Korean J. Chem. Eng.*, vol. 26, no. 4, pp. 1040–1046, 2009, doi: 10.1007/s11814-009-0173-z.
- [107] M. Bončina, A. Apelblat, and M. Bešter-Rogač, "Dilute aqueous solutions with formate ions: A conductometric study," *J. Chem. Eng. Data*, vol. 55, no. 5, pp. 1951–1957, 2010, doi: 10.1021/je900903w.
- [108] A. Mikołajczuk, A. Borodzinski, P. Kedzierzawski, L. Stobinski, B. Mierzwa, and R. Dziura, "Deactivation of carbon supported palladium catalyst in direct formic acid fuel cell," *Appl. Surf. Sci.*, vol. 257, no. 19, pp. 8211–8214, 2011, doi: 10.1016/j.apsusc.2011.04.078.
- [109] K. A. Bogdanowicz, P. Sístat, J. A. Reina, and M. Giamberini, "Liquid crystalline polymeric wires for selective proton transport, part 2: Ion transport in solid-state," *Polymer (Guildf.)*, vol. 92, pp. 58–65, 2016, doi: 10.1016/j.polymer.2016.03.080.

KHCO₃/CO₂ electroreduction for fuel cell applications

Reaction and reactor optimization, prototyping with 3D printing and automatic testing.

APPENDIX

KHCO₃/CO₂ electroreduction for fuel cell applications*Reaction and reactor optimization, prototyping with 3D printing and automatic testing.***List of publications**

Authors: Adrianna Nogalska, Andreu Bonet Navarro, and Ricard Garcia-Valls.

Title: *MEA Preparation for Direct Formate/Formic Acid Fuel Cell—Comparison of Palladium Black and Palladium Supported on Activated Carbon Performance on Power Generation in Passive Fuel Cell.*

Journal: *Membranes*

Volume: 10

Pages: 1-10

Year: 2020

Authors: Andreu Bonet Navarro, Adrianna Nogalska and Ricard Garcia-Valls.

Title: *Direct Electrochemical Reduction of Bicarbonate to Formate Using Tin Catalyst.*

Journal: *Electrochem*

Volume: 2

Pages: 64-70

Year: 2021

Congresses

Authors: Andreu Bonet, Adrianna Nogalska, Ricard Garcia Valls

Title: "Chemical reactors manufactured by SLA and FDM 3D printing technologies."

Poster/Oral: Oral

Name of Congress: 14th Mediterranean Congress of Chemical Engineering.

Place: Fira Gran Vía, Barcelona, Spain

Date: Virtual Event: 16-20 November 2020----**Face-to-face:** 14-17 September 2021

Authors: Andreu Bonet Navarro, Adrianna Nogalska, Ricard Garcia Valls, Eva Chinarro Martín

Title: "*Catalizador a base de Ceria para electroreducción de CO₂ en bicarbonato a formiato para pilas de combustible.*"

Poster/Oral: Poster

Name of Congress: LVII Congreso Nacional de la SECV

Place: Universitat Jaume I, Castellón

Date: 26-29 October 2020

KHCO₃/CO₂ electroreduction for fuel cell applications

Reaction and reactor optimization, prototyping with 3D printing and automatic testing.

Code used for calculation of HCOOH production

(Python)

Define the function used for calculating the total charge passed through the electrodes during all the experiment

def calculate_total_charge(excel_file_name):

DataF = pd.read_excel(excel_file_name, 'Sheet1')

time = DataF["Time (s)"]

current = DataF["WE(1).Current (A)"]

Total_Charge = 0

length = len(time) - 1

for i in range(length):

try:

**Total_Charge = Total_Charge + (time[i+1] - time[i]) *
current[i]**

except Exception as e:

print(e, i)

return Total_Charge * -1

Define the function used for calculating the faradaic efficiency

**def eficiencia_faradiaca(DMSO_mass, DMSO_density, DMSO_volume,
DMSO_Molecular_Weight, DMSO_Moles, D2O_mass, D2O_density, D2O_vol-
ume, Total_volume_in_eppendorf, Reference_mass, Reference_volume, Refer-
ence_density, Sample_volume, Sample_density, Dilution_ratio, Total_Vol-
ume_NMR, DMSO_concentration_in_NMR_Tube, DMSO_Integral,
CH₃COOH_Integral, Ratio_CH₃COOH_DMSO, CH₃COOH_NMR_Concentra-
tion, Concentration_ratio, CH₃COOH_Concentration, Total_Charge,
CH₃COOH_Charge, Total_cathodic_volume, Total_CH₃COOH_moles, Farada-
ic_Efficiency, excel_file_name, Reaction_rate, Electroreduction_Time,**

**Total_Bicarbonate_moles, Bicarbonate_Concentration, Conversion,
CH₃COOH_Concentration_mM):**

Define the input parameters for calculations

```
DMSO_density = 1.1004
DMSO_volume = (DMSO_mass / DMSO_density) / 1000
DMSO_Molecular_Weight = 78.13
DMSO_Moles = DMSO_mass / DMSO_Molecular_Weight
D2O_density = 1.107
D2O_volume = (D2O_mass / D2O_density) / 1000
Total_volume_in_eppendorf = (D2O_volume + DMSO_volume)
DMSO_concentration_in_eppendorf = DMSO_Moles / Total_vol-
ume_in_eppendorf
Reference_density = 1.1
Reference_volume = (Reference_mass / Reference_density) / 1000
Sample_volume = 0.0006
Sample_density = 1
Total_Volume_NMR = Sample_volume + Reference_volume
Dilution_ratio = Reference_volume / Total_Volume_NMR
DMSO_concentration_in_NMR_Tube = DMSO_concentration_in_eppen-
dorf * Dilution_ratio
Ratio_CH3COOH_DMSO = CH3COOH_Integral / (DMSO_Integral / 2)
CH3COOH_NMR_Concentration = DMSO_concentra-
tion_in_NMR_Tube * Ratio_CH3COOH_DMSO
Concentration_ratio = Total_Volume_NMR / Sam-ple_volume
```

Define the output parameters or results

```
CH3COOH_Concentration = (CH3COOH_NMR_Concentration * Concen-
tration_ratio)
CH3COOH_Concentration_mM = CH3COOH_Concentration * 1000
Total_CH3COOH_moles = CH3COOH_Concentration * To-tal_ca-
thodic_volume
CH3COOH_Charge = Total_CH3COOH_moles * 6 * 96485.3365
Faradaic_Efficiency = (CH3COOH_Charge / Total_Charge) * 100
```

KHCO₃/CO₂ electroreduction for fuel cell applications*Reaction and reactor optimization, prototyping with 3D printing and automatic testing.*

```

    Reaction_rate = (Total_CH3COOH_moles / Electroreduction_Time) *
1000000000
    Total_Bicarbonate_moles = Bicarbonate_Concentration * Total_ca-
thodic_volume
    Conversion = (Total_CH3COOH_moles / Total_Bicarbonate_moles) *
100

    return DMSO_concentration_in_NMR_Tube, CH3COOH_Concentra-
tion, CH3COOH_Concentration_mM, Total_Charge, CH3COOH_Charge, Fara-
daic_Efficiency, Reaction_rate, Conversion

# Define main function

def main():

    print("Electroreduction performance calculations")
    print("The units of each parameter are specified in parentheses")

    DMSO_mass = float(input("DMSO mass (g): "))
    D2O_mass = float(input("D2O mass (g): "))
    Reference_mass = float(input("Reference mass (g): "))
    DMSO_Integral = float(input("DMSO Integral: "))
    CH3COOH_Integral = float(input("CH3COOH Integral: "))
    Total_cathodic_volume = float(input("Total cathodic volume (L): "))
    Electroreduction_Time = float(input("Electroreduction Time (s): "))
    userinput = input("Excel Name: ")
    Bicarbonate_Concentration = float(input("Bicarbonate concentration (M):
"))

    DMSO_density = 1.1004
    DMSO_volume = (DMSO_mass / DMSO_density) / 1000
    DMSO_Molecular_Weight = 78.13
    DMSO_Moles = DMSO_mass / DMSO_Molecular_Weight
    D2O_density = 1.107
    D2O_volume = (D2O_mass / D2O_density) / 1000
    Total_volume_in_ependorf = (D2O_volume + DMSO_volume)

```

```
DMSO_concentration_in_ependorf = DMSO_Moles / Total_vol-  
ume_in_ependorf  
Reference_density = 1.1  
Reference_volume = (Reference_mass / Reference_density) / 1000  
Sample_volume = 0.0006  
Sample_density = 1  
Total_Volume_NMR = Sample_volume + Reference_volume  
Dilution_ratio = Reference_volume / Total_Volume_NMR  
DMSO_concentration_in_NMR_Tube = DMSO_concentration_in_epen-  
dorf * Dilution_ratio  
Ratio_CH3COOH_DMSO = CH3COOH_Integral / (DMSO_Integral / 2)  
CH3COOH_NMR_Concentration = DMSO_concentra-  
tion_in_NMR_Tube * Ratio_CH3COOH_DMSO  
Concentration_ratio = Total_Volume_NMR / Sample_volume  
CH3COOH_Concentration = (CH3COOH_NMR_Concentration * Con-  
centration_ratio)  
CH3COOH_Concentration_mM = CH3COOH_Concentration * 1000  
excel_file_name = userinput  
Total_Charge = calculate_total_charge(excel_file_name)  
Total_CH3COOH_moles = CH3COOH_Concentration * Total_ca-  
thodic_volume  
CH3COOH_Charge = Total_CH3COOH_moles * 6 * 96485.3365  
Faradaic_Efficiency = (CH3COOH_Charge / Total_Charge) * 100  
Reaction_rate = Total_CH3COOH_moles / Electroreduc-tion_Time  
Total_Bicarbonate_moles = Bicarbonate_Concentration * Total_ca-  
thodic_volume  
Conversion = (Total_CH3COOH_moles / Total_Bicarbonate_moles ) *  
100
```

try:

```
resultat1, resultat2, resultat3, resultat4, resultat5, resultat6, re-  
sultat7, resultat8 = eficien-cia_faradiaca (DMSO_mass, DMSO_density,  
DMSO_volume, DMSO_Molecular_Weight, DMSO_Moles, D2O_mass,  
D2O_density, D2O_volume, Total_volume_in_ependorf, Reference_mass, Ref-  
erence_volume, Reference_density, Sample_volume, Sample_density, Dilu-  
tion_ratio, Total_Volume_NMR, DMSO_concentration_in_NMR_Tube,  
DMSO_Integral, CH3COOH_Integral, Ratio_CH3COOH_DMSO,
```

KHCO₃/CO₂ electroreduction for fuel cell applications*Reaction and reactor optimization, prototyping with 3D printing and automatic testing.*

CH₃COOH_NMR_Concentration, Concentration_ratio, CH₃COOH_Concentration, Total_Charge, CH₃COOH_Charge, Total_cathodic_volume, Total_CH₃COOH_moles, Faradaic_Efficiency, excel_file_name, Reaction_rate, Electroreduction_Time, Total_Bicarbonate_moles, Bicarbonate_Concentration, Conversion, CH₃COOH_Concentration_mM)

Print results

```

print("DMSO concentration in NMR Tube (M) : ", round(resultat1, 5))

print("CH3COOH Concentration (M) : ", round(resultat2, 6))
print("CH3COOH Concentration (mM) : ", round(resultat3, 2))
print("Total Charge : ", round(resultat4, 1))
print("CH3COOH Charge : ", round(resultat5, 2))
print("Faradaic Efficiency (%) : ", round(resultat6, 2))
print("Reaction rate (nM/s) : ", round(resultat7, 2))
print("Conversion (%) : ", round(resultat8, 4))

except Exception as e:
    print(e)

if __name__ == "__main__":
    main()

```

Code used for calculation of CH₃COOH production

(Python)

```
def calculate_total_charge(excel_file_name):

    DataF = pd.read_excel(excel_file_name, 'Sheet1')
    time = DataF["Time (s)"]
    current = DataF["WE(1).Current (A)"]

    Total_Charge = 0

    length = len(time) - 1

    for i in range(length):
        try:
            Total_Charge = Total_Charge + (time[i+1] - time[i]) *
current[i]
        except Exception as e:
            print(e, i)

    return Total_Charge * -1

def eficiencia_faradiaca(DMSO_mass, DMSO_density, DMSO_volume,
DMSO_Molecular_Weight, DMSO_Moles, D2O_mass, D2O_density, D2O_vol-
ume, Total_volume_in_ependorf, Reference_mass, Reference_volume, Refer-
ence_density, Sample_volume, Sample_density, Dilution_ratio, Total_Vol-
ume_NMR, DMSO_concentration_in_NMR_Tube, DMSO_Integral, HCOOH_In-
tegral, Ratio_HCOOH_DMSO, HCOOH_NMR_Concentration, Concentration_ra-
tio, HCOOH_Concentration, Total_Charge, HCOOH_Charge, Total_cathodic_vol-
ume, Total_HCOOH_moles, Faradaic_Efficiency, excel_file_name, Reaction_rate,
Electroreduction_Time, Total_Bicarbonate_moles, Bicarbonate_Concentration,
Conversion, HCOOH_Concentration_mM):

    DMSO_density = 1.1004
    DMSO_volume = (DMSO_mass / DMSO_density) / 1000
    DMSO_Molecular_Weight = 78.13
```

KHCO₃/CO₂ electroreduction for fuel cell applications*Reaction and reactor optimization, prototyping with 3D printing and automatic testing.*

```

DMSO_Moles = DMSO_mass / DMSO_Molecular_Weight
D2O_density = 1.107
D2O_volume = (D2O_mass / D2O_density) / 1000
Total_volume_in_eppendorf = (D2O_volume + DMSO_volume)
DMSO_concentration_in_eppendorf = DMSO_Moles / Total_vol-
ume_in_eppendorf
Reference_density = 1.1
Reference_volume = (Reference_mass / Reference_density) / 1000
Sample_volume = 0.0006
Sample_density = 1
Total_Volume_NMR = Sample_volume + Reference_volume
Dilution_ratio = Reference_volume / Total_Volume_NMR
DMSO_concentration_in_NMR_Tube = DMSO_concentration_in_eppen-
dorf * Dilution_ratio
Ratio_HCOOH_DMSO = HCOOH_Integral / (DMSO_Integral / 6)
HCOOH_NMR_Concentration = DMSO_concentration_in_NMR_Tube *
Ratio_HCOOH_DMSO
Concentration_ratio = Total_Volume_NMR / Sample_volume
HCOOH_Concentration = (HCOOH_NMR_Concentration * Con-centra-
tion_ratio)
HCOOH_Concentration_mM = HCOOH_Concentration * 1000
Total_HCOOH_moles = HCOOH_Concentration * Total_cathodic_vol-
ume
HCOOH_Charge = Total_HCOOH_moles * 2 * 96485.3365
Faradaic_Efficiency = (HCOOH_Charge / Total_Charge) * 100
Reaction_rate = (Total_HCOOH_moles / Electroreduc-tion_Time) *
1000000000
Total_Bicarbonate_moles = Bicarbonate_Concentration * Total_ca-
thodic_volume
Conversion = (Total_HCOOH_moles / Total_Bicarbonate_moles ) * 100

return DMSO_concentration_in_NMR_Tube, HCOOH_Concentration,
HCOOH_Concentration_mM, Total_Charge, HCOOH_Charge, Faradaic_Effi-
ciency, Reaction_rate, Conversion

def main():

```

```
print("Electroreduction performance calculations")
print("The units of each parameter are specified in parentheses")

DMSO_mass = float(input("DMSO mass (g): "))
D2O_mass = float(input("D2O mass (g): "))
Reference_mass = float(input("Reference mass (g): "))
DMSO_Integral = float(input("DMSO Integral: "))
HCOOH_Integral = float(input("HCOOH Integral: "))
Total_cathodic_volume = float(input("Total cathodic volume (L): "))
Electroreduction_Time = float(input("Electroreduction Time (s): "))
userinput = input("Excel Name: ")
Bicarbonate_Concentration = float(input("Bicarbonate concentration (M):
"))

DMSO_density = 1.1004
DMSO_volume = (DMSO_mass / DMSO_density) / 1000
DMSO_Molecular_Weight = 78.13
DMSO_Moles = DMSO_mass / DMSO_Molecular_Weight
D2O_density = 1.107
D2O_volume = (D2O_mass / D2O_density) / 1000
Total_volume_in_ependorf = (D2O_volume + DMSO_volume)
DMSO_concentration_in_ependorf = DMSO_Moles / Total_vol-
ume_in_ependorf
Reference_density = 1.1
Reference_volume = (Reference_mass / Reference_density) / 1000
Sample_volume = 0.0006
Sample_density = 1
Total_Volume_NMR = Sample_volume + Reference_volume
Dilution_ratio = Reference_volume / Total_Volume_NMR
DMSO_concentration_in_NMR_Tube = DMSO_concentration_in_epen-
dorf * Dilution_ratio
Ratio_HCOOH_DMSO = HCOOH_Integral / (DMSO_Integral / 6)
HCOOH_NMR_Concentration = DMSO_concentration_in_NMR_Tube *
Ratio_HCOOH_DMSO
Concentration_ratio = Total_Volume_NMR / Sample_volume
HCOOH_Concentration = (HCOOH_NMR_Concentration * Concentra-
tion_ratio)
```

KHCO₃/CO₂ electroreduction for fuel cell applications*Reaction and reactor optimization, prototyping with 3D printing and automatic testing.*

```

HCOOH_Concentration_mM = HCOOH_Concentration * 1000
excel_file_name = userinput
Total_Charge = calculate_total_charge(excel_file_name)
Total_HCOOH_moles = HCOOH_Concentration * Total_cathodic_vol-
ume
HCOOH_Charge = Total_HCOOH_moles * 2 * 96485.3365
Faradaic_Efficiency = (HCOOH_Charge / Total_Charge) * 100
Reaction_rate = Total_HCOOH_moles / Electroreduction_Time
Total_Bicarbonate_moles = Bicarbonate_Concentration * Total_ca-
thodic_volume
Conversion = (Total_HCOOH_moles / Total_Bicarbonate_moles ) * 100

```

```

try:

```

```

    resultat1, resultat2, resultat3, resultat4, resultat5, resultat6, re-
sultat7, resultat8 = eficiencia_faradiaca (DMSO_mass, DMSO_density,
DMSO_volume, DMSO_Molecular_Weight, DMSO_Moles, D2O_mass,
D2O_density, D2O_volume, Total_volume_in_eppendorf, Reference_mass, Ref-
erence_volume, Reference_density, Sample_volume, Sample_density, Dilu-
tion_ratio, Total_Volume_NMR, DMSO_concentration_in_NMR_Tube,
DMSO_Integral, HCOOH_Integral, Ratio_HCOOH_DMSO,
HCOOH_NMR_Concentration, Concentration_ratio, HCOOH_Concentration, To-
tal_Charge, HCOOH_Charge, Total_cathodic_volume, Total_HCOOH_moles, Far-
adaic_Efficiency, excel_file_name, Reaction_rate, Electroreduction_Time, To-
tal_Bicarbonate_moles, Bicarbonate_Concentration, Conversion, HCOOH_Con-
centration_mM)

```

```

    print("DMSO concentration in NMR Tube (M) : ", round(re-
sultat1, 5))

```

```

    print("HCOOH Concentration (M) : ", round(resultat2, 6))
    print("HCOOH Concentration (mM) : ", round(resultat3, 2))
    print("Total Charge : ", round(resultat4, 1))
    print("HCOOH Charge : ", round(resultat5, 2))
    print("Faradaic Efficiency (%) : ", round(resultat6, 2))
    print("Reaction rate (nM/s) : ", round(resultat7, 2))
    print("Conversion (%) : ", round(resultat8, 4))

```



```
except Exception as e:  
    print(e)
```

```
if __name__ == "__main__":  
    main()
```

KHCO₃/CO₂ electroreduction for fuel cell applications*Reaction and reactor optimization, prototyping with 3D printing and automatic testing.***Code used for solutions preparation****(Python)****# Define function for potassium bicarbonate solution preparation****def Potassium_Bicarbonate_Solution():****Potassium_Bicarbonate_Concentration = float(input("Desired Potassium Bicarbonate Concentration (M) "))****Potassium_Bicarbonate_Volume = float(input("Desired Potassium Bicarbonate Volume (L) "))****Potassium_Bicarbonate_Purity = float(input("Commercial Potassium Bicarbonate Purity % "))****Potassium_Bicarbonate_Molar_Mass = 100.115 #g/mol****Potassium_Bicarbonate_Mass = (Potassium_Bicarbonate_Volume * Potassium_Bicarbonate_Concentration * Potassium_Bicarbonate_Molar_Mass) / (Potassium_Bicarbonate_Purity / 100)****print ("You have to weight " + str(round(Potassium_Bicarbonate_Mass, 4)) + " g of the Commercial Potassium Bicarbonate and dilute it into a " + str((Potassium_Bicarbonate_Volume * 1000)) + "ml Volumetric Flask")****# Define function for sodium bicarbonate solution preparation****def Sodium_Bicarbonate_Solution():****Sodium_Bicarbonate_Concentration = float(input("Desired Sodium Bicarbonate concentration (M) "))****Sodium_Bicarbonate_Volume = float(input("Desired Sodium Bicarbonate Volume (L) "))****Sodium_Bicarbonate_Purity = float(input("Commercial Sodium Bicarbonate Purity % "))****Sodium_Bicarbonate_Molar_Mass = 84.007 #g/mol****Sodium_Bicarbonate_Mass = (Sodium_Bicarbonate_Volume * Sodium_Bicarbonate_Concentration * Sodium_Bicarbonate_Molar_Mass) / (Sodium_Bicarbonate_Purity / 100)**

```
print ("You have to weight " + str(round(Sodium_Bicarbonate_Mass, 4)) +  
" g of the Commercial Sodium Bicarbonate and dilute it into a " + str((Sodium_Bi-  
carbonate_Volume * 1000)) + "ml Volumetric Flask")
```

```
# Define function for sulfuric acid solution preparation
```

```
def Sulfuric_Acid_Solution():
```

```
    Sulfuric_Acid_Concentration_Desired = float(input("Desired Sulfuric  
Acid Concentration (M) "))
```

```
    Sulfuric_Acid_Volume_Desired = float(input("Desired Sulfuric Acid  
Volume (L) "))
```

```
    Sulfuric_Acid_Purity = float(input("Commercial Sulfuric Acid Purity (%  
w/w) "))
```

```
    Sulfuric_Acid_Density = float(input("Commercial Sulfuric Acid Density  
(g/mL) "))
```

```
    Sulfuric_Acid_Molar_Mass = 84.007 #g/mol
```

```
    Sulfuric_Acid_Mass_Commercial = Sulfuric_Acid_Volume_Desired *  
Sulfuric_Acid_Concentration_Desired * Sulfuric_Acid_Molar_Mass / (Sulfu-  
ric_Acid_Purity / 100)
```

```
    Sulfuric_Acid_Volume_Commercial = Sulfuric_Acid_Volume_Desired *  
Sulfuric_Acid_Concentration_Desired * Sulfuric_Acid_Molar_Mass / (Sulfu-  
ric_Acid_Purity / 100) / (Sulfuric_Acid_Density)
```

```
print ("You have to weight " + str(round(Sulfuric_Acid_Mass_Commer-  
cial, 4)) + "g or pipette " + str(round(Sulfuric_Acid_Volume_Commercial, 4)) + "mL  
of the Commercial Sulfuric Acid Solution and dilute it into a " + str((Sulfu-  
ric_Acid_Volume_Desired * 1000)) + "mL Volumetric flask")
```

```
# Define function for chlorohydric acid solution preparation
```

```
def Clorhidric_Acid_Solution():
```

```
    Clorhidric_Acid_Concentration_Desired = float(input("Desired Clorhi-  
dric Acid Concentration (M) "))
```

```
    Clorhidric_Acid_Volume_Desired = float(input("Desired Clorhidric  
Acid Volume (L) "))
```

KHCO₃/CO₂ electroreduction for fuel cell applications*Reaction and reactor optimization, prototyping with 3D printing and automatic testing.*

```

Clorhidric_Acid_Purity = float(input("Commercial Clorhidric Acid Pu-
rity (% w/w) "))

```

```

Clorhidric_Acid_Density = float(input("Commercial Clorhidric Acid
Density (g/ml) "))

```

```

Clorhidric_Acid_Molar_Mass = 36.46 #g/mol

```

```

Clorhidric_Acid_Mass_Commercial = Clorhidric_Acid_Volume_Desired
* Clorhidric_Acid_Concentration_Desired * Clorhidric_Acid_Molar_Mass /
(Clorhidric_Acid_Purity / 100)

```

```

Clorhidric_Acid_Volume_Commercial = Clorhidric_Acid_Volume_De-
sired * Clorhidric_Acid_Concentration_Desired * Clorhidric_Acid_Molar_Mass /
(Clorhidric_Acid_Purity / 100) / (Clorhidric_Acid_Density)

```

```

print ("You have to weight " + str(round(Clorhidric_Acid_Mass_Com-
mercial, 4)) + " g or pipette " + str(round(Clorhidric_Acid_Volume_Commercial, 4))
+ " mL of the Commercial Chlorohydric solution and dilute it into a " + str((Clorhi-
dric_Acid_Volume_Desired * 1000)) + " mL Volumetric flask")

```

```

# Define function for hydrogen peroxide solution solution preparation

```

```

def Hydrogen_Peroxide_Solution():

```

```

    Hydrogen_Peroxide_Concentration_Desired = float(input("Hydrogen
Peroxide Concentration (M) "))

```

```

    Hydrogen_Peroxide_Volume_Desired = float(input("Desired Hydrogen
Peroxide Volume (L) "))

```

```

    Hydrogen_Peroxide_Purity = float(input("Commercial Hydrogen Perox-
ide Purity (% w/w) "))

```

```

    Hydrogen_Peroxide_Density = float(input("Commercial Hydrogen Per-
oxide Density (g/ml) "))

```

```

    Hydrogen_Peroxide_Molar_Mass = 34.0147 #g/mol

```

```

    Hydrogen_Peroxide_Mass_Commercial = Hydrogen_Peroxide_Vol-
ume_Desired * Hydrogen_Peroxide_Concentration_Desired * Hydrogen_Perox-
ide_Molar_Mass / (Hydrogen_Peroxide_Purity / 100)

```

```

    Hydrogen_Peroxide_Volume_Commercial = Hydrogen_Peroxide_Vol-
ume_Desired * Hydrogen_Peroxide_Concentration_Desired * Hydrogen_Perox-
ide_Molar_Mass / (Hydrogen_Peroxide_Purity / 100) / (Hydrogen_Peroxide_Den-
sity)

```

```
print ("You have to weight " + str(round(Hydrogen_Peroxide_Mass_Commercial, 4)) + "g or pipette " + str(round(Hydrogen_Peroxide_Volume_Commercial, 4)) + "mL of the Commercial Hydrogen Peroxide Solution and di-lute it into a " + str((Hydrogen_Peroxide_Concentration_Desired * 1000)) + "mL Volumetric flask")
```

```
def main():
```

```
    # Solutions definitions
    #solutions = {}
    #solutions['Potassium Bicarbonate'] = Potassium_Bicarbonate_solution
    #solutions['Sulfuric Acid'] = Potassium_Bicarbonate_solution

    solutions = ['Potassi-um_Bicarbonate_Solution','Sodium_Bicarbonate_Solution','Clorhidric_Acid_Solution','Sulfuric_Acid_Solution','Hydrogen_Peroxide_Solution']
    solutions_functions = [Potassium_Bicarbonate_Solution ,Sodium_Bicarbonate_Solution ,Clorhidric_Acid_Solution ,Sulfuric_Acid_Solution ,Hydrogen_Peroxide_Solution ]
    print('\nThe available solutions are:')

    #for solution in solutions:
    #    print('\t',solution)

    for i in range(len(solutions)):
        print ('\t', i ,',', solutions[i])

    # Ask user for desired solution
    index = int(input("\nWhat solution do you want to prepare? (type the number of the solution listed above) (The units you should use in each parameter appear in parentheses after the parameter) \n"))

    if index > len(solutions) or index < 0:
        print('Introduced number doesn\'t correspond to any solution in the list')
```

KHCO₃/CO₂ electroreduction for fuel cell applications*Reaction and reactor optimization, prototyping with 3D printing and automatic testing.***return****solutions_functions[index]()****# Call solution function****#if solution in solutions:****# solutions[solution]()****#else:****# print(solution, ' not in list')****if __name__ == '__main__':****main()**

Code used for NMR spectra processing and analysis

(Python)

Insert basic parameters of the NMR instrument

```
sw = 6395.862  
obs = 400.1324  
car= 2400.78
```

Insert the name of the folder with all the NMR data to process

```
Name_of_Folder = 'T1'
```

Define function to detect the peaks

```
def remove_ranges(uc_, excluded_ranges):  
    filt = []  
    for excluded_range in excluded_ranges:  
        filt_ = np.where((uc_.ppm_scale() < excluded_range[0]) | (uc_.ppm_scale() > excluded_range[1]))[0]  
        if len(filt):  
            filt = np.intersect1d(filt_, filt)  
        else:  
            filt = filt_  
    return filt  
def get_range(x, included_range, shift=0):  
    return np.where((x > included_range[0]) & (x < included_range[1]))[0]  
def get_max_peak_idx(data, peaks_idx):  
    peak_values = [data[i] for i in peaks_idx]  
    peak_max_idx = np.argmax(peak_values)  
    return peaks_idx[peak_max_idx]
```

Define function to process all the data and transform it into plottable data

```
def get_data(data_path, p0, p1, sw, obs, car, peak_thresh, excluded_ranges=[[4, 6]]):  
    dic, data = ng.varian.read(data_path)  
    data = ng.proc_base.zf_size(data, 32768) # zero fill to 32768 points
```

KHCO₃/CO₂ electroreduction for fuel cell applications*Reaction and reactor optimization, prototyping with 3D printing and automatic testing.*

```

data = ng.proc_base.fft(data) # Fourier transform
data = ng.proc_base.ps(data, p0=p0, p1=p1) # phase correction
# data = ng.proc_autophase.autops(data, "acme")
data = ng.proc_base.di(data) # discard the imaginaries
data = ng.proc_bl.baseline_corrector(data)
# Prepare unit conversion object to work with ppm
uc_ = ng.fileiobase.unit_conversion(data.size, True, sw, obs, car)
frq = uc_.ppm_scale()
# Filter Water Peak
filt = remove_ranges(uc_, excluded_ranges=excluded_ranges)
# Get peaks
# peak_table = ng.peakpick.pick(data, pthres=2e4, algorithm='downward')
peak_table = ng.peakpick.pick(data, pthres=peak_thresh, algorithm='down-
ward')
peaks_idx = [int(i) for i in peak_table['X_AXIS'] if i in filt]
# Calculate shift of with DMSO reference peak
reference_peak_DMSO_idx = get_max_peak_idx(data, peaks_idx)
reference_shift = uc_.ppm_scale()[reference_peak_DMSO_idx] - 2.71
# Calculate position of principal peaks
# Plot NMR X-Y #
x = (uc_.ppm_scale() - reference_shift)
y = data
# NMR plot peaks #

peak_locations_ppm = [uc_.ppm(i)-reference_shift for i in peak_table['X_AXIS']
if i in filt]
peak_amplitudes = data[[elm for elm in peak_table['X_AXIS'].astype('int') if elm
in filt]]
x_point = np.array(peak_locations_ppm)
y_point = peak_amplitudes
return x, y, x_point, y_point, reference_shift

# Brute force autophase in the given interval

from tqdm import tqdm

def get_range_values(x, y, included_range, reference_shift):

```



```
    range_idx = get_range(x, included_range=included_range, shift=reference_shift)
    return y[range_idx]

def integrate_range(x, y, int_range, reference_shift):
    return get_range_values(x, y, int_range, reference_shift).sum()

p0_min = 24
p0_max = 25
p1_min = -21
p1_max = -20
integration_values = []
for p0 in tqdm(np.arange(p0_min, p0_max, 1)):
    for p1 in np.arange(p1_min, p1_max, 1):
        # for p1 in [-68]:
            x, y, x_point, y_point, reference_shift = get_data("T1", p0=p0, p1=p1, sw=sw,
            obs=obs, car=car, peak_thresh=5e3)

# y_peak_left = get_range_values(x, y, [2.3, 2.5], reference_shift)
# y_peak_right = get_range_values(x, y, [2.5, 2.7], reference_shift)
# Integrate reference peak
peak_integration = integrate_range(x, y, [2.9, 2.5], reference_shift)
# integration_values.append({'p0': p0, 'p1': p1, 'int': peak_integration})
left_peak_integration = integrate_range(x, y, [2.3, 2.5], reference_shift)
right_peak_integration = integrate_range(x, y, [2.5, 2.7], reference_shift)
integration_diff = np.abs(left_peak_integration - right_peak_integration)
integration_values.append({'p0': p0, 'p1': p1, 'diff': integration_diff})
# plot_nmr(x*-1, y, x_point*-1, y_point)
integration_values[:10]

min_idx = np.argmin([val['diff'] for val in integration_values])
integration_values[min_idx]

# Define the plotting parameters with altair for online observation

import pandas as pd
import altair as alt
```

KHCO₃/CO₂ electroreduction for fuel cell applications*Reaction and reactor optimization, prototyping with 3D printing and automatic testing.*

```

def plot_nmr(x, y, x_point, y_point):
    df = pd.DataFrame({
        'x': x,
        'y': y
    })
    alt.data_transformers.disable_max_rows()
    line_chart = alt.Chart(df).mark_line().encode(
        x=alt.X(
            'x:Q',
            scale=alt.Scale(
                domain=(-2.7, -2.3),
                clamp=True,
            ),
            axis=alt.Axis(),
        ),
        # order=alt.Order('x', orient=alt.AxisOrient('left')),
        y=alt.Y(
            'y',
            scale=alt.Scale(
                domain=(-1e2, 2e3)
            )
        )
    ).interactive().properties(
        width=1000,
        height=500
    )
    # Plot points

    df_points = pd.DataFrame({
        'x': x_point,
        'y': y_point
    })
    points = alt.Chart(df_points).mark_circle(
        color='red',
        size=15,
    ).encode(
        x='x:Q',

```

```

    y='y:Q',
)
# 2.62 - 2.5 - 2.324
# 2.7 - 2.3
return line_chart + points

# Define the used parameters to plot and plot the spectra

x, y, x_point, y_point, _ = get_data(Name_of_Folder, p0=-20.0000000000002, p1=-
25.00000000000001, sw=sw, obs=obs, car=car, peak_thresh=1.5e4)
plot_nmr(x*-1, y, x_point*-1, y_point)

p0 = -20
p1 = -25

# Integration of the peaks in the given ranges

peak_integration_Acetic = integrate_range(x, y, [1.8, 2.0], reference_shift)
print("Acetic integral :" + str(peak_integration_Acetic))
peak_integration_DMSO = integrate_range(x, y, [2.4, 3.0], reference_shift)
print("DMSO integral :" + str(peak_integration_DMSO))
peak_integration_Formic = integrate_range(x, y, [8.3, 8.6], reference_shift)
print("Formic integral :" + str(peak_integration_Formic))

ratio_in_percentage_Formic_DMSO = (peak_integration_Formic / peak_integra-
tion_DMSO) * 100
ratio_in_percentage_Acetic_DMSO = (peak_integration_Acetic / peak_integra-
tion_DMSO) * 100

print(("ratio_in_percentage_Formic_DMSO :" + str(round(ratio_in_percentage_For-
mic_DMSO, 2))))
print(("ratio_in_percentage_Acetic_DMSO :" + str(round(ratio_in_percentage_Ace-
tic_DMSO, 2))))

# Plot and extract the data with matplotlib and ready for publishing

import nmrplug as ng

```

KHCO₃/CO₂ electroreduction for fuel cell applications*Reaction and reactor optimization, prototyping with 3D printing and automatic testing.*

```

import numpy as np
import matplotlib.pyplot as plt
import matplotlib.pyplot as ax
from matplotlib.ticker import AutoMinorLocator, FormatStrFormatter

dic, data = ng.varian.read(Name_of_Folder)
data = ng.proc_base.zf_size(data, 32768) # zero fill to 32768 points
data = ng.proc_base.fft(data) # Fourier transform
data = ng.proc_base.ps(data, p0=p0, p1=p1) # phase correction
# data = ng.proc_autophase.autops(data, "acme")
data = ng.proc_base.di(data) # discard the imaginaries
data = ng.proc_bl.baseline_corrector(data)

def get_uc_(data_path, p0, p1, sw, obs, car, peak_thresh, excluded_ranges=[(4, 6)]):
    dic, data = ng.varian.read(data_path)
    data = ng.proc_base.zf_size(data, 32768) # zero fill to 32768 points
    data = ng.proc_base.fft(data) # Fourier transform
    data = ng.proc_base.ps(data, p0=p0, p1=p1) # phase correction
    # data = ng.proc_autophase.autops(data, "acme")
    data = ng.proc_base.di(data) # discard the imaginaries
    data = ng.proc_bl.baseline_corrector(data)
    # Prepare unit conversion object to work with ppm
    uc_ = ng.fileibase.unit_conversion(data.size, True, sw, obs, car)
    return uc_

uc_ = get_uc_(Name_of_Folder, p0=p0, p1=p1, sw=sw, obs=obs, car=car,
peak_thresh=1e6)
plot_nmr(x*-1, y, x_point*-1, y_point)

_ _ _ _ reference_shift = get_data(Name_of_Folder, p0=p0, p1=p1, sw=sw,
obs=obs, car=car, peak_thresh=5e3)
plot_nmr(x*-1, y, x_point*-1, y_point)

ppm_scale = uc_.ppm_scale()

```

```
# read in the integration limit
```

```
peak_list = np.recfromtxt("limits_new.in")
```

```
# plot the spectrum
```

```
fig = plt.figure()
ax = fig.add_subplot(111)
ax.set_xlim([9, 0])
ax.set_ylim([-10000, 50000])
plt.xlabel('ppm', fontsize = 12, fontname = 'Palatino Linotype')
plt.ylabel('Intensity (arbitrary units)', fontsize = 12, fontname = 'Palatino Linotype')
plt.title('Proton NMR of cathodic compartment products', fontsize = 14, fontname = 'Palatino Linotype')
ax.axvline(1.9, 0.14, 0.1, color='darkblue', linewidth = 0.50,)
ax.axvline(2.71, 0.14, 0.1, color='darkblue', linewidth = 0.50)
ax.axvline(8.44, 0.14, 0.1, color='darkblue', linewidth = 0.50)
ax.text(1.9, -7000, '1.9', fontname='Palatino Linotype', fontsize = 10, horizontalalignment='center', color = 'darkblue')
ax.text(2.71, -7000, '2.71', fontname='Palatino Linotype', fontsize = 10, horizontalalignment='center', color = 'darkblue')
ax.text(8.44, -7000, '8.44', fontname='Palatino Linotype', fontsize = 10, horizontalalignment='center', color = 'darkblue')
plt.grid()
for tick in ax.get_xticklabels():
    tick.set_fontname("Palatino Linotype")
for tick in ax.get_yticklabels():
    tick.set_fontname("Palatino Linotype")

from matplotlib.ticker import AutoMinorLocator, FormatStrFormatter
ax.xaxis.set_minor_locator(AutoMinorLocator())
ax.yaxis.set_minor_locator(AutoMinorLocator())

#plt.grid()

ax.plot(ppm_scale - reference_shift, data, 'k-', linewidth = 0.50, color = 'darkred')
```

KHCO₃/CO₂ electroreduction for fuel cell applications

Reaction and reactor optimization, prototyping with 3D printing and automatic testing.

prepare the output file

```
f = open("area.out", 'w')  
f.write("#Name\tStart\tStop\tArea\n")
```

```
name, start, end = peak_list[0]
```

loop over the integration limits

```
min_val = uc_(start + reference_shift, "ppm")  
max_val = uc_(end + reference_shift, "ppm")  
if min_val > max_val:  
    min_val, max_val = max_val, min_val
```

extract the peak

```
peak = data[min_val:max_val + 1]  
peak_scale = ppm_scale[min_val:max_val + 1]
```

plot the integration lines, limits and name of peaks

```
ax.plot(peak_scale-reference_shift, (peak.cumsum() / 100. + peak.max())/40, 'g-', lin-  
ewidth = 0.60)
```

```
#ax.plot(peak_scale-reference_shift, [0] * len(peak_scale), 'b-')
```

```
text_height = min(peak.max(), 25000)
```

```
ax.text(  
    peak_scale[0] - 0.2,  
    text_height + 6500,  
    name.decode('utf-8').replace('_', ' '),  
    fontsize=8, fontname = 'Palatino Linotype')
```

write out the integration info

```
tup = (name, peak_scale[0], peak_scale[-1], peak.sum())
f.write("%s\t%.3f\t%.3f\t%E\n" % tup)

name, start, end = peak_list[1]

# loop over the integration limits

min_val = uc_(start + reference_shift, "ppm")
max_val = uc_(end + reference_shift, "ppm")
if min_val > max_val:
    min_val, max_val = max_val, min_val

# extract the peak

peak = data[min_val:max_val + 1]
peak_scale = ppm_scale[min_val:max_val + 1]

# plot the integration lines, limits, and name of peaks

ax.plot(peak_scale-reference_shift, (peak.cumsum() / 100. + peak.max())/1, 'g-', lin-
ewidth = 0.60)

#ax.plot(peak_scale-reference_shift, [0] * len(peak_scale), 'b-')

text_height = min(peak.max(), 25000)

ax.text(
    peak_scale[0],
    text_height,
    name.decode('utf-8').replace('_', ' '),
    fontsize=8, fontname = 'Palatino Linotype')

# write out the integration info

tup = (name, peak_scale[0], peak_scale[-1], peak.sum())
f.write("%s\t%.3f\t%.3f\t%E\n" % tup)
```

KHCO₃/CO₂ electroreduction for fuel cell applications

Reaction and reactor optimization, prototyping with 3D printing and automatic testing.

```
name, start, end = peak_list[2]

# loop over the integration limits

min_val = uc_(start + reference_shift, "ppm")
max_val = uc_(end + reference_shift, "ppm")
if min_val > max_val:
    min_val, max_val = max_val, min_val

# extract the peak

peak = data[min_val:max_val + 1]
peak_scale = ppm_scale[min_val:max_val + 1]

# plot the integration lines, limits, and name of peaks

ax.plot(peak_scale-reference_shift, (peak.cumsum() / 100. + peak.max())/1, 'g-', lin-
ewidth = 0.60)

#ax.plot(peak_scale-reference_shift, [0] * len(peak_scale), 'b-')

text_height = min(peak.max(), 25000)

ax.text(
    peak_scale[0],
    text_height,
    name.decode('utf-8').replace('_', ' '),
    fontsize=8, fontname = 'Palatino Linotype')

# write out the integration info
tup = (name, peak_scale[0], peak_scale[-1], peak.sum())
f.write("%s\t%.3ft%.3ft%E\n" % tup)
#ax.plot(8.45, 20000, 'g-')
# close the output file and save the plot
f.close()
fig.savefig("plot.png", dpi=300, bbox_inches='tight')
```


Curriculum vitae

KHCO₃/CO₂ electroreduction for fuel cell applications*Reaction and reactor optimization, prototyping with 3D printing and automatic testing.***CURRICULUM VITAE**

Andreu Bonet Navarro was born in 1995 in Deltebre, Spain. He obtained a B.AS in Chemistry at Universitat Rovira i Virgili in Tarragona, where he developed a project focused on crystallography. He then pursued a M.SC Nanotechnology at the same university in 2017-2018, in collaboration with FiCMA research group where he kept working on material science and nanotechnology. Afterwards, Andreu moved his priority interests in research fields, then he started to be interested in renewable energies and embarked a doctoral thesis in Eurecat in collaboration with MEMTEC group in URV. During his thesis he worked on electroreduction of CO₂ meanwhile he got passionate about 3D printing, chemical engineering, automation, and programming skills that boosted his value on his working field. He published 2 articles during his research.